PLASTIC DEFORMATION OF GERMANIUM SINGLE CRYSTALS.

by

W. Bonfield.

Thesis submitted for the
degree of Doctor of Philosophy
in the University of London.

July, 1961.

Metallurgy Department,
Imperial College,
London. S.W.7.

Abstract.

A study was made of the plastic deformation of germanium single crystals. Specimens oriented for single slip were strained in tension at elevated temperatures ($> 400^{\circ}C$). Deformation at a constant strain rate is characterised by a pronounced yield point, followed by an extensive easy glide region. The size and nature of the yield point depend sensitively on the initial dislocation density and orientation of the specimen, strain rate and temperature, but are not significantly affected by either the surface condition of the specimen or the presence of small amounts of impurity.

A yield point is not observed on unloading and reloading in the easy glide region. It is found that a return of the yield point on loading is only effected by reducing the dislocation density of the deformed specimen to a level approaching that of the undeformed specimen.

The yield point phenomenon is explained in terms of the number and velocity of dislocations. It is concluded that grown in dislocations provide the operative dislocation sources.

The flow stress in the easy glide region is found to be a sensitive function of the dislocation density, strain rate and temperature. From these results a physical model of flow stress is developed, in which the contributions are the internal stress field and the stress to move certain dislocation "dragging points".

Some preliminary observations on the nature of work-hardening are also made.

CONTENTS

Page

I. INTRODUCTION AND REVIEW OF LITERATURE

1. Introduction.

Germanium provides a convenient model substance for a study of the mechanisms of plastic deformation. The commercial use of germanium in semi-conductor devices has resulted in the technology of the material being well developed. Consequently germanium single crystals can be readily prepared by established zone refining and crystal pulling techniques. The single crystals produced by these techniques are of high crystalline perfection; the usual dislocation density of an undeformed single crystal is of the order 10^3 cm^{-2}. (Even after considerable deformation the dislocation density is only of the order 10^7 cm^{-2}). These values of dislocation density are much smaller than the comparable values in most metal crystals and facilitate observations of dislocations during deformation. A sensitive etching technique can be used for the study of dislocations in germanium. As a 1 : 1 correlation between etch pits and dislocations on certain planes has been established, this comparatively simple technique enables quantitative measurements of dislocation density to be made. The special electrical properties of germanium also provide useful

information. A knowledge of the resistivity of a single crystal allows an accurate evaluation of the concentration of any electrically active impurity.

Until comparatively recently little attention had been given to the plasticity of germanium. In view of the advantages of germanium as a model substance, it was felt that a comprehensive study of the plasticity might prove of value.

Single crystal specimens, oriented for single slip, were strained in tension at a constant rate. To avoid brittle fracture of the specimens testing temperatures above 400°C had to be used. Deformation was characterised by a pronounced yield point, followed by an extensive easy glide region.

We first investigated the nature of the yield point phenomenon. A study was made of the effects on the yield point of the initial dislocation density, impurity, strain rate, temperature, orientation and surface. A yield point was not observed on reloading the specimen in the easy glide region, and a survey was made of the annealing conditions necessary to effect a return of the yield point.

Secondly the flow stress in the easy glide region was investigated; the effects of dislocation

density, strain rate and temperature being determined. A quantitative study of this parameter was aided by its excellent reproducibility.

The easy glide region was followed by a region of multiple slip and work-hardening. This region was not comprehensively studied, but some preliminary observations were made.

In the discussion of the results, we first develop a physical model of the flow stress. An explanation of the yield point phenomenon is then suggested. Finally an assessment of the nature of the operative dislocation sources is made.

Many problems associated with the plasticity of germanium still remain to challenge the researcher. One experimental result was that, after certain conditions of fast cooling from the annealing temperature, a yield point was observed on retesting. This effect, which is thought to be due to point defects, deserves a more thorough investigation. The wider problems of the detailed nature of dislocation nucleation and multiplication, work-hardening and the ductile-brittle transition are still outstanding. It is felt that a combined research using stress pulsing techniques and electron microscopy, as well as tensile deformation, would provide the most profitable approach.

The following review of literature has two main sections. The first section relates specifically to the properties of germanium and other materials with a diamond structure. The properties of germanium which differ from the more familiar properties of metals are described, i.e. sections are included on the nature of dislocations in the diamond structure, and electrons and point defects in germanium. A critical review of the previous work on the plastic deformation of germanium is made.

In the second section, a general account of the yield point, flow stress and work-hardening in metal and lithium fluoride crystals is given. In contrast to the small amount of work on the plasticity of germanium, the problems of the nature of the yield point and flow stress of metal crystals have received a comprehensive study. The results obtained and the theories evolved from the researches on metal crystals provide a convenient starting point from which to consider the problem of plasticity in germanium. In the same category are the recent studies of the plasticity of lithium fluoride crystals. These results are of special interest as lithium fluoride has a crystalline perfection approaching that of germanium. A detailed account of all the work on metals and lithium fluoride

would be out of place in the present literature review. Instead an attempt is made to give a general picture of the main effects and theories.

2. Dislocations in the diamond structure.

2.1 Simple dislocations.

Germanium, like silicon and diamond, has a covalently bonded structure. The lattice is of the diamond cubic type, which can be visualized as two interpenetrating face centred cubic lattices. Each atom is bonded to four neighbours situated at the corners of a regular tetrahedron, with the valence bonds oriented in <111> directions. The slip plane and direction have been established as the {111} and <110> respectively.

There are three types of simple dislocations in the diamond structure :-

(a) 60° dislocations

This type of dislocation was first considered by Read[1,2] and Schockley[3]. Fig. 1a shows the normal diamond structure and Fig.1b the structure containing a 60° dislocation. The dislocation axis runs in the $[01\bar{1}]$ direction on the (111) plane. The slip or Burgers' vector is in the $[1\bar{1}0]$ direction, i.e. at 60° to the dislocation axis. Above the slip plane is a row of atoms that have no neighbours on the plane

below. These atoms, each of which has a dangling unpaired electron, form the edge of an atomic plane that ends on the slip plane.

(b) Screw dislocations.

Hornstra[4] has considered in detail the properties of screw dislocations in the diamond structure. The simplest form of screw dislocation is shown in Fig.2a. The screw character may be seen by comparing the normal hexagon 7 - 8 - 9 - 10 - 11 - 12 - 7 with the structure 13 - 2 - 3 - 14 - 15 - 16 - 17. In the first case atom 7 is the beginning and end of the loop, in the latter case there is a gap between 13 and 17 (equal to the Burgers' vector).

Another possible screw configuration (shown in Fig.2b) is derived by breaking the bonds 2 - 3, 4 - 5, etc. and forming double bonds between the atoms 1 - 2, 3 - 4, 5 - 6, etc. The dislocation is split into two components occupying neighbouring channels.

(c) Edge dislocations.

The structure of a simple edge dislocation (also due to Hornstra[4]) is shown in Fig. 3a. The dislocation axis runs in the $[1\bar{1}0]$ direction, the Burgers vector is in the [110] direction and the slip plane is the (001) plane. Dangling bonds are associated with the atoms in the extra half plane (which is shown

in heavy type in Fig. 3a). As the edge dislocation is not a slip dislocation, it is less important in the present studies than the 60° and screw dislocations.

Fig. 3b shows an edge dislocation without any dangling bonds. It is derived[4] from Fig. 3a by omitting the atoms with dangling bonds and connecting the remaining free bonds.

The two configurations cannot be simply transformed into one another by electronic re-arrangement (as in the case of the two screw configurations). Presumably this transformation can only occur, at a high temperature, by the diffusion of vacancies or interstitial atoms.

2.2 Partial dislocations.

It is not feasible to re-arrange a 60° dislocation. However Schockley[3] pointed out that the nature of the dislocation would be quite different if slip occurred between the 2nd and 3rd plane instead of the 1st and 2nd plane. This would involve breaking three times as many bonds per atom. The dislocation could reduce its elastic energy by splitting into partials.

The number of distinguishable partial dislocations in the diamond lattice is much greater than in

the face centred cubic lattice, due to the two types of octahedral planes. The two adjacent octahedral planes, connected by three bonds per atom , differ from the next similar pair of planes by a rotation around a common normal of $\pi/3$. The regular stacking is given by :

a b c a b c etc.

where a, b, c, represent pairs of similar planes.

A {111} plane stacking fault can be constructed by the removal or insertion of a pair of planes, forming an intrinsic or extrinsic stacking fault respectively.

The partial dislocation can have various structures, depending on the type of stacking fault and its Burgers vector. All the various possibilities were considered in detail by Hornstra[4].

The partials, associated with a 60° dislocation with Burgers vector $\frac{1}{2}$ a [110] have Burgers vectors of $\frac{1}{6}$ a [211] and $\frac{1}{6}$ a [12$\bar{1}$]. These partials both have their stacking fault in a 111 plane. However an extended dislocation lying fully in one plane is not possible in the diamond structure. Haasen and Seeger[5] have shown that a stable form of extended dislocation can be formed by the combination of a perfect dislocat-

ion on one plane and a partial dislocation on the other plane of the pair. For a partial dislocation with an intrinsic stacking fault, combination with a perfect dislocation involves rotation of whole ribbons of atoms, near the stacking fault plane, through 90^{o}. A combination of a partial dislocation with an extrinsic stacking fault, with a perfect dislocation, is not likely as two ribbons on successive planes must rotate simultaneously.

The stacking fault of a partial need not lie in a {111} plane, in which case the partial dislocation is sessile.

2.3 Other dislocations.

Hornstra[4] has also studied the properties of more complex dislocations. He suggested that every dislocation can be resolved into steps of the simple dislocations discussed previously. The alternation of different orientations of the axis was thought of as a series of jogs. All types of dislocations that could be built up from two simple dislocations were considered. An example is shown in Fig. 4. There are six possible combinations of two simple dislocations with the same Burgers vector ($\frac{1}{2}$ a [110]), which are shown in Table 1.

TABLE I (After Hornstra)

	Axis of Dislocation	Glide Plane	Angle Between Axis & Burgers Vector.
(1)	<211>	(111)	30°
(2)	<211>	(111)	90°
(3)	<211>	(311)	73°
(4)	<211>	(110)	55°
(5)	<100>	(110)	90°
(6)	<100>	(100)	45°

The edge dislocation with a (110) glide plane (No.5) has been observed as a constituent of a small angle tilt boundary.

3. Experimental observations of dislocations.

3.1 Etching techniques.

Etching is an important method of studying dislocations in germanium. Sensitive etching techniques have been developed which enable dislocations to be revealed as etch pits. Moreover, as a 1 : 1 correlation has been established between the etch pits and dislocations on certain planes, etching provides a simple method of determining the dislocation density of germanium.

Vogel[6,7] established a 1 : 1 correlation

between etch pits and edge dislocations in a low angle boundary. The difference in lattice orientation on either side of a small angle boundary was measured by an X-ray technique. From this the expected dislocation spacing in the boundary was derived, using Burgers' model of a low angle grain boundary. The agreement of the expected dislocation spacing with the observed etch pit spacing was excellent. It was concluded that the etch pits mark the points of emergence of edge dislocations.

Later Vogel[8] studied the dislocation densities of plastically bent germanium. Single crystals were bent to various radii of curvature (r) and the observed etch pit densities on {111} planes were compared with the dislocations densities (ρ) calculated from

$$\rho = 1/rb \quad - \quad 3.1 \qquad \ldots\ldots$$

b - Burgers vector.

The results are shown in Table 2.

TABLE 2 (After Vogel)

Radius of curvature (cm)	Calculated dislocation density ($\times 10^6$ cm^{-2})	Observed etch pit density ($\times 10^6$ cm^{-2})
3.4	7.8	12.8
5.2	6.8	9.6
14.3	1.9	5.6
28.2	0.9	2.5

From the results it can be seen that after deformation the etch pit density was larger than the calculated dislocation density. However a short anneal reduced the observed etch pit density and gave a reasonable agreement with the calculated dislocation density.

The etching technique also enables the distribution of dislocations to be studied. Vogel[8] noted the following changes in distribution on annealing the deformed specimens :

(1) There was a migration of dislocations from the high density areas near the surface to the low density areas at the neutral axis.

(2) The dislocations moved into walls normal to the slip plane, giving a polygonised structure.

3.2 Decoration technique.

A decoration technique has been developed for the study of dislocations in silicon. Dash[9] decorated silicon with copper and, using an infra red image tube in conjunction with a microscope, observed lines of copper connecting all the etch pits on the top and bottom surfaces.

The decoration technique enables the nature of dislocations to be studied. Some of the observat-

ions made by Dash were :

(1) Dislocations, in certain crystals, were generated by Frank-Read sources.

(2) In the range 900° - 1100°C the dislocation loops had crystallographically oriented segments if the deformation was "rapid". At "slower" deformation rates, at the higher temperatures, the dislocations were irregular and not confined to a single glide plane.

(3) The screw component of a dislocation loop moved more slowly than the edge component.

3.3 Thin film electron microscopy.

Little work has been performed on the electron microscopy of thin films of germanium. Philips[10] examined the dislocations in germanium produced by indentation. He found that indentation at 550°C produced an irregular array of dislocations. Annealing the deformed specimen at 750°C for 90 hours, caused a re-arrangement of the dislocation lines into a more orderly structure. Indenting the thin film at higher temperatures (800°C) produced a fully polygonised structure.

4. Plastic deformation and the yield point phenomenon in germanium.

4.1 Delay time and plastic creep at a constant load.

Germanium is brittle at room temperature. However Gallacher[11] demonstrated that above 500°C, germanium can be plastically deformed, with slip occurring on {111} planes. A delay time before deformation was observed at temperatures below 600°C. The delay time decreased as the temperature was raised, from five minutes at 500°C to a few seconds at 600°C.

Seitz[12] suggested that the temperature dependent delay time is related to the freeing, by thermal fluctuations, of edge dislocations locked by impurity atoms. The delay time is described by :-

At a constant load

$t = t_o \exp(Q/RT)$ - (4.1)

with $t_o = 10^{-5}$ sec.

$Q = 28{,}000$ cal/mole.

t_o - delay time in pure crystals with no locking points.

Q - activation energy to free dislocations from locks.

Patel[13] also investigated the effect of delay time. He used approximately the same stress level as

as Gallacher, but found longer delay times in the range 400° - 500°C and no delay at 550°C. These differences probably resulted from small variations in the experimental conditions used by the two workers. Later work by Treuting[14] showed that the delay time depended sensitively on the applied load. He found that at 600°C the delay time decreased from 195 secs. at an applied stress of 900 p.s.i. to 42 secs. with an applied stress of 2370 p.s.i. Therefore the delay times would only be comparable if the loading conditions were exactly reproduced. Patel derived a similar equation to equation (4.1), with :

$$t_o = 3 \times 10^{-10} \text{ sec.}$$

$$Q = 39{,}000 \text{ cal/mole.}$$

Patel suggested that the locking impurity may be copper.

Van Bueren[15] and Penning[16] and De Wind have made a comprehensive study of the full creep curves of germanium single crystals, loaded in tension and in bending. The characteristics of the creep curve were :

(1) An "initial" period in which very little plastic strain occurred. A real delay time did not exist in carefully prepared specimens. The specimens deformed immediately although slowly.

(2) A "steady state" period during which

the creep rate was much larger than in the initial period and fairly constant.

(3) A period when the creep rate decreased again due to the onset of work hardening.

Increasing the testing temperature or loading stress resulted in :

(1) A decrease in the lengths of the three periods.

(2) An increase in the creep rate during the steady state period.

The initial period can be described by a cubic time law. The inverse strain rate $(\dot{\varepsilon}_s)^{-1}$ during the steady state period is represented by :

(1) At constant stress (σ)

$(\dot{\varepsilon}_s)^{-1} \sim \exp Q/kT$ Q - activation energy.

with $Q \sim 1.5 - 2$ e.v.

(2) At constant temperature (T)

$(\dot{\varepsilon}_s)^{-1} \sim \exp(-a\sigma)$

with $a \sim 10^{-7}$ dyne^{-1}cm^2.

The creep curves were independent of the dislocation density of the specimen at densities below 5×10^5 cm^{-2}. At higher densities, the creep rate was proportional to the dislocation density of the specimen.

Van Bueren suggested that the "grown in" dislocation density has little influence on the deformation characteristics of the specimen. This does not seem to be a reasonable conclusion as :

(1) At densities greater than 5×10^5 cm^{-2} the creep rate was proportional to the dislocation density of the specimen.

(2) There was a considerable scatter in the experimental results.

(3) The specimens tested were not oriented for single slip. Therefore any effect due to the number of dislocations, may be observed by any work-hardening produced by multiple slip.

The addition of oxygen to germanium crystals decreased both the length of the initial period and the stationary creep rate. It was suggested that oxygen inhibited the dislocation sources.

Van Bueren[17] has suggested a theory of creep. On the application of a stress, dislocation sources can emit dislocations in intervals of time (t_1) given by :

$$t_1 = \theta + \frac{\delta}{v} \quad \cdots\cdots \quad (1.2)$$

v - velocity of dislocation loops.

δ - distance between successive loops.

θ - possible delay time.

The expansion of the loops and the number of loops both increase proportionally with time (t). The total dislocation density (ρ) increases quadratically with time.

$$\rho = \frac{N}{t_1} \cdot \Pi v t^2 \quad \ldots\ldots \quad (4.3)$$

N - number of dislocations.

The strain rate ($\dot{\varepsilon}$) is given by :

$$\dot{\varepsilon} = \rho b v \quad \ldots\ldots \quad (4.4)$$

$$= \frac{\Pi N b v^2 . t^2}{t_1} \quad \ldots\ldots \quad (4.5$$

Ultimately the dislocation loops reach the surface of the specimen and a "stationary state" corresponding to period two of the creep curve is reached. The time which must elapse before the "stationary state" begins is of order d/v, where d is the dimension of the specimen.

For $t < d/v$ $\quad \varepsilon = \frac{\Pi N b v^2 .}{3 t_1} t^3 \quad \ldots\ldots \quad (4.6)$

$t > d/v$ $\quad \varepsilon_s = \frac{\Pi N b d^2}{t_1} \quad t - \frac{2}{3}\frac{d}{v} \quad \ldots\ldots \quad (4.7)$

$$\dot{\varepsilon}_s = \frac{\Pi N b d^2}{t_1} \quad \ldots\ldots \quad (4.8)$$

Van Bueren's assumptions seem reasonable for an experimental situation in which single slip is occurring.

4.2 Variable load experiments.

(a) Compressive loading.

Patel and Alexander[18] investigated the effects of temperature, orientation and impurity content on the compressive stress-strain characteristics of germanium single crystals. The load-unload technique was used; i.e. the specimen was allowed to deform for 15 seconds after the application of the load, the load was then removed and the strain measured. This method of testing is not the most suitable, in view of the marked dependence of flow stress on strain rate, and yield points were not observed.

The results obtained were :

(1) The rate of work-hardening decreased with increase in the testing temperature.

(2) Specimens with a <111> orientation work-hardened the most rapidly. For orientations near the <100> - <111> and <111> - <110> boundaries, double slip occurred. (This was in spite of the orientations lying in a region favouring single slip).

(3) Annealing a deformed specimen for 30 minutes at 800°C gave a slight decrease in dislocation density. After 16 hours at 900°C a reduction of a factor of 5 in dislocation density was obtained.

(4) No difference in stress-strain behaviour was found between intrinsic germanium ($<10^{14}$ atoms/cc impurity) and 0.06 Ωcm germanium ($\sim 10^{17}$ atoms/cc impurity).

(5) The dislocation density of a specimen with two parallel {111} faces increased rapidly from 5×10^{3} cm^{-2} initially to $2 \times 10^{6} cm^{-2}$ after 1% strain. The density then increased more slowly to approximately $8 \times 10^{7} cm^{-2}$ after 6% strain.

(b) Tensile loading.

No comprehensive study of the tensile deformation of germanium at a constant strain rate has been made Treuting[14] deformed 0.1 Ωcm germanium single crystals, of nearly <110> orientation, in tension at 600°C under an atmosphere of helium gas. He found that slip occurred on {111} planes in a <110> direction. The deformation was inhomogeneous, localised rotations being observed. After deformation the structure was polygonised with a domain size of $\sim 2 \times 10^{3} cm^{-2}$.

Treuting deformed one specimen under continuous loading and noted a sharp yield point, followed by a region of work-hardening. A yield point was not observed on unloading and reloading the specimen. Subsequent annealing of the deformed specimen did not effect a return of the yield point.

Carreker[19] deformed a few 2 - 20 Ω cm germanium single crystal specimens with <111> orientation, in air using an Instron machine. A yield point was observed at 550°C and 600°C, but not above 625°C. The reproducibility was not very good as a second specimen tested at 600°C did not give a yield point. Further the testing of specimens with <111> orientations, which exhibit rapid work-hardening, is likely to mask any small yield point effects. The flow stress was sensitive to the rate of straining. At 650°C with an elongation rate of 0.005"/min. yielding occurred at 2000 p.s.i. and fracture at 7% elongation, at 0.05"/min. fracture occurred at 4500 p.s.i. with no apparent elongation. Stopping the elongation caused the stress to relax to a lower value.

Treuting and Carreker suggested that the yield point can be explained in terms of the impurity locking of dislocations (See section 6.1a) Certain of the experimental results are typical of the effects due to impurity locking. They are :

(1) A sharp yield point is produced on continuous loading.

(2) The yield point is not observed on unloading and reloading after the lower yield point.

However a return of the yield point by strain

ageing has not been effected. Further, the smallness of the number of specimens tested and the scatter in the results obtained, indicate that a far more comprehensive series of experiments is required to understand the nature of the yield point mechanism.

4.3 Other current research.

Since our research was started (1958), Patel and co-workers have been continuing their study of the plastic deformation of germanium. The full details of this work have not yet been published and a critical review is not possible. However the information obtained from the published abstracts is considered in the discussion section.

4.4 The flow stress of germanium single crystals.

A model of flow stress at a constant strain rate has been proposed by Van Bueren[20]. The model was based on his creep results and some flow stress measurements of Alexander. (See Discussion).

The creep results (see Section 4.1) indicated that the stationary creep rate ($\dot{\varepsilon}_s$) is given by :

$$\dot{\varepsilon}_s = \frac{\Pi N b d^2}{t_1} \qquad \ldots\ldots\ldots \qquad (4.8)$$

also $$t_1 = \theta + \frac{\delta}{v} \qquad \ldots\ldots\ldots \qquad (4.2)$$

hence assuming θ is small

$$\dot{\varepsilon}_s = \frac{\Pi N b d^2}{\delta} \cdot v \qquad \ldots\ldots \qquad (4.9)$$

It was also found that the stationary creep rate ($\dot{\varepsilon}_s$) depends exponentially on the stress (σ) and temperature (T)

$$\dot{\varepsilon}_s = \dot{\varepsilon}_{s_o} \exp - (Q_1 - \sigma V)/kT \quad \ldots. \quad (4.10)$$

Q_1 - activation energy.

V - activation volume

$\dot{\varepsilon}_{s_o}$ - constant.

The flow stress results indicated that the flow stress at a constant strain rate varies :

(1) exponentially with temperature,

(2) with the logarithm of the strain rate.

Van Bueren extended equation (4.10) to include these results by considering the variation of the activation volume with temperature.

The activation volume (V) is given by :

$$V = l\, b^2 \qquad \ldots\ldots\ldots \qquad (4.11)$$

where l is the distance between "dragging points" along a dislocation line. The dragging points are sites at which the dislocation mobility under stress has become limited. The points can only be made to move by supplying the stress dependent activation energy (Q),

given by :

$$Q = Q_1 - \sigma V \quad \ldots\ldots\ldots \quad (4.12)$$

Van Bueren suggested that the distance l varies with temperature given by :

$$l = l_o \exp(-U/kT) \quad \ldots\ldots\ldots \quad (4.13)$$

where μ is the free energy difference between a mobile and immobile dragging point.

Rearranging equation (4.10) gives :

$$\sigma = \frac{Q_1}{V} + \frac{kT}{V} \ln \frac{\dot{\varepsilon}_s}{\dot{\varepsilon}_{s_o}} \quad \ldots\ldots\ldots \quad (4.14)$$

substituting V for $\dot{\varepsilon}_s$ (from equation 4.9)

l " V (from equation 4.13)

gives :

$$\sigma = Q_1 + kT \ln \frac{\delta \dot{\varepsilon}_s}{\Pi N b d^2 V_o} \frac{1}{b^2 l_o} \exp(U/kT) \quad \ldots(4.15)$$

Van Bueren then assumed that a similar experimental situation prevails in a tensile test, and that the flow stress (σ_t) at a constant strain rate ($\dot{\varepsilon}_t$) is given by :

$$\sigma_t = Q_1 + kT \ln \frac{\delta \dot{\varepsilon}_s}{\Pi N b d^2 V_o} \frac{1}{b^2 l_o} \exp(U/kT) \quad \ldots \quad (4.16)$$

Q_1 was defined as the energy to remobilize a dragging point, containing apart from U an energy term

related to a re-arrangement mechanism. It was suggested that if the dragging points were diffusion locks due to vacant atomic sites, the energy difference could represent the migration energy of an interstitial atom or a vacancy. The derived values of activation energy were :

$$Q_1 \sim 1.7 \text{ e v}$$
$$U \sim 0.6 \text{ e v.}$$

Van Bueren considered that equation (4.16) only applies to the post yield flow stress and not to the initial yield point.

In its basic form (equation 4.14) Van Bueren's equation is similar to that derived by Seeger for thermally activated dislocation motion (see Section 6.2). It differs in the absence of a term due to the internal stress field and the use of a variable activation volume. Van Bueren's model is further examined and its validity tested in the Discussion section.

Haasen[21] has proposed a simple theory of the post yield flow stress. He considered that a 60° dislocation has a micro crack along its axis. As the dislocation moves the micro crack has to diffuse along with it. The following equation was derived :

$$\sigma_f = \frac{vkT}{b^2 D_o} e^{\frac{U}{kT}} \quad \ldots \quad (4.17)$$

v - dislocation velocity.

D_o - diffusivity of crack.

μ - activation energy to move crack.

4.5 Plastic deformation of "heavily-doped" germanium.

Only a few experiments have been performed on the plastic properties of "heavily doped" germanium (i.e. > 10^{18} atoms/cm^3 impurity). The results are conflicting and lacking in detail. The upper yield point at 500°C of germanium heavily doped with gallium was found[22] to be approximately twice that of germanium doped with arsenic in the same concentration. The results were interpreted in terms of the effect of the impurity on the concentration of vacancies, and possibly on the size of condensed vacancy loops.

Cummerow and Cherry[23] lightly deformed dislocation free arsenic doped (10^{19} atoms/cm^3) and gallium doped (10^{19} atoms/cm^3) germanium, in bending at 500°C. A well defined neutral region, with no etch pits, was observed. On annealing at 600°C for 5 minutes, dislocations, as revealed by etch pits, spread into the neutral region in the p-type (gallium doped) specimen. No movement of dislocations in the n-type (arsenic doped) specimen was observed until the annealing temperature was raised to 700°C. The higher temperature

required to move the dislocations in the n-type specimen was interpreted as due to arsenic providing a more effective impurity locking of dislocations. This result is in conflict with that of Patel.

Suzuki[24] found that the size of the yield point decreased as the concentration of doping impurity was increased. At a concentration greater than 10^{19} atoms $/cm^3$, no yield point was observed. Suzuki confirmed the observations of Cummerow and Cherry, p-type samples did not exhibit a yield point above 600°C , whereas n-type samples gave a yield point up to 800°C. The locking energies were estimated as 1.4 e.v.for p-type and 1.8 e.v.for n-type germanium.

4.6 Dislocations produced by crystal growth.

Single crystals of germanium are generally prepared by the Czochralskitechnique, in which a seed is slowly withdrawn from the melt under an argon atmosphere or vacuum. The usual dislocation density of the grown crystal is $10^3 - 10^4$ cm^{-2}. Using after heater techniques to reduce the cooling rate, crystals of even higher perfection can be prepared.

Billig[25] and Penning[26] have studied the nature of the as grown dislocation arrays. The distribution obtained depended on the crystallographic

orientation and the experimental conditions. Dislocations are produced during the cooling of the crystal drawn from the melt. The inhomogeneous temperature gradient in the crystal produces thermal stresses, which are released at high temperatures by the generation and movement of dislocations.

The geometry of the observed dislocation patterns can be explained in one of two ways. These are :

(a) Only a small part of the thermal stress is released by plastic flow. Then the deformation pattern is determined primarily by the elastic stress distribution and the geometry of the available glide systems.

(b) Complete plastic release occurring. The flow pattern then no longer reflects the original elastic distribution.

It was found that the observed dislocation distributions could best be explained by assuming only a little plastic flow occurred. Hence we can conclude that even at very high temperatures near melting point, dislocations in germanium have only a restricted mobility.

4.7 The yield point phenomenon in silicon.

The similarity in structure of germanium and silicon make any observations of yield point effects

in silicon of special interest.

Pearson[27] et al. tested silicon rods and whiskers in bending over a range of temperature. Above 600°C both rods and whiskers deformed plastically with a sharp yield point. The yield point could be regained by ageing; rods tested at 800°C and held at a constant stress for 2 hours, regained about one half of the yield point. Pearson suggested that the results can be explained by the impurity locking of dislocations. It was suggested that the oxygen content was about 10^{18} atoms/cc, which was more than enough to saturate all the dislocations.

The yield stress was the same for rods annealed at 800°C and 1200°C. It was suggested that this indicated that all the dislocations were still saturated at the higher temperature, and that the condensation temperature was > 1200°C.

From $c = c_0 \exp(U/kT)$ ..... (6.2)
(See section 6.1)

$U > 1.4$ e.v.

It was concluded that the binding energy (U) is chemical rather than elastic.

However this experiment is not very conclusive. The load was applied by hand, and as the deformation properties of germanium (and probably also

of silicon) are particularly sensitive to the applied strain rate, this method is not likely to produce very critical results. A critical experiment would be to test an oxygen free specimen, with a low dislocation density, at a constant strain rate.

Recently Sylwestrowicz[28] has deformed <111> oriented silicon specimens over a range of temperature. He found that samples with a low oxygen content gave either a very small yield point or no yield point at all. The initial dislocation density did not affect the stress-strain characteristics. However, these results are not very significant. The deformation properties of germanium, and probably also of silicon, are very sensitive to the specimen orientation. As the <111> orientation produces very rapid work-hardening, any effect due to the number and velocity of dislocations was not likely to be observed.

5. Electrons and point defects in germanium.

5.1. Introduction.

In germanium at the absolute zero of temperature the valence band is exactly full and the conduction band (0.79 e.v. above valence band) is empty. At room temperature there are sufficient free electrons and holes to produce an intrinsic conductivity approximately a factor of 10^7 smaller than in metals. The

product of the concentrations of electrons and holes is a constant. Foreign atoms, i.e. trivalent (acceptor) atoms or pentavalent (donor) atoms also produce a finite extrinsic(positive or negative carrier) conductivity. The conductivity ($\emptyset$) (of extrinsic germanium) depends on the number (n or p or both) and mobility (M) of the charge carriers.

$$\emptyset = n.M\,\varepsilon \qquad \ldots\ldots \qquad (5.1)$$

ε = charge on carrier.

Hence a knowledge of the conductivity (or resistivity) and the mobility enables an evaluation of the concentration of electrically active impurity to be made.

5.2 The effect of plastic deformation.

Plastic deformation increases the number of lattice imperfections and results in :

(1) A reduction in the mobility of charge carriers due to increased effect of scattering by dislocations.

(2) An increase in acceptor concentration (n-type germanium is converted to p-type after sufficient deformation).

Tweet[29] measured the temperature variation of the resistivity and Hall coefficient of plastically bent and annealed germanium. Part of the acceptors

introduced by the deformation annealed out in 1 hour at 700°C. It was suggested that these acceptors are vacancies, the residual acceptors being associated with dislocations. High temperature deformation produced only dislocation type acceptors.

5.3 The effect of quenching.

It has been found that the acceptor density in germanium can be increased by rapid cooling from a high temperature. The possibility of point defects having an effect on the yield point phenomenon makes a review of this work useful.

Theurerer and Scaff[30] noticed that rapidly cooling n-type germanium from 850°C caused a conversion to p-type. Annealing the specimen at 500°C caused a reversion to n-type. The results were interpreted in terms of an increase in acceptor density due to the quenching, followed by an annealing out of acceptors. Acceptors were obtained in experiments where the cooling rate varied from quenching[31] to radiation cooling[32].

Later work[33,34] showed that copper has similar properties to the acceptors, i.e. solubility, diffusivity and annealing properties. It was concluded that copper causes the conversion (copper has a maximum

solubility in germanium at 850°C. Quenching from this temperature causes the retention of copper in solid solution which acts as acceptor centres. Annealing causes the copper to precipitate and reduces the acceptor density).

Later workers took great care to remove copper impurity before starting quenching experiments. It was found[35] that 95% of the copper can be removed by heating at 920°C in vacuum.

Mayburg[36] found that radiation cooling from 830°C produced 2 x 10^{14} acceptors/cc, which were thought to be vacancies. Logan[37] quenched germanium into ethyleneglycol, giving a much faster cooling rate than Mayburg, but found the acceptor density to be about 5 times less. It was not possible to quench in acceptor centres in germanium of high dislocation density (10^6 cm^{-2}), the centres presumably being annihilated on dislocations during the quenching. Hopkins and Clarke[38], taking great care to avoid contamination, quenched at 170°C/min. and obtained even fewer acceptors than Logan. It was suggested[39] that the different acceptor densities obtained were due to different dislocation densities, rapid quenching possibly giving some plastic deformation.

Letaw[40] identified quenched-in acceptors as

vacancies with an energy of formation of 2 e.v. The point defects introduced by quenching annealed out in a few minutes at 350°C. This annealing time was much smaller than that required to anneal out acceptors produced by plastic deformation. It was suggested[41,5] that the nature of the defects is different, quenching producing single vacancies and deformation divacancies.

6. Plasticity of metals and lithium fluoride.

6.1 The yield point phenomenon.

(a) Impurity locking of dislocations

The nature of the yield point phenomenon in metals has been rigorously investigated. Some of the metals and alloys in which the effect has been observed are :

(1) Mild steel, containing carbon or nitrogen.
(2) Single crystals[42] of iron containing carbon,
(3) Polycrystalline molybdenum[43] containing nitrogen,
(4) Single crystals of β brass[44], zinc[45] and cadmium[46] containing nitrogen,
(5) α brass[44],
(6) Aluminium[47,48] alloys.

The main features of the phenomenon are :

(1) A fall in stress from the upper to lower yield point during the first loading.

(2) The absence of a yield point on immediate reloading.

(3) The return of the yield point after a suitable ageing treatment.

Cottrell[49] has proposed a theory of the yield point in terms of the locking of dislocations by impurity atoms. The presence of an impurity atom produces a distortion in the metal lattice, which enables it to react with the stress field around a dislocation. With sufficient impurity atoms, the dislocations are anchored along their entire length to fixed positions in the crystal. To produce plastic flow the dislocations must be pulled away from the atmospheres of the impurity atoms. The strong affinity between a dislocation and its atmosphere, means that the force required to separate the dislocations from their atmospheres will be greater than the subsequent force required to keep them in motion. The release of dislocations makes the start of plastic deformation and as the dislocations can move under a reduced load, the material yields under a decreasing stress. On unloading and immediate reloading, the dislocations are no longer anchored by impurity atom atmospheres and a yield point is not observed. On ageing the impurity atoms diffuse back to the freed dislocations, which become locked

again by the atmospheres. A yield point is then obtained on retesting.

Cottrell and Bilby[50] considered the elastic interaction between solute interstitial atoms and the hydrostatic stress field of an edge dislocation. If the hydrostatic pressure of a stress field at some point is p and the change in volume produced by a solute atom is Δv, the atom is bound to this point by an energy :

$$U = p \Delta v \qquad \ldots\ldots\ldots \quad (6.1)$$

In the case of carbon and nitrogen in body centred cubic iron an additional effect is important. The distortion produced by the solute atom is not spherically symmetrical, a local body centred tetragonal configuration being formed. By producing this tetragonal distortion, as well as a volume expansion, these atoms can interact with both shear and hydrostatic stress fields. This enables them to react with screw dislocations (with stress fields of pure shear) about as strongly as they react with edge dislocations.

Each dislocation gathers around itself an atmosphere of solute atoms. The equilibrium concentration (c) of solute atoms at a point where the binding energy is U, is :

$$c = c_o \exp (U/kT) \quad \ldots \quad (6.2)$$

c_o - average concentration.

If the temperature is lowered the atmosphere of solute atoms becomes saturated, i.e. $(c - c_o)\ \Delta v$ approaches the limit set by the maximum dilation at the centre of the dislocation. When the atmosphere becomes saturated the Maxwellian distribution of equation (6.2) is no longer satisfied and the atmosphere condenses into a line of solute atoms, lying parallel to the dislocation at the position of maximum binding.

For iron

substituting $c = 1$

$U = U_{max} \sim 0.5$ e.v.

$c_o = 10^{-4}$

gives the condensation temperature

$To = 700^{\circ}K.$

The reaction of carbon and nitrogen with dislocations in iron gives an exceptionally large binding energy. In face centred cubic metals the binding is weaker and the condensation temperature occurs at low temperatures. This is because many substitional solute atoms, particularly in face centred cubic metals, produce only spherically symmetrical distortions

and so should hardly interact with screw dislocations. Indirect anchoring of screw dislocations can occur by the formation of two partial dislocations[51], one of which must have a substantial edge component.

(b) The release process

Yielding occurs by nucleation in an area of high stress concentration and subsequent spreading through the rest of the material. Careful observations have shown that the abrupt yielding of certain metal crystals only occurs after a delay time. The occurrence of a delay time and an upper yield point have been interpreted by Fisher[52] in terms of a thermally activated release process. Fisher suggested that under the action of a shear stress, a thermally activated breakaway of dislocation segments from their pinning points occurs. It was assumed that this is a consecutive process, as a certain number of pinning points have to be released successively. The energy required for this process reaches a maximum value as a function of the length of the dislocation that has broken loose. The maximum energy is regarded as the activation energy (to be supplied by thermal vibration) for the breakaway of a dislocation segment. No more energy is required to further extend the free length. The assumption of a consecutive process means that

the rate of the process depends strongly on the stress. The activation energy is inversely proportional to the stress, and the delay time and inverse strain rate depend on the stress (σ) and temperature T through an exponential factor of the form $e^{c/\sigma T}$

Cottrell[53] criticised Fisher's theory on the ground that the concept of line tension cannot be applied to very short dislocation lengths. He suggested that the important factor is the change in core energy of a dislocation when it pulls loose from an impurity atmosphere. Such a derivation leads to a less strong dependence of activation energy (Wo) on stress ($Wo \sim \sigma^{-\frac{1}{3}}$)

(c) Other dislocation-impurity interactions

Other types of impurity atom-dislocation interactions have been suggested.

(1) Suzuki interaction[54]

In face centred cubic metals the dislocations may be split into partial dislocations separated by a stacking fault. The difference in structure of the stacking fault compared with the matrix, may mean that the solubility of the impurity atoms in each is different. Such a free energy difference may produce an effective binding energy of the impurity atom to the extended dislocation.

(2) Snoek ordering[55]

It has been suggested that the interstitial carbon atoms in iron can occupy three types of position, which differ according to the direction of tetragonality caused by the interstitial atom. Normally these three positions are equivalent, but in the stress field of a dislocation, a state of order in the distribution is created depending on which direction of tetragonality complies best with the local stress conditions. To move a dislocation, the order must be removed, giving a higher yield stress.

(d) Unloading effects.

The Cottrell theory of impurity locking suggests that unloading, followed by immediate reloading, is a reversible process. However interrupted tensile tests at low temperatures on aluminium and copper single[56,57,58] crystals, have shown that a small yield point may be obtained on reloading. Haasen and Kelly[59] noted yield points in interrupted tensile tests on nickel and aluminium and suggested that the effect is of general occurrence in face centred cubic single crystals at low temperatures ($< 300^{o}K$). They suggested that on unloading, sessile dislocations are created by dislocation interactions. The sessile dislocations anchor the relaxing dislocations and produce a yield

point on reloading. Later work by Makin[60] supported this theory.

Other workers[61,62] found an unloading effect in alloy single crystals. Bolling[63] suggested that the effect is likely to be of general occurrence.

(e) Work softening effects.

Cottrell and Stokes[64,65] found a work softening effect in aluminium single crystals. A sharp yield point was produced on straining at 300°K after cold working at 90°C. Intermediate annealing reduced or eliminated the yield point drop. It was suggested that the effect is due to a work softening effect. The combined influence of stress and temperature produces an unlocking of the sessile dislocations at the head of piled up groups (produced by cold working). The piled up groups can then partly collapse and many dislocations are released for slip.

6.2 The flow stress and work-hardening of f.c.c.metals

The stress strain curve of face centred cubic single crystals can be divided into three parts :

(a) Stage I - this is the easy glide region with only one operative slip system.

(b) Stage II - multiple slip occurs, the slope $d\sigma/d\varepsilon$ is practically independent of the temperature and impurity concentration.

(c) Stage III - the slope $d\sigma/d\varepsilon$ is a function of the temperature.

The present study has been mainly of the flow stress of germanium in the easy glide region, i.e. corresponding to stage I of the stress-strain curve in f.c.c. metals. However a general review of the current theories of stages II and III in f.c.c. metals is included for completeness.

The contributions to the flow stress of a metal may be :

(1) The Peierls force, i.e. the force to move a dislocation in a perfect lattice. It is thought to be small in f.c.c. metals, but large in b.c.c. metals at low temperatures.

(2) The elastic interaction between parallel dislocations producing an internal stress field given by :

$$\sigma = \alpha b G \sqrt{\rho} \quad \ldots\ldots\ldots \quad (6.3)$$

α - depends on nature of dislocations.
G - shear modulus.
ρ - dislocation density.

(3) Impurity locking effects.

(4) Lattice obstacles such as precipitates or forest dislocations.

The flow stress of a deformed metal increases with the amount of strain, i.e. the metal work-hardens. Taylor[66] suggested that work-hardening is due to the elastic interaction of parallel dislocations. As the dislocation number increases, the internal stress due to elastic interactions also increases. Taylor equated the internal stress field to the applied shear stress (σ) and derived a parabolic equation :

$$\sigma = \text{constant} \frac{\varepsilon}{L} \quad \ldots\ldots \quad (6.4)$$

ε - strain.

L - distance moved by each dislocation.

Such a relation does not describe the observed linear stress-strain relation in the easy glide and stage II regions.

Various workers, notably Seeger[67], have shown that a linear work-hardening law can be obtained using a model in which piled up groups of dislocations act as sources of internal stress. As deformation proceeds, the number of Cottrell-Lomer barriers (which originate from the coalescence of two extended dislocations on intersecting slip planes) increases. Easy glide continues until each operative dislocation source is completely surrounded by barriers. The extent of the easy glide region depends largely on

the orientation of the specimen.

Seeger suggested that during stage II the mean path length of successively released dislocations decreases, due to the continuous formation of new Cottrell-Lomer barriers. The work-hardening is determined by the elastic interaction of parallel groups of piled up dislocations. The constant rate of work-hardening is assumed to be due to a constant number of piled up dislocations per source.

Friedel[68] also assumed that the main source of work-hardening in stage II is the obstruction of Cottrell-Lomer barriers. He assumed that the barriers are all formed together at the beginning of stage II and then remain constant in number, with the number of dislocations per pile up increasing continuously. This theory gives a large work-hardening coefficient. Friedel reduces this to the order of the observed work-hardening coefficient by considering the effect of the back stress of the dislocations on their own source.

Objections to Friedel's theory are :

(1) The inherent instability under stress reversal of the dislocation distribution.

(2) The observed inverse proportionality of slip line length with strain.

In stage III the rate of work-hardening decreases

with increasing temperature. Thermal fluctuations are required to overcome :

(1) Cottrell-Lomer barriers by break through or cross slip.

(2) Intersecting dislocations.

Seeger[67] has considered the theory of thermally activated dislocation motion. He considered that the activation energy (U) depends on the net stress, i.e. the applied stress (σ) minus the internal stress field (σ_a) due to the elastic interaction of parallel dislocations.

$$U = Uo - V (\sigma - \sigma_a) \quad ..... \quad (6.5)$$

Uo - energy to form a jog or constriction.

V is the activation volume given by :

$$V = l_o b d \quad ..... \quad (6.6)$$

l_o - distance between obstacles.

d - distance through which work is done in "cutting" obstacles.

The rate of strain ($\dot{\varepsilon}$) is given by :

$$\dot{\varepsilon} = N \Lambda b \nu_o \exp \frac{- Uo - V (\sigma - \sigma_a)}{kT} \quad ..... \quad (6.7)$$

N - number of dislocations per unit volume.

Hence

$$\sigma = \sigma_G + \frac{U_o - kT \ln N A b \nu_o / \dot{\varepsilon}}{V} \quad \ldots\ldots \quad (6.8)$$

A - area swept out.

ν_o - atomic frequency factor.

Thus the flow stress is composed of a temperature independent elastic term and a temperature dependent term.

When $T > T_o$ where $T_o = U_o/k \ln NAb \nu_o/\dot{\varepsilon}$

$$\sigma = \sigma_G \quad \ldots\ldots\ldots \quad (6.9)$$

The electron microscope studies of thin films of metals by various workers have indicated certain objections to the work-hardening theory of Seeger. These objections are :

(1) In single and polycrystalline metals, in stages II and III, the most characteristic arrangement of dislocations is in thick tangled regions separating regions comparatively free from dislocations. Arrangements of dislocations on slip lines are seen only in metals of very low stacking fault energy (Cu + 7% Al austenitic steel).

(2) Piled up groups of dislocations are observed at grain boundaries in metals of low stacking fault energy, but not in the body of the grain. There is no evidence of Cottrell-Lomer locks long enough to

anchor piled up groups.

Bailey and Hirsch[69] showed that the flow stress of copper and silver single crystals is given by :

$$\sigma = \alpha G b / l \quad \ldots\ldots\ldots \quad (6.10)$$

l - distance between dislocation in the dense region.

Hirsch[70] showed that vacancy jogs can exert a resistance to the movement of a screw dislocation. The intersection of two screw dislocations produces a jog, which is a pure edge dislocation. However, the activation energy for the jog to move conservatively along the screw dislocation, is greater than the activation energy for non-conservative motion. Hence the jog moves with the dislocation, creating a row of vacancies and exerting a resistance to the movement. The resistance is temperature independent, as due to the restraint of the row of vacancies, temperature fluctuations can only move the dislocation a single atomic distance. A temperature dependence occurs only when the vacancies can diffuse away from the dislocation. Interstitial jogs move more easily, in a conservative manner, along the dislocation and only affect the dislocation motion at low temperature.

It was suggested that in stage II :

(1) Considerable secondary slip occurs.

(2) The dislocations move until the jog density stops them.

(3) The dislocation network, much of which is produced by the secondary slip, is responsible for a considerable part of the flow stress.

Clearly the problems associated with the work-hardening of f.c.c. metals are not yet resolved and further work is required to test the validity of the competing theories.

6.3 Plastic deformation of lithium fluoride.

Johnston and Gilman[71,72,73,74,75], have made a comprehensive study of deformation mechanisms in lithium fluoride single crystals. These studies are of interest for the new ideas evolved, particularly as lithium fluoride has a crystalline perfection approaching that of germanium.

The movements of individual dislocations (revealed as etch pits), were studied under various stress pulses. Measurements of the distances moved enabled the dislocation velocities to be calculated. The dislocation velocities obtained ranged from 10^{-7} to 10^{5} cm/sec. The main results were :

(1) There was a minimum stress for dislocation motion.

(2) The dislocation velocity was very

sensitive to the applied stress.

(3) At a given stress the edge components moved faster than the screw components.

The stress and temperature dependence of the dislocation velocity (v) from 25°C to -50°C is given by :

$$v \propto \sigma^m e^{-E/kT} \quad \ldots\ldots\ldots \quad (6.11)$$

where E ~ 0.7 e.v.

σ - applied stress.

m - a constant for a given crystal, but varies from 15 - 25 for crystals of different hardness.

The multiplication of a glide dislocation, as it moved through the crystal, was a function of the applied stress and the dislocation velocity. A glide band formed which widened as deformation proceeded. The dislocation density in the glide band reached a saturation value which was not exceeded until the specimen was covered by glide bands.

A mechanism for dislocation multiplication was proposed, involving the formation of jogs on screw dislocations by cross glide. The smaller jogs move with the dislocation leaving behind point defects. Jogs of intermediate size (3 - 300 b) are immobile and remained connected to the moving dislocation by pairs of closely spaced dislocations. These pairs

require an appreciable stress to by pass one another and form new loops. The multiplication rate increases with stress because more pairs can be separated at higher stresses. With very large jogs multiplication follows continuously from cross glide.

The average dislocation density increased linearly with the plastic strain. It was suggested that the strain hardening is caused by the defects that are left behind by the expanding dislocation loops. The number of such defects is proportional to the area swept out by the moving loops and therefore to the plastic strain.

The yield stress of lithium fluoride was influenced by :

(1) Impurities,

or (2) Clusters of vacancies, which provide resistance to dislocation motion.

The yield stress was not influenced at all by the number or distribution of the grown-in dislocations, which were not observed to move during the deformation.

The macroscopic plastic properties of lithium fluoride were also determined by bending tests at a constant strain rate in a hard machine. The nature of the deformation depended on the surface condition of the specimen. The two limiting cases were :

(1) Specimens with a polished surface gave a large yield point.

(2) Specimens with surfaces containing large numbers of defects and dislocations yielded at a lower stress and gave only a small or no yield point.

It was suggested that the yield point is a function of the number and velocity of the dislocations. The applied strain rate ($\dot{\varepsilon}$) is given by :

$$\dot{\varepsilon} = b \rho \bar{v} \qquad \ldots\ldots\ldots \qquad (6.12)$$

ρ - dislocation density.

$\bar{v}$ - average dislocation velocity.

b - Burgers vector.

As dislocation multiplication occurs, the dislocation velocity required to maintain the applied strain rate decreases. The stress for dislocation motion is a function of the dislocation velocity. Hence the decrease in stress is accompanied by a decrease in stress, giving a yield point. As the change in velocity governs the size of the yield point, a specimen with a high initial dislocation density gives only a small yield point.

Stress strain curves were calculated from the observed dependence of dislocation velocity on stress and of dislocation density on strain. These were

found to differ from the observed curves by an amount attributable to work-hardening.

The importance of the lithium fluoride work is in showing that the deformation characteristics of crystals of high perfection can be understood simply in terms of the number and velocity of dislocations.

II. EXPERIMENTAL METHOD.

7. Specimen preparation.

7.1 Growth of germanium single crystals.

Germanium single crystals were supplied by the Royal Radar Establishment. The crystals were grown by the Czochralski technique; i.e. by the steady withdrawal of a seed from a crucible of molten germanium. The orientation of the seed was such that the growth axis of the crystal was along the direction at the centre of the unit stereographic triangle. (This enabled a maximum number of specimens oriented for single slip to be prepared from a single crystal). An argon atmosphere was used to minimise oxygen contamination. The usual dimensions of the crystals were :

length ~ 5 cm.

diameter ~ 2 - 3 cm.

Three types of germanium single crystal were supplied, as follows :

(1) 50 Ω -cm, intrinsic.

(2) 5 Ω -cm, doped with indium.

(3) 0.05 Ω -cm, doped with gallium.

Knowing the resistivity of germanium, an evaluation of the electrically active impurity concentration can be made. The approximate correlation is as follows:

50 Ω cm $< 10^{14}$ atoms/cc impurity.

5 Ω cm $\sim 10^{15}$ " "

0.05 Ω cm $\sim 10^{17}$ " "

The first crystals supplied had a grown-in dislocation density of $1 \times 10^{3} cm^{-2}$. An improvement in the growth technique reduced the grown-in dislocation density of later crystals to $5 \times 10^{2} cm^{-2}$.

7.2 Preparation of specimens from single crystals.

The following procedure was employed to prepare tensile specimens, oriented for single slip, from the single crystals. Great care was needed at all stages of the preparation, due to the brittle nature of germanium at room temperature.

(1) A back reflection Laue X-ray of the crystal was taken. From the X-ray, a stereogram was plotted to check that the growth axis of the crystal was oriented along the direction at the centre of the unit stereographic triangle.

(2) The crystal was cut, with a diamond coated slitting wheel, into 3 mm. wide slices parallel to the growth axis, i.e. the length of each slice was approximately oriented along the direction at the centre of the unit stereographic triangle.

(3) A back reflection Laue X-ray of each slice, mounted on an aluminium pad, was taken, the stereo-

gram plotted and the orientation of the slice accurately determined. The aluminium pad was then attached (in an equivalent position to that on the specimen holder) to the table of a wire saw, which could be adjusted in a horizontal and vertical plane relative to the cutting wire. The table was suitably adjusted and a rectangular section (26 mm x 10 mm x 3 mm) cut from the slice, with the length oriented accurately along the direction at the centre of the unit stereographic triangle.

[The details of the wire saw, shown in Fig. 5, are as follows :

A continuous length of 0.005" tungsten wire is wound around a grooved drum (A) with a single strand of wire near the centre of the drum passing over the two pulleys (B). The wheel is driven by a motor, which is reversed by a switch about every 10 seconds. The crystal (D) is mounted on the adjustable table (E) and can be cut along most crystallographic planes by suitable adjustment. Carborundum abrasive is fed to the wire to cut through the crystal, the speed of cutting being controlled by the position of the weight (M) along the pivoted rod (F).]

(4) The 3 mm dimension of the rectangular section was reduced by hand grinding until the section just fitted into a slit of width 2.7 mm, in a simple

jig. The jig consists of a stainless steel plate with a slit along its centre. The plate, which is supported by two bearings mounted on a steel base, can be rotated through 360° and locked in any position.

The section was secured in the slit with resinous wax, with its two long edges parallel to the length of the plate. The jig was mounted on the magnetic base of a grinding machine, with the section normal to the $\frac{1}{2}$" diamond coated wheel. The plate was locked in the horizontal plane and a portion removed from near one end of the specimen, forming a shoulder. Then the plate was rotated through 180°, locked, and a shoulder formed in an equivalent position on the other side of the section. This procedure was repeated to form two shoulders at the other end of the section. Hence we obtained an I shaped specimen. The usual dimensions of the specimen were :

Total length - 4.0 cm.

Gauge length (distance between shoulder - 2.5 cm.

Cross sectional area - 5 - 8 sq.mm.

The above procedure gave very uniform shoulders, which were square to within 0.001".

(5) The specimen was cleaned in toluene and then hand ground with successively finer

carborundum powders to give a smooth surface. Particular attention was paid to the corners of the shoulders, these were carefully radiused with carborundum powder carried on a fine silica rod.

(6) A back reflection X-ray was taken, the stereogram plotted, and the orientation of the tension axis of the specimen accurately determined. Most of the specimens had orientations within 2^{o} of the direction at the centre of the unit stereographic triangle.

(7) The ground specimen was chemically polished for 2 minutes in CP4 solution (30 c.c. HNO_3, 15 c.c. HF, 15 c.c. CH_3COOH, 0.5 c.c. Br_2), which produced a bright, smooth surface.

7.3 Resistivity measurements.

The resistivity of the tensile specimens, in the ground condition, was determined using the 4 probe technique[76]. The principle of the method is shown in Fig. 6.

Four colinear point contacts (P) are made on a flat surface (S). The voltage (V) developed between the two inner contacts is measured when a current (I) is passed through the sample via the outer contacts. It can be shown that for a semi-infinite sample :

$$V = \frac{I\rho}{2\Pi}\left(\frac{1}{W} + \frac{1}{X} - \frac{1}{W+X} - \frac{1}{X+Y}\right) \quad \ldots\ldots \quad (7.1)$$

where ρ is the resistivity of the sample. With uniform spacing $W = X = Y = Z$ this reduces to :

$$V = \frac{I\rho}{2\pi Z} \qquad \ldots\ldots\ldots \qquad (7.2)$$

The probe head used consists of four equally spaced steel needles, with each needle individually sprung to accommodate any surface irregularities.

The voltage between the inner probes was measured by means of a potentiometer, using a null deflection method. A current (I), variable up to 1 m A, was passed to the outer probes. This produced a current (I_1) between the two inner probes, the magnitude of which could be varied up to 1 m A by varying a series resistor. The potentiometer galvanometer deflection was reduced to zero by adjusting a series of standard resistors to obtain the balancing resistance R. The ratio of I_1/I was adjusted so as to give a large balancing resistance.

The balancing voltage $V = I_1 R$ .... (7.3)

Hence resistivity $\rho = \frac{V}{I} \cdot 2\pi Z$ ... (7.4)

The resistivity was measured at various positions along the specimen to determine the reproducibility. The variation along a specimen was usually $< 10\%$.

7.4 Dislocation density measurements.

The dislocation density of a section from each crystal was determined by microscopic etch pit counts

on 111 planes. A back reflection Laue X-ray of the crystal was taken, and the crystal was sectioned on a 111 plane, using the adjustable wire saw. The cut surface was then ground and etched with CP4 solution.

8 The tensile machine.

8.1 The general arrangement.

The hard beam tensile machine was designed by Dr. R.L.Bell and constructed at the Royal Radar Establishment. The basic arrangement of the machine is shown in Fig. 7.

The machine is mounted on a solid base (A), which is carried on three adjustable supports (B). Three columns constitute the external frame members (C). Two rods (D) pass from the cross head (2), through plates (3) and (4) to the bottom plate (5). Plates (3) and (4) are coupled together by two sleeves (F). The three innermost rods (G) pass from plate 6 to the bottom plate 5.

The central pull rod (H) is in two sections. The top section is secured at one end to the 200 lb. beam (10" x 1" x 0.347") mounted on plate 4, and at the other end to the top of the tensile specimen. The bottom section is secured at one end to the tensile specimen, and the other end has a ball which mates with a spherical socket in the bottom plate.

A 6" diameter furnace (I) is symmetrically placed around the pull rod. The counter weight (J) is secured by three tension wires to the top of the furnace.

The lead screw (K) (20 t.p.i. x 3/4" diameter) is secured to plates (1) and (3) and passes through a threaded hole in the cross head. Back lash in the lead screw is prevented by 3 tension wires (E), which are loaded by weights situated in the columns (C). The circular rod (L), supported by two bearings (M), has a central worm which connects with the lead screw (K) through a toothed wheel. This rod (L) can be rotated by hand or connected via a flexible coupling and connecting rod to a motor.

Particular features of the machine are as follows :

(a) Furnace.

A schematic arrangement of the furnace is shown in Fig. 8.

The pull rod (H) is centrally positioned within a 1" diameter quartz tube (F), which is threaded (10 t.p.i.) and wound with 20 S.W.G. Kanthal wire (total resistance = 10Ω). The top and middle thirds of the winding are shunted with resistances to obtain a uniform temperature gradient. A fixed resistance (3Ω), selected by trial experiments, is placed across

the middle third of the winding. The top third of the winding is shunted with a variable resistance which enables small adjustments to be made during the experiments. The quartz tube is secured to the top plate of the furnace by a molybdenum flange and hangs free in the furnace. Cooling water (U) from a constant head tank passes around the outside of the furnace, and is also circulated through the top and bottom plates of the furnace and a small spiral around the pull rod.

The temperature of the furnace is determined by two thermocouples (R) secured to the top and bottom of the specimen. Argon gas, to prevent oxidation of the specimen, is introduced into the furnace through a hole (T) in the base plate. A small positive pressure is maintained to counterbalance gas leakage from the furnace.

Great care was taken in the early experiments to ensure a constant voltage across the furnace winding. The furnace current was drawn from six 12 volt accumulators, which were constantly charged at a current just less than the discharge current. This system gave only a small variation of voltage with time. Later tests were generally performed at a faster strain rate. For these tests it was found that the a.c. mains supply, stabilised with a voltage regulator, gave an adequately stable voltage. The furnace input was controlled by a variac and a series rheostat.

(b) The extension of the specimen

Rotation of the rod (L) causes a rotation of the worm, which connects through a toothed wheel to the lead screw (K). A clockwise rotation of the lead screw moves the cross head (2) and the bottom plate (5) downwards, while the plates 3 and 4 remain fixed in position. The result is that the specimen extends and the beam deflects to accommodate the movement. The deflection of the beam was calibrated in terms of the applied load by a dead loading technique (See Section 9.1). Hence measurements of the deflection of the beam enable the loads on the specimen to be determined.

The rotation of the lead screw is measured by a carriage calibrated in 360 divisions (One complete rotation of the lead screw gives a vertical movement of $^{1}/_{20}$")

(c) The measurement of the beam deflection

The details of the deflection measurement are shown in Fig.9. A hardened steel rhomb is enclosed by a plate (W) attached to the pull rod and a semicircular section (X) attached to plate 4. The semicircular section is carried on a copper-beryllium support, the position of which can be varied by an adjuster (Y). As the beam is deflected, W moves past X causing a rotation of the rhomb. A mirror, forming part of an

optical lever system, is fixed to the end of the rhomb and its rotation causes a deflection of a light spot on a graduated scale. The optical lever system, which gives a magnified beam deflection of about 400 : 1, is shown in Fig. 10.

(d) Straining mechanism.

The rod (L) is connected, via a flexible coupling and connecting rod, to the output shaft of a motor driven gear box. The speed of the motor is maintained constant with time by a servo control mechanism. Five motor speed settings are available from 400 r.p.m. to 5300 r.p.m. The motor can be run in a clockwise or anti-clockwise direction.

The schematic arrangement of the gear box is as follows :

Motor — 1 : 2 — A) 1 : 5 – 1 : 100 / B) 1 : 1 – 1 : 100 / C) — 1 : 100 — 20 t.p.i. lead screw.

Using different gear trains and motor speed settings, the rate of motion of the cross head can be varied from 2.4×10^{-4} "/min to 1.6"/min. The details are as follows : -

Motor Setting		1	2	3	4	5
Cross head motion ("/min)	Gear train					
	A	2.4×10^{-4}	6.9×10^{-4}	1.2×10^{-3}	2.8×10^{-3}	3.2×10^{-3}
	B	1.2×10^{-3}	3.4×10^{-3}	5.9×10^{-3}	1.4×10^{-2}	1.6×10^{-2}
	C	1.2×10^{-1}	3.4×10^{-1}	5.9×10^{-1}	1.4	1.6

9. Experimental techniques.

9.1 Calibration of apparatus.

The magnified deflection of the beam for a given load, was determined by dead loading of the pull rod. The load was increased in increments of ~ 4.7 kg. up to a maximum of about 42 kg. The maximum load gave a deflection of about 33 cm. The deflection of the beam was directly proportional to the applied load (Fig.11). A very small hysteresis loop was observed on unloading.

The deformation of a "dummy" molybdenum specimen, at a constant strain rate, showed that the elastic deflection increased linearly with the extension of the specimen.

9.2 Securing the specimen in the tensile machine.

Great care has to be taken in securing the specimen to the pull rod, due to the brittle nature of

germanium at room temperature. The arrangement employed is shown in Fig.12. Two split molybdenum chucks are used to secure the specimen to the two sections of the pull rod. Each chuck has two recesses, one to receive the specimen shoulder and the other the flange at the end of the pull rod. The halves of each chuck are secured together with molybdenum wire. Small holes in the chucks allow the thermocouples to make contact with the surface of the specimen.

9.3 Experimental procedure.

The cross sectional area of the specimen was measured with a micrometer, the variation of the cross sectional area along the gauge length (distance between shoulders) also being determined. The gauge length was measured with a ruler (which gave sufficient accuracy).

Then the specimen was secured to the pull rod and the thermocouples placed in position. The position of the specimen in the furnace was adjusted until the ball of the bottom section of the pull rod was nearly touching the socket in the bottom plate. This ensured that correct alignment was maintained when the load was applied.

Argon was passed into the furnace for 30 minutes to completely expel all the air. Cooling

water was also allowed to circulate during this period.

Then the furnace current was increased gradually until the required temperature was attained. The temperatures at the top and bottom of the specimen were measured. The temperature gradient along the specimen was minimised by adjustment of the top shunt to about $1^{\circ}C$, after which the furnace was allowed to equilibriate for 15 minutes.

The specimen was then strained at the selected strain rate. The deflection of the light spot on the graduated scale was noted for each 5 or 10 divisions of the calibrated carriage. Temperature measurements were made before, during and after the test to check the uniformity of the conditions.

After the test, the specimen was unloaded by hand and the furnace current switched off, the specimen cooling at about $70^{\circ}C$/minute to room temperature. The surface of the specimen remained bright during the test and the nature and distribution of the slip lines could be examined.

From the results a graph of beam deflection (load) versus carriage position (extension) was plotted. Reference to the calibration graph of beam deflection versus load enabled the load (P) at any point on the graph to be determined. Hence knowing the cross

sectional area (A), the tensile stress (σ_t) at any point could be determined :

$$\sigma_t = \frac{P}{A} \qquad \ldots\ldots\ldots \qquad (9.1)$$

The resolved shear stress[77] is given by :

$$\sigma = \frac{P}{A} \sin \chi \cos \lambda . \qquad \ldots\ldots \qquad (9.2)$$

χ - angle between slip plane and tension axis.

λ - angle between slip direction and tension axis.

These angles could be obtained from the stereogram of the specimen and the resolved shear stress calculated.

The plastic elongation at any point was determined by counting the number of divisions from the elastic region to the point. The number of divisions (d) could be converted into the plastic specimen extension from :

$$e = d \,/\, 7200" \qquad \ldots\ldots\ldots \qquad (9.3)$$

Knowing the gauge length (L) the tensile strain (ε_t) was determined from :

$$\varepsilon_t = \frac{e}{L} \qquad \ldots\ldots\ldots \qquad (9.4)$$

The glide strain (ε) is given by :

$$\varepsilon = \frac{1}{\sin \chi_o} \left(\sqrt{d^2 - \sin^2 \lambda_o} - \cos \lambda_o \right) \ldots\ldots \qquad (9.5)$$

χ

where $D = \frac{L + e}{L}$

χ_o - initial angle between slip plane and tension axis.

λ_o - initial angle between slip direction and tension axis.

The angles could be obtained from the stereogram of the specimen and the glide strain calculated.

9.4 Dislocation density measurements

The dislocation density of a specimen was determined by microscopic etch pit counts on a 111 plane intersecting the primary slip plane. The dislocation density at various stages of deformation was determined by stopping the straining, unloading and sectioning specimens across the gauge length. At least two specimens were sectioned at each stage of the deformation.

9.5 Annealing treatment.

Deformed specimens were sealed in an evacuated quartz tube, to avoid contamination and heated in a resistance furnace. The annealing temperature was regulated to $\pm$ 5°C by a controller. A recorder was used to provide a check of the temperature conditions during long time treatments. The specimens were heated slowly to the annealing temperature and furnace cooled (5°C/min) after the anneal. The surface

of the specimen was not affected by the annealing and remained bright.

III. EXPERIMENTAL RESULTS.

10. Introduction.

The terminology used in the results section is defined as follows :

The term yield point represents the fall in stress from the upper yield point to the lower yield point.

The term elastic limit represents the point on the deflection (load) - carriage position (extension) graph at which the extension ceases to be linear.

The post yield flow stress represents the flow stress in the easy glide region after the lower yield point.

The relaxed stress represents the stress to which the machine relaxes on stopping the straining.

The experimental results are divided into four sections, as follows :

(11) The yield point phenomenon.

In this section there is a description of the yield point observed on first loading, the effects of unloading and reloading after the lower yield point, and the conditions necessary to effect a return of the yield point. The effects of other factors on the yield point such as initial dislocation density, impurity

strain rate, temperature, orientation, surface and rate of cooling, are also described.

(12) The post yield flow stress.

This section contains an account of the effects of dislocation density, strain rate and temperature on the post yield flow stress. The relaxed stress effects are also described.

(13) Work hardening in germanium.

The preliminary observations made on stage II work-hardening are given in this section.

(14) Experimental errors.

The final section contains an assessment of the various experimental errors.

11. The yield point phenomenon.

11.1 The yield point on first loading.

(a) The stress-strain curve.

Tensile specimens, oriented to a direction at the centre of the unit stereographic triangle, were prepared from three types of germanium single crystals:

(1) 50 Ω-cm intrinsic germanium (with an electrically active impurity concentration of $< 10^{14}$ atoms/cc.)

(2) 5 Ω-cm indium doped germanium (with an electrically active impurity concentration of approximately 10^{15} atoms/cc.)

(3) 0.05 Ω-cm gallium doped germanium (with an electrically active impurity concentration of approximately 10^{17} atoms/cc.)

The specimens were strained in tension at a constant rate of $1 \times 10^{-4} sec^{-1}$ at 560°C. Deformation was characterised by a pronounced yield point, the stress falling by approximately 40% from the upper to the lower yield point. A typical graph of the yield point is shown in Figs. 13a and 13b.

The main features of deformation observed in 13 tensile tests were :

(1) The resolved shear stress at the elastic limit varied from 1.1 to 2.0 kg/mm^2.

(2) The upper yield point occurred after approximately 0.2% glide strain. The resolved shear stress at the upper yield point varied from 1.2 to 2.15 kg/mm^2.

(3) The stress decreased from the upper yield point at a rate ($d\sigma/d\varepsilon$) of ~400 gms/mm^2 until about 1% glide strain, and then more slowly ($d\sigma/d\varepsilon$ ~ 200 gms/mm^2) to the lower yield point. (The maximum relaxation rate of the machine was about 650 gms/mm^2).

(4) The lower yield point occurred after approximately $2\frac{1}{2}$% glide strain. The resolved shear

stress at the lower yield point varied between 0.95 - 1.10 kg/mm^2.

(5) Easy glide continued at the lower yield point stress until 4 - 8% glide strain.

The large variations in the elastic limit and upper yield stress are probably due to their sensitivity to any small changes in experimental conditions. In contrast, the reproducibility of the lower yield stress suggests that it is a more fundamental property of the material.

The effects of added impurity on the upper and lower yield stresses are shown in Table 3. We found that the three types of crystal tested gave similar yield points. The variation in the upper yield stress between specimens of different resistivity was no greater than the variation between different specimens of the same resistivity. The lower yield stress was very reproducible for all three types of crystal. We conclude that the addition of small amounts of gallium or indium to germanium does not affect the initial yield point.

(b) Observations of slip lines and dislocation density during the tensile test.

The first slip lines were observed between the elastic limit and the upper yield point. (These initial

slip lines completely traversed the specimen, making it impossible to decide by direct observation whether surface or internal sources were the operative ones). At the upper yield point about 5% of the surface area, usually near the shoulder of the specimen, was covered with slip lines. As deformation proceeded, one or more Luders bands (See Fig.14) spread through the specimen. After about 1% glide strain the surface was completely covered with slip lines. The number of slip lines further increased until the lower yield point and then remained constant during the easy glide region.

Slip occurred mainly on one {111} system, at an angle of approximately 45° to the tension axis, during the yield point and easy glide region. Some localised secondary slip (at ~ 80° to the tension axis) was also observed near the shoulders in about 40% of the specimen. This localised secondary slip did not significantly affect the nature of the easy glide region.

The dislocation density of the undeformed specimen was about $1 \times 10^{3} cm^{-2}$, with the dislocations (as revealed by etch pits) in a random arrangement. At the upper yield point, the dislocation density in the slipped region was about $1 \times 10^{6} cm^{-2}$, with the dislocations situated along slip lines. After 1%

TABLE 3

Temperature - 560°C

Strain rate - $1 \times 10^{-4} sec^{-1}$

Crystal	Specimen number	Resolved shear stress at U.Y.P. (kg/mm^2)	Resolved shear stress at L.Y.P. (kg/mm^2)
P.H. 90 (50 Ω cm)	2	1.70	1.05
	3	1.60	1.10
	4	1.55	1.10
H.C. 11 (50 Ω cm)	1	1.20	0.95
	2	1.90	1.05
	4	2.15	1.05
	5	2.00	1.10
	7	1.90	1.00
H.C. 12 (50 Ω cm)	1	1.35	1.05
P.H. 91 (0.05 Ω cm)	4	1.20	1.00
	5	1.40	1.05
H.C. 33 (5 Ω cm)	1	1.65	1.10
	6	2.05	1.10

glide strain, when the specimen was completely covered with slip lines, the overall dislocation density was about $3 \times 10^6 cm^{-2}$. The dislocation density increased to about $7 \times 10^6 cm^{-2}$ (See Fig.15) at the lower yield point and then remained constant during the easy glide region.

11.2 Unloading and reloading effects.

Interrupting the straining during the easy glide region caused the stress to decrease exponentially with time from the post yield flow stress. After 5 minutes the stress had relaxed to about 60% of the post yield flow stress. (The effect is discussed in more detail in Section 12.4).

On reloading the specimen from the relaxed stress, the stress increased to the post yield flow stress before deformation continued. If the specimen was completely unloaded and then reloaded, deformation again continued at the post yield flow stress. We conclude that the effect of unloading and reloading is completely reversible.

Unloading and reloading the specimen in the elastic region did not affect the nature of the yield point.

11.3 The return of the yield point.

(a) The effect of annealing.

The deformed specimens were unloaded in the easy glide region after the lower yield point. They were then annealed in vacuum at various temperatures, furnace cooled to room temperature and retested at 560°C. The effects of annealing on the post yield flow stress are shown in Tables 4 and 5 and Fig.16.

It was found that :

(1) Annealing the deformed specimens at 600°C for 70 hours had no effect on the post yield flow stress on retesting at 560°C.

(2) Annealing the deformed specimens at temperatures higher than 600°C, produced a reduction in the post yield flow stress on retesting at 560°C. The reduction in the post yield flow stress increased as the annealing temperature was raised; the maximum reduction (of about 30%) being obtained after an anneal of 800°C for 70 hours.

There was no immediate work hardening on retesting the annealed specimens. Easy glide continued at the reduced value of stress for 2 - 5% glide strain.

(3) Annealing the deformed specimens at 900°C for 70 hours, produced a yield point on retesting at 560°C. The size of the yield point increased with the

TABLE 4

Post yield flow stress (kg/mm^2)	Annealing treatment	Flow stress after annealing (kg/mm^2)
1.05	70 hrs. at 600°C	1.05
1.05	70 hrs. at 700°C	0.85 - 0.95
1.05	70 hrs. at 800 - 850°C	0.70 - 0.75

TABLE 5

Annealing treatment	Resolved shear stress at U.Y.P. (kg/mm^2)	Resolved shear stress at L.Y.P. (kg/mm^2)
70 hrs. at 900°C	0.78 - 0.84	0.70 - 0.75
236 hrs. at 900°C	0.80 - 0.88	0.72 - 0.76

time of anneal. After an anneal at 900°C for 236 hours, the maximum yield drop on retesting at 560°C, was approximately 20% of the upper yield stress. A typical graph at the regained yield point is shown in Fig.16.

The features of the regained yield point were similar to those observed during the initial yield point :

(1) The stress decreased from the upper yield point at a "fast" rate until about 0.5% glide strain. The stress then decreased more slowly to the lower yield point (1% glide strain).

(2) Easy glide continued at the lower yield stress for 2 - 5% glide strain.

The resolved shear stresses at the upper and lower yield points of the regained yield point were lower than those in the initial yield point. (See Table 5).

(b) <u>The variation of the dislocation density during annealing and subsequent retesting.</u>

The dislocation density of the deformed specimens (See Fig.15) was about $7 \times 10^6 cm^{-2}$. The effects of annealing on the dislocation density of the specimens were :

(1) Annealing the deformed specimens at 600°C

did not affect the dislocation density.

(2) Annealing the deformed specimens at temperatures above 600 °C, caused a reduction in dislocation density. An anneal of 70 hours at 800°C reduced the dislocation density to 5 x $10^5 cm^{-2}$. (See Fig.17). The distribution of etch pits was more random, with only a few straight lines of etch pits along slip lines. Anneals at 900°C for 70 and 236 hours reduced the average dislocation density to 1 x 10^5 and 9 x $10^4 cm^{-2}$ (See Fig.18), respectively; the distribution of etch pits being completely random.

The effects of retesting at 560°C on the dislocation densities of the annealed specimens were :

(1) For specimens annealed at 600 - 850°C, easy glide continued and the dislocation density remained constant.

(2) For specimens annealed at 900°C, the dislocation density increased during the regained yield point to about 6 x $10^5 cm^{-2}$ at the lower yield point. The dislocation density then remained constant during the easy glide region.

When the annealing treatment was sufficient to reduce the dislocation density to about 1 x $10^5 cm^{-2}$, a yield point was regained. As the dislocation density was further reduced, the size of the regained yield

point increased. Therefore it seems probable that the regained yield point is a function of the dislocation density of the specimen.

The upper and lower yield stresses of the regained yield point were lower than those of the initial yield point. However the dislocation density in the undeformed state ($1 \times 10^{3} cm^{-2}$) was lower than the minimum density obtained by annealing ($9 \times 10^{4} cm^{-2}$). As the dislocation density of the annealed specimen was reduced to this minimum value, the upper and lower yield stresses tended to increase. It seems likely that, if the dislocation density of the annealed specimen could be reduced to the same level as in the undeformed state, the upper and lower yield stresses would be comparable.

This was confirmed by testing an undeformed specimen, with a dislocation density similar to that of the annealed specimens. The specimen was prepared from a section of crystal with a higher than usual dislocation density ($\sim 3 \times 10^{4} cm$). The deformation characteristics of this specimen were similar to those of the annealed specimens. The result is shown in Table 6.

Annealing the undeformed specimens at high temperatures did not affect the yield point observed

TABLE 6

Temperature -560°C Strain rate - 1 x 10^{-4} sec^{-1}

Crystal	Specimen number	Dislocation density (cm^{-2})	Resolved shear stress at U.Y.P. (kg/mm^2)	Resolved shear stress at L.Y.P. (kg/mm^2)
P H 90 (50Ω cm)	5	3 x 10^4	0.90	0.70

TABLE 7

Temperature - 560°C Strain rate - 1 x 10^4 sec^{-1}

Crystal	Specimen number	Preliminary annealing treatment	Resolved shear stress at U.Y.P. (kg/mm^2)	Resolved shear stress at L.Y.P. (kg/mm^2)
H C 12 (50 Ω cm)	2	70 hrs at 800°C	1.80	1.10
	3	1 hr at 700°C	1.50	1.00
H C 33 (5 Ω cm)	3	70 hrs at 800°C	1.50	1.10
-Indium doped	5	1 hr at 700°C	2.10	1.05
	7	70 hrs at 900°C	2.50	1.10

on first loading. The undeformed specimens were annealed in vacuum at various temperatures, furnace cooled to room temperature and tested at 560°C. It was found that the upper and lower yield stresses were similar to those obtained with specimens which had not been annealed. The results are shown in Table 7.

The annealing did not reduce the dislocation density of the undeformed specimens, which remained at ~ 1 x $10^3 cm^{-2}$.

(c) The effect of added impurity on the annealing of the deformed specimens.

The effects of increasing the impurity levels in deformed and annealed specimens were determined. The specimens were deliberately contaminated with elements known to have a high diffusion coefficient in germanium.

(1) The effect of nickel.

(a) A deformed specimen, with a dislocation density of 7 x $10^6 cm^{-2}$, was completely nickel plated and annealed at 700°C. for 1 hour. This treatment was sufficient for the nickel to diffuse into the specimen, but not to significantly affect the dislocation density. The specimen was then furnace cooled and the surfaces ground and chemically polished. On retesting the specimen at 560°C, the results were :

(1) No yield point was observed.

(2) The post yield flow stress (1.05 kg/mm^2) was not altered.

(b) The deformed specimen was again nickel plated and then annealed at 800°C for 70 hours. This treatment enabled the nickel to diffuse into the specimen and also reduced the dislocation density. Again the specimen was furnace cooled, ground and chemically polished. On retesting the specimen at 560°C, the results were :

(1) No yield point was observed.

(2) The post yield flow stress was reduced to 0.9 kg/mm^2. This value of flow stress was higher than that observed for nickel-free specimens similarly annealed and tested (0.70 - 0.75 kg/mm^2). The increase in flow stress may be due to solid solution hardening of the lattice by the nickel.

(2) <u>The effect of interstitial gas atoms</u>

Similar experiments, under the same temperature and time conditions, were performed annealing the specimen in :

(a) air,

(b) forming gas (Nitrogen + 10% hydrogen).

In all cases, no yield point was observed on retesting and the post yield flow stress was unchanged.

We conclude that increasing the impurity level in the germanium does not effect a return of the yield point on retesting. Even under annealing conditions, when both the impurity atoms and the dislocations are mobile, no effective locking of dislocations occurs.

11.4 Other factors influencing the yield point phenomenon.

(a) The dislocation density of the undeformed specimen.

We have shown previously that a higher dislocation density in the undeformed specimen resulted in lower values of the upper and lower yield stresses on testing. It was also found that a reduction in the initial dislocation density raised the upper and lower yield stresses on testing. Specimens of dislocation density $5 \times 10^{2} cm^{-2}$ tested at $560^{\circ}C$, at a strain rate of $1 \times 10^{-4} sec^{-1}$ failed by brittle fracture before any appreciable plastic flow occurred. The resolved shear stress at fracture varied between 2.2 - 2.4 kg/mm^{2}. The details are shown in Table 8.

To avoid brittle fracture the specimens had to be deformed at a higher testing temperature. On deformation at $620^{\circ}C$, at a strain rate of $1 \times 10^{-4} sec^{-1}$, a yield point was observed. A typical yield point is shown in Fig.19. The main features of the yield point observed in 8 tensile tests were :

TABLE 8

Temperature 560°C. Strain rate 1 x 10^{-4} sec^{-1}

Crystal	Specimen number	Resolved shear stress at fracture (kg/mm^2)
H C 101 (50 Ω cm)	1	2.4
	2	2.3
H C 102 (50 Ω cm)	1	2.2

TABLE 9

Temperature 620°C. Strain rate 1 x 10^{-4} sec^{-1}

Crystal	Specimen number	Resolved shear stress at U.Y.P. (kg/mm^2)	Resolved shear stress at L.Y.P. (kg/mm^2)
H C 101 (50Ω cm)	7	1.05	0.88
	9	1.22	0.96
H C 102 (50Ω cm)	4	1.07	0.92
	5	1.10	0.94
	6	1.08	0.94
	7	1.10	0.90
	8	1.28	0.96
	9	1.24	0.91

TABLE 10

Post yield flow stress (kg/mm^2)	Annealing treatment	Dislocation density after anneal (cm^{-2})	Post yield flow stress after anneal (kg/mm^2)
0.92	70 hrs at 700°C	-	0.8
0.92-0.94	70 hrs at 800°C	1 x 10^6	0.73 - 0.78
			Resolved stress at U.Y.P. / Resolved stress at L.Y.P
0.92	100 hrs at 900°C		0.72 / 0.69

(1) The resolved shear stress at the elastic limit varied between 1.0 - 1.1 kg/mm^2.

(2) The upper yield point occurred after about 0.2% glide strain. The resolved shear stress at the upper yield point varied from 1.1 to 1.2 kg/mm^2.

(3) The stress decreased at a "fast" rate from the upper yield point to about 0.5 % glide strain, and then more slowly to the lower yield point.

(4) The lower yield point occurred after about 1% glide strain. The resolved shear stress at the lower yield point varied from 0.88 - 0.95 kg/mm^2.

(5) Easy glide continued at the lower yield point stress until 3 - 6% glide strain.

Details of the upper and lower yield stresses obtained are shown in Table 9.

Deformation occurred in a similar manner to that described previously for specimens with an initial density of $10^3 cm^{-2}$. (The specimens with an initial dislocation density of $10^3 cm^{-2}$ will be designated Type A specimens and those with an initial density of $5 \times 10^2 cm^{-2}$ will be designated Type B specimens). The deformation was heterogeneous, one or more Luders bands spreading throughout the specimen. The dislocation density at the lower yield point was $1 \times 10^7 cm^{-2}$ and remained constant during the easy glide region. This value of dislocation density was higher than the corresponding density observed in Type A crystals.

Type B specimens exhibited similar unloading and annealing effects to those of Type A specimens. The details of the results are shown in Table 10. We found that :

(1) Unloading in the easy glide region followed by immediate reloading did not affect the post yield flow stress.

(2) Annealing the deformed specimens at temperatures above 600°C, gave a reduced post yield flow stress on retesting at 620°C. There was no immediate work-hardening and easy glide continued at the reduced value of stress until 2 - 5% glide strain. The reduction in flow stress on retesting at 620°C increased as the annealing temperature was raised.

(3) The reduction in post yield flow stress was associated with a reduction in dislocation density. The dislocation density in the deformed condition was higher than in Type A specimens and this resulted in longer annealing times being required to reduce the dislocation density to a given value.

(4) Annealing the deformed specimen at 900°C gave sufficient reduction in dislocation density for a yield point to be regained on retesting at 620°C.

(b) Strain rate.

The yield point was found to depend sensitively on the applied strain rate; reducing the applied strain rate reduced the upper and lower yield point stresses.

(a) Type A specimens

A typical graph of the deformation of a Type A specimen at a strain rate of $2 \times 10^{-5} sec^{-1}$ at 560°C, is shown in Fig.20. The main features of the yield point observed in 4 tensile tests were :

(1) The resolved shear stress at the elastic limit varied from 0.67 - 0.80 kg/mm^2.

(2) The upper yield point occurred after 0.2% glide strain. The resolved shear stress at the upper yield point varied from 0.72 - 0.86 kg/mm^2.

(3) The stress decreased from the upper yield point at a "fast" rate to about 1% glide strain, and then more slowly to the lower yield point.

(4) The lower yield point occurred after about 2% glide strain. The resolved shear stress at the lower yield point varied from 0.53 - 0.63 kg/mm^2.

(5) Easy glide continued at the lower yield stress until 4 - 8% glide strain.

Details of the upper and lower yield point stresses are shown in Table 11.

In Table 12 and Fig.20 the results are compared with those obtained using a strain rate of $1 \times 10^{-4} sec^{-1}$. We found that reducing the strain rate by a factor of 5 :

(1) Reduced the resolved shear stresses at the upper and lower yield point by a factor of ~2.

(2) Did not significantly alter the % glide strain at the upper and lower yield points.

(b) Type B. specimens

Similar effects were observed with Type B specimens on varying the strain rate. The deformation characteristics of specimens deformed at 650°C at different strain rates are compared in Table 13 and Fig.21.

For Type B crystals, a reduction of 5 in applied strain rate :

(1) Reduced considerably the resolved shear stress at the upper and lower yield point.

(2) Did not significantly alter the % glide strain at the upper and lower yield point.

(c) Temperature.

The yield point was found to depend sensitively on the testing temperature; increasing the testing temperature reduced the upper and lower yield stresses.

The deformation characteristics of Type A specimens tested at the same strain rate, but at different temper-

TABLE 11

Crystal	Specimen number	Resolved shear stress at U.Y.P. (kg/mm^2)	Resolved shear stress at L.Y.P. (kg/mm^2)
pH 73 (0.05Ω cm)	1	0.83	0.55
pH 91 (0.05Ω cm)	2	0.72	0.53
-gallium doped	3	0.78	0.63
pH 74 (50 Ω cm)	2	0.86	0.54

TABLE 12

Temperature = 560°C

Strain rate	$2 \times 10^{-5} sec^{-1}$	$1 \times 10^{-4} sec^{-1}$
Resolved shear stress at elastic limit (kg/mm^2)	0.67 - 0.80	1.1 - 2.4
U.Y.P. - % glide strain	0.2	0.2
- resolved shear stress (kg/mm^2)	0.72 - 0.86	1.2 - 2.5
Inflexion - % glide strain	~ 1.0	~ 1.0
L.Y.P. - % glide strain	~ 2.0	~ 2.0
- resolved shear stress (kg/mm^2)	0.53 - 0.63	0.95 - 1.10

TABLE 13

Temperature = 650°C

Strain rate	2×10^{-5} sec^{-1}	1×10^{-4} sec^{-1}
Resolved shear stress at the elastic limit	0.57	0.93
U.Y.P. - % glide strain	~ 0.2	~ 0.2.
- resolved shear stress (kg/mm^2)	0.62	1.03
Inflexion - % glide strain	~ 0.5	~ 0.5
L.Y.P. - % glide strain	~ 1.0	~ 1.0
- resolved shear stress (kg/mm^2)	0.48	0.80

atures, are shown in Table 14.

The effects of increasing the testing temperature from 560°C to 650°C, at a constant strain rate were :

(1) To reduce the resolved shear stresses at the upper and lower yield points by a factor of about 2.

(2) To reduce the % glide strain at the upper and lower yield point.

The previous experiments on Type A specimens, enables a comparison between Type A and Type B specimens to be made at a given temperature (650°C).

The results are shown in Table 15 and Fig.22.

The Type B specimen (with the lower initial dislocation density) had higher upper and lower yield stresses. The higher upper yield stress suggests that the initial "grown in" dislocation density is important in the nucleation of yielding. The higher lower yield stress can be correlated with the larger dislocation density obtained on deformation of Type B specimens.

(d) Orientation.

The deformation characteristics were found to depend on the orientation of the specimen. The results were :

(1) Single slip orientations.

The results obtained on deformation of specimens oriented for single slip (i.e. the tension axis at the

TABLE 14

Type A Specimens

Strain rate = $1 \times 10^{-4} sec^{-1}$

Temperature	560°C	650°C
Resolved shear stress at elastic limit (kg/mm^2)	1.1 - 2.1	0.60
U.Y.P. - % glide strain	~ 0.2	~ 0.2
- resolved shear stress (kg/mm^2)	1.2 - 2.2	0.64
Inflexion - % glide strain	~ 1.0	~ 0.5
L.Y.P. - % glide strain	~ 2.0	~ 1.0
- resolved shear stress (kg/mm^2)	0.95 - 1.10	0.50

TABLE 15

Temperature 650°C

Strain rate $1 \times 10^{-4} sec^{-1}$

Crystal type	A	B
Dislocation density in the undeformed state (cm^{-2})	1×10^{3}	5×10^{2}
Resolved shear stress at elastic limit (kg/mm^{2})	0.60	0.93
U.Y.P. - % glide strain	~ 0.2	~ 0.2
- resolved shear stress (kg/mm^{2})	0.64	1.03
Inflexion - % glide strain	~ 0.5	~ 0.5
L.Y.P. - % glide strain	~ 1.0	~ 1.0
- resolved shear stress (kg/mm^{2})	0.50	0.80

centre of the unit stereographic triangle) have been described in detail. Deformation is characterised by a large yield point, followed by an easy glide region.

(2) Double slip orientations.

The deformation of a Type A specimen, oriented along a direction near the {111} - {100} boundary, produced marked multiple slip. Intersecting slip lines were observed at 36° and 38° to the tension axis. Some further slip lines at 78° to the tension axis were present near the shoulders of the specimen.

The specimen was deformed at $560^{\circ}C$ at a strain rate of $2 \times 10^{-5} sec^{-1}$. A graph of the deformation is shown in Fig.23. The deformation characteristics were:

(1) The resolved shear stress at the elastic limit was 0.80 kg/mm^2.

(2) The upper yield point occurred after 0.3% glide strain. The resolved shear stress at the upper yield point was 0.85 kg/mm^2.

(3) The stress decreased at a uniform rate from the upper to the lower yield point, no inflexion being observed.

(4) The lower yield point occurred after 1% glide strain. The resolved shear stress at the lower yield point was 0.78 kg/mm^2.

(5) There was no easy glide region, work-hardening

occurring after the lower yield point.

Comparing the results with those obtained on single slip specimens, we find :

(1) The size of the yield point was smaller. The upper yield stress was of the same order, but the lower yield stress was higher.

(2) The nature of the yield point was different:

(a) No inflexion was observed.

(b) The lower yield point occurred after a smaller % glide strain.

(3) No easy glide region was observed after the lower yield point.

(3) <u>< 111 > orientations.</u>

A Type A specimen of <111> orientation was deformed at 560°C, at a strain rate of $2 \times 10^{-5} sec^{-1}$. On yielding pronounced multiple slip was observed. A graph of the deformation is shown in Fig.23. The deformation characteristics were :

(1) No yield point was observed.

(2) The resolved shear stress at the elastic limit was 0.90 kg/mm^2. After the elastic limit, the specimen work-hardened rapidly until fracture at a resolved shear stress of 2.4 kg/mm^2 and 4% glide strain

(e) Surface.

The deformation characteristics were not sensitive to the surface condition of the specimen. Specimens with different surface conditions were tested, as follows:

(1) With a chemically polished surface.

(2) With an oxidised surface.

(3) With a specimen which had been ground, but not chemically polished. The grinding caused considerable surface damage and would be expected to increase the dislocation density at the surface of the specimens.

The deformation characteristics of the oxidised and ground specimens were similar to those of the chemically polished specimens, described previously.

We conclude that the effect of surface is not important in the deformation process

(f) The effect of the cooling rate from the annealing temperature.

The cooling rate from the annealing temperature was found to affect the deformation characteristics of the annealed specimens. The deformation characteristics of annealed specimens, which were furnace cooled ($5^{\circ}C$/min) to room temperature before retesting, have been previously described. Annealing a Type A deformed specimen at $850^{\circ}C$ for 70 hours, followed by furnace cooling to room temperature, gave the following results

on retesting at 560°C at 1 x 10^{-4} sec^{-1}:

(1) No yield point was observed.

(2) The post yield flow stress was reduced to 0.70 - 0.75 kg/mm^2.

Annealing a similar specimen under identical conditions, followed by air cooling to room temperature, gave the following results on retesting at 560°C at 1 x 10^{-4} sec^{-1} :

(1) A small yield point was observed. The resolved shear stress decreased from 0.80 kg/mm^2 at the upper yield point to 0.75 kg/mm^2 at the lower yield point. The lower yield point occurred after 0.8% glide strain. No inflexion in the stress-strain curve occurred between the upper and lower yield point.

(2) There was an absence of a yield point on unloading after the lower yield point followed by immediate reloading. Easy glide continued at the post yield flow stress of 0.75 kg/mm^2.

The effect of cooling rate was not investigated further. The yield point observed may be due to the locking of dislocations by point defects, formed by the rapid cooling from a high temperature.

12. The post yield flow stress.

The post yield flow stress is defined as the flow stress in the easy glide region after the lower

yield point. The effects of dislocation density, strain rate and temperature on the post yield flow stress were determined.

12.1 The effect of dislocation density.

The effects of dislocation density on the post yield flow stress have been previously described (see Section 11.3a,b). The post yield flow stress was very sensitive to the dislocation density of the specimen. For a Type A specimen reducing the dislocation density from $7 \times 10^{6} cm^{-2}$ to $5 \times 10^{5} cm^{-2}$ reduced the post yield flow stress from 1050 gms/mm^{2} to 700 gms/mm^{2}, on testing at 560°C at $1 \times 10^{-4} sec^{-1}$.

12.2 The effect of strain rate.

The variation of post yield flow stress with strain rate was determined in the easy glide region. The post yield flow stress was determined for a given strain rate and then for a second faster strain rate. Then the specimen was retested at the first strain rate to check that work-hardening (giving an increase in dislocation density) had not occurred. In this way the variation of post yield flow stress with strain rate was determined with a constant dislocation density specimen.

The strain rate was varied from $4 \times 10^{-6} sec^{-1}$ to $2 \times 10^{-3} sec^{-1}$ at a constant given temperature.

The variation was also determined at different constant temperatures. Specimens of different dislocation density were used :

(1) Type A specimens

(a) Deformed specimens ($\rho = 7 \times 10^6 cm^{-2}$)

(b) Annealed specimens ($\rho = 5 \times 10^5 cm^{-2}$)

(2) Type B specimens

(a) Deformed specimens ($\rho = 1 \times 10^7 cm^{-2}$)

(b) Annealed specimens ($\rho = 1 \times 10^6 cm^{-2}$)

The results are shown in Table 16. We found that :

(1) The post yield flow stress was sensitively dependent on the applied strain rate. An increase in the strain rate of 500 increased the post yield flow stress by a factor of about 2. A plot of the post yield flow stress against the logarithm of the strain rate gave a reasonable straight line (see Figs.24,25), except for some deviations at the highest strain rate. (It should be noted that this plot gave only a slightly better fit than a log. - log. plot (see Fig.26).

(2) At a constant temperature, the slope $d\sigma/d \log_e \dot{\varepsilon}$ was independent of the dislocation density of the specimen (Figs. 24,25).

(3) The slope $d\sigma/d \log_e \dot{\varepsilon}$ decreased as the testing temperature was increased. (Figs. 24,25).

TABLE 16

(a) Type A specimens

Temp. (°C)	Dislocation density (cm^{-2})	Flow stress at a given strain rate (sec^{-1})				
		4×10^{-6}	2×10^{-5}	1×10^{-4}	2.4×10^{-4}	2×10^{-3}
		kg/mm^2	kg/mm^2	kg/mm^2	kg/mm^2	kg/mm^2
560	7×10^6	-	0.73	1.00	1.20	F
560	5×10^5	-	0.58	0.75	0.90	1.20
620	5×10^5	0.37	0.48	0.60	0.73	1.00
670	5×10^5	0.32	0.41	0.54	0.62	0.86

F - fractured

(b) Type B specimens

Temp. (°C)	Dislocation density (cm^{-2})	Flow stress at a given strain rate (sec^{-1})				
		4×10^{-6}	2×10^{-5}	1×10^{-4}	2.4×10^{-4}	2×10^{-3}
		kg/mm^2	kg/mm^2	kg/mm^2	kg/mm^2	kg/mm^2
560	1×10^7	0.80	1.01	1.22	1.42	F
560	1×10^6	0.63	0.83	1.04	1.20	1.60
620	1×10^7	0.63	0.79	1.01	1.11	1.40
620	1×10^6	0.50	0.65	0.78	0.90	1.16
705	1×10^7	0.35	0.47	0.59	0.69	0.86
705	1×10^6	0.29	0.39	0.51	0.60	0.78
775	1×10^6	0.21	0.29	0.36	0.42	0.52

12.3 The effect of temperature.

The variation of post yield flow stress with temperature, at a constant strain rate, was determined in the easy glide region. The post yield flow stress was determined at a given temperature and then for a second, lower temperature. Then the specimen was re-tested at the first temperature to check that work-hardening (giving an increase in dislocation density) had not occurred. In this way, the variation of post yield flow stress with temperature was determined with a constant dislocation density.

The variation of post yield flow stress with temperature was determined at various constant strain rates. The temperature was varied from 780°C to the temperature at which brittle fracture occurred for a given strain rate.

Specimens of different dislocation density were tested:

(1) Type A specimens.

(a) Deformed specimens ($\rho = 7 \times 10^6 cm^{-2}$)

(b) Annealed specimens ($\rho = 5 \times 10^5 cm^{-2}$)

(2) Type B specimens

(a) Deformed specimens ($\rho = 1 \times 10^7 cm^{-2}$)

(b) Annealed specimens ($\rho = 1 \times 10^6 cm^{-2}$)

The results are shown in Table 17. We found that :

Table 17a

Type A specimens

The experiments on Type A specimens were preliminary ones, in which the temperature was varied up to 670°C.

Strain rate = 1×10^{-4} sec^{-1}

$\rho = 5 \times 10^5$ cm^{-2}		$\rho = 7 \times 10^6$ cm^{-2}	
Temp (°C)	P.y. flow stress (kg/mm^2)	Temp (°C)	P.y. flow stress (kg/mm^2)
670	0.54	670	0.62
646	0.57	640	0.73
637	0.55 - 0.59	632	0.7 - 0.78
620	0.60	615	0.84
590	0.70	585	0.91
570	0.74	570	0.98
560	0.75 - 0.77	560	1.00
543	0.83	540	1.15
523	0.90	515	1.25
480	F 1.4	500	F 1.9

F - brittle fracture.

Table 17b

Type B specimens

Strain rate = 4×10^{-6} sec^{-1}

$\rho = 1 \times 10^6$ cm^{-2}		$\rho = 1 \times 10^7$ cm^{-2}	
Temp (°C)	P.y. flow stress kg/mm^2	Temp (°C)	P.y. flow stress kg/mm^2
775	0.21	775	0.24
752	0.23	756	0.25
732	0.26	724	0.29
715	0.28	716	0,35
705	0.29	705	0.35
696	0.30	686	0.39
690	0.32	674	0.43
654	0.41	658	0.48
620	0.46 - 0.50	652	0.49
560	0.63	640	0.58
550	0.68	620	0.62 - 0.68
510	0.87	610	0.63 - 0.70
500	1.00	570	0.78
480	0.94 - 1.10	560	0.80
440	1.2	520	0.98 - 1.10
400	F 1.65	490	1.10 - 1.30
		440	F 1.75

F - brittle fracture.

Table 17c

Type B specimens

Strain rate (sec^{-1})	Brittle fracture temperature (°C) $\rho = 1 \times 10^6$ cm^{-2}	$\rho = 1 \times 10^7$ cm^{-2}
4×10^{-6}	440	460
2×10^{-5}	460	480
1×10^{-4}	490	510
2.4×10^{-4}	510	530
2×10^{-3}	550	560

(1) The post yield flow stress decreased rapidly with increasing temperature (see Figs. 27,28). A plot of the logarithm of stress against the reciprocal of the temperature gave a reasonable straight line (see Fig. 29).

(2) The slope $d\sigma/dT$ depended on the dislocation density of the specimen. At any given temperature, the slope $d\sigma/dT$ of the deformed specimen was greater than that of the annealed specimen (Figs. 27,28).

(3) The slope $d\sigma/dT$ for a given dislocation density specimen was independent of the applied strain rate.

(4) The ductile brittle transition temperature increased as the applied strain rate increased. (A comprehensive survey of the ductile brittle effect was not made. The absolute values of ductile brittle transition temperature obtained are approximate and apply only to the particular experimental conditions used. However their importance is in showing the large effect of strain rate on the ductile brittle transition).

12.4 The relaxed stress.

Interrupting the straining during the easy glide region caused the stress to relax with time to a lower value, which became approximately constant after 5 minutes. Typical experimental curves of

deflection (load) versus time are shown in Fig. 30. The effects of strain rate, dislocation density and temperature on the relaxed stress were determined.

The results were :

(1) At a constant temperature and dislocation density, the relaxed stress was independent of the post yield flow stress; i.e. the stress always relaxed to the same value regardless of the initial applied strain rate. Typical results are shown in Table 18 and Fig. 31.

(2) The relaxed stress was a function of the dislocation density of the specimen. An annealed specimen always relaxed to a lower stress than a deformed specimen. Typical results are shown in Table 19 and Fig. 31.

(3) The relaxed stress decreased as the temperature was increased. Typical results are shown in Table 20 and Fig. 31.

(4) The relaxed stress could be correlated with the initial departure from the elastic region on straining. (Fig. 31).

13. Work-hardening.

A comprehensive study of work-hardening was not made. However some preliminary observations were made on the effects of strain rate, temperature and

TABLE 18

Crystal type	Temp. (^{o}C)	Strain rate (sec^{-1})	Post yield flow stress (kg/mm^2)	Relaxed stress (kg/mm^2)
"B" ($1x10^{6}cm^{-2}$	620	1×10^{-4}	0.78	0.26
	620	4×10^{-6}	0.50	0.26

TABLE 19

Crystal type	Dislocation Density (cm^{-2})	Strain rate (sec^{-1})	Temp. (^{o}C)	Post Yield flow stress (kg/mm^2)	Relaxed stress (kg/mm^2)
A	7×10^{6}	1×10^{-4}	560	1.05	0.70
A	5×10^{5}	1×10^{-4}	560	0.75	0.37
B	1×10^{7}	4×10^{-6}	620	0.63	0.54
B	1×10^{6}	4×10^{-6}	620	0.50	0.26

TABLE 20 (Type "B" specimens)

Temp. (^{o}C)	Relaxed stress (kg/mm^2)	
	Annealed ($\rho = 1 \times 10^{6}cm^{-2}$)	Deformed ($\rho = 1 \times 10^{7}cm^{-2}$)
620	0.26	0.54
650	0.24	-
690	0.22	-
705	0.21	0.26
775	0.17	0.22

orientation on stage II of the stress strain curve.

For a specimen oriented initially for single slip, the start of work-hardening was correlated with the appearance of pronounced secondary slip. As secondary slip continued, the specimen work-hardened. The stress always increased linearly with the strain during stage II of work-hardening. The work-hardening coefficient ($d\sigma/d\varepsilon$) depended on :

(1) The applied strain rate.

The work hardening coefficient ($d\sigma/d\varepsilon$) increased with an increase in strain rate. The values are shown in Table 21.

(2) The temperature.

Increasing the testing temperature reduced the work-hardening coefficient. The values are shown in Table 22.

(3) The orientation of the specimen.

The work-hardening coefficient was very sensitive to the orientation of the specimen. The results are shown in Table 23 and Fig. 23.

Stage II was followed by a small region in which the variation of stress with strain became parabolic (stage III). Stage III was followed by the fracture of the specimen. No stage III was observed for specimens of <111> orientation, for which the variation

TABLE 21

Strain rate (sec^{-1})	$2x10^{-5}$	$1x10^{-4}$
Stage II $d\sigma/d\varepsilon$ (gms/mm^2 % ε)	20 - 30	55 - 60

Temperature $560^{\circ}C$.

TABLE 22

Temperature ($^{\circ}C$)	560	650
State II $d\sigma/d\varepsilon$ (gm/mm^2 % ε)	55 - 60	40 - 45

Strain rate $1 \times 10^{-4} sec^{-1}$

TABLE 23

Initial Orientation	Stage II $d\sigma/d\varepsilon$ (gms/mm^2 % ε)
Centre of unit triangle - single slip	20 - 30
Near {100} - {111} boundary - double slip	80
< 111 > - multiple slip	350

Temperature $560^{\circ}C$.

Strain rate $2 \times 10^{-5} sec^{-1}$

of stress with strain remained linear until the final fracture.

These preliminary results suggest that the nature of work-hardening is not the same as in metal crystals.

14. Experimental errors.

14.1 Resolved shear stress.

The resolved shear stress (σ) is determined from the equation :

$$\sigma = \frac{P}{A} \sin\chi \cos\lambda \quad \ldots\ldots \qquad (9.2)$$

P - applied load.

A - cross-sectional area.

χ - angle between slip plane and tension axis.

λ - angle between slip direction and tension axis.

The calculation of the resolved shear stress involved measurements of :

(a) The applied load.

The calibrated scale, on which the magnified deflection of the beam was measured, could be read to the nearest 0.5 mm. As the total deflection varied from 5 - 25 cm., the maximum error in measuring the deflection was about 0.4 - 2.0 %.

The observed deflection (cm) was converted into the applied load (kg) using the calibration graph. The error involved in the determination, plotting and

reading of the calibration graph was probably small (<1%).

Hence the maximum error in the measurement of the applied load was probably about 3%.

(b) The cross sectional area.

The specimens had a regular, almost square cross section which was measured with a micrometer. The maximum variation, along the length of the specimen, in each of the two measured dimensions was about 0.05 mm. The overall dimensions of the cross section were about 0.25 cm x 0.25 cm. Hence the maximum error was about 2% in a particular dimension, and about 4% in the cross sectional area.

(c) The orientation factor.

The angles χ and λ could be measured to the nearest $\frac{1}{2}^{\circ}$ from the stereogram plotted from a Laue back reflection X-ray of the specimen. Measurement of the angles between the slip lines and the tension axis on two adjacent faces of the specimen provided a check of these values.

The angles χ and λ were approximately 45°. A typical measurement was :

$$\chi = 43^{\circ}$$

$$\lambda = 44^{\circ}$$

i.e. $\sin \chi \cos \lambda = 0.49$

Hence the maximum error in sin χ cos λ was small (1%).

We conclude that the maximum error in the resolved shear stress was about 8%.

14.2 Glide strain.

The tensile strain (ε_t) is given by :

$$\varepsilon_t = \frac{e}{L} \quad \ldots\ldots\ldots \quad (9.4)$$

e - extension.

L - original length.

The glide strain is given by :

$$\varepsilon = \frac{1}{\sin \chi_o} \left(\sqrt{d^2 - \sin^2 \lambda_o} - \cos \lambda_o \right) \quad \ldots\ldots (9.5)$$

with $d = \frac{L + e}{L}$

χ_o - the initial angle between the slip plane and tension axis.

λ_o - the initial angle between the slip direction and tension axis.

The calculation of glide strain involved measurements of :

(a) Extension.

During the tensile experiments the deflection of the beam was measured as a function of the carriage position, which could be read to the nearest $\frac{1}{2}$ division (1 division corresponds to 3.5×10^{-3}mm extension).

A graph was plotted of deflection versus carriage position, from which the plastic extension at various points was determined. The error involved in the determination of a particular extension depended largely on the amount of the extension. The error involved in determination of the upper yield point extension was large, whereas that in the lower yield point extension was much smaller.

At the upper yield point

Total plastic extension ~ 10 divisions

i.e. maximum error in reading

carriage position ~ 10 %.

At the lower yield point

Total plastic extension ~ 60 divisions

i.e. maximum error in reading

carriage position ~ 2 %.

The error in plotting and reading the deflection - carriage position graph was probably small (<1%).

(b) Initial length.

The initial length measured was the distance between the shoulders of the specimen. This distance, of about 2.5 cm, was measured with a ruler, which could be read to 0.5 mm. Hence the maximum error involved in the measurement was about 4%.

(c) The orientation factor.

The angles χ_o and λ_o could be measured to the nearest $\frac{1}{2}^o$ (χ_o and λ_o were about 45^o). Hence the maximum error in the orientation factor in equation (9.5) was small (1%).

We conclude that the maximum error in the glide strain varied from about 16% at the upper yield point to about 8% at the lower yield point.

14.3 Strain rate.

The strain rate ($\dot{\varepsilon}$) is given by :

$$\dot{\varepsilon} = \frac{\dot{\varnothing}}{l} \quad \ldots\ldots \quad (14.1)$$

$\dot{\varnothing}$ - rate of motion of cross head.

l - length of specimen.

The calculation of the strain rate involved measurements of :

(a) The cross head motion.

The rate of motion of the cross head was determined by measuring the output speed from the gear box, the time for a given number of revolutions of the output shaft being determined. The error involved in measuring the output speed was negligible.

(b) The specimen length.

The error involved in measuring the specimen (discussed previously) was about 4%. As the specimen

extends, the strain rate decreases due to the increase in length. This effect was neglected in the calculation of strain rate and would give a maximum error of about 5%.

We conclude that the maximum error in the calculation of strain rate was about 9%.

14.4 Dislocation density.

The dislocation density was determined by microscopic etch pit counts on a {111} plane, assuming a 1 : 1 correlation between etch pits and dislocations. The number of etch pits in about 20 fields was counted and the average etch pit number derived. The area of the field was accurately measured with a graticule.

The following errors were involved in the determination of dislocation density :

(a) The error involved in counting the etch pits was small (2%).

(b) The density of etch pits, at "low" dislocation densities ($< 5 \times 10^5 cm^{-2}$) was not very uniform. The etch pit number could vary by a factor of 2 in different fields. By counting about 20 fields the error due to the scatter in number was reduced. The average number derived had a probable error of about 10%. At higher densities the distribution of etch pits was more uniform and the error smaller.

(c) No allowance was made for the angle between the slip plane and the etch plane, which gives an error in the area of about 6%.

We conclude that the maximum error in the dislocation density measurements was about 18%.

IV. DISCUSSION OF RESULTS.

15. Introduction.

The discussion of the results is presented in three sections, as follows :

(16) The post yield flow stress.

In this section a physical model of the post yield flow stress is developed from the experimental results.

(17) The yield point phenomenon.

An explanation of the yield point phenomenon is suggested in this section. A short discussion of the nature of the dislocation sources is also included.

(18) Other results.

Finally the relevance of recently published work is considered.

16. The post yield flow stress.

16.1 Selection of basic model.

From the experimental results we derived empirical relations between strain rate, temperature and the post yield flow stress. We found that a plot of the flow stress versus the logarithm of the strain rate gave a slightly better fit than a logarithm - logarithm plot. For this reason Seeger's equation of flow stress, rather than those of Haasen and Gilman,

is used as a basis from which to examine the experimental results. In this model, derived for thermally activated dislocation motion (see Review of Literature), flow stress may be expressed as :

$$\sigma = \sigma_G + \frac{U_o}{V} + \frac{kT}{V} \ln \frac{\dot{\varepsilon}}{\dot{\varepsilon}_o} \qquad \ldots\ldots\ldots (16.1)$$

σ_G - internal stress field

V - activation volume.

$\dot{\varepsilon}$ - strain rate.

$\dot{\varepsilon}_o$ - constant.

16.2 Effect of strain rate.

Seeger's model requires a logarithmic strain rate ($\dot{\varepsilon}$) dependence of flow stress (σ). This dependence was observed experimentally, a plot of σ versus $\ln \dot{\varepsilon}$ giving a straight line (with some minor deviations at the highest strain rate).

From equation (16.1), at a given temperature, the slope $d\sigma/d \ln \dot{\varepsilon}$ is given by :

$$\frac{d}{d \ln \dot{\varepsilon}} = \frac{kT}{V} \qquad \ldots\ldots\ldots (16.2)$$

Hence from the slope, a value of the activation volume (V) at a given temperature can be derived.

From the experimental results, we find :

(1) The slope $d\sigma/d \ln \dot{\varepsilon}$ varies with the testing temperature, the slope increasing with decreasing

temperature. We conclude that the activation volume is not constant, but varies with the testing temperature. The activation volume increases with increasing temperature.

In Seeger's model the activation volume, (which is independent of temperature) depends on the distance l between "obstacles" along a dislocation. The activation volume is given by :

$$V = l\ b\ d \qquad \ldots\ldots\ldots \qquad (16.3)$$

$$\sim l\ b^2$$

d - distance through which work is done in cutting obstacle.

In germanium the obstacles are likely to be the "dragging points" (probably dangling bonds) along a dislocation. Hence the increase in activation volume with increasing temperature reflects a similar increase in the distance (l) between dragging points along a dislocation.

From the results on Type B specimens we can calculate the activation volume (V) and distance (l) between dragging points along a dislocation at various temperatures. The calculations are shown in Table 22. As the tests were all reversible, the change in the distance (l) between dragging points with temperature must occur almost instantaneously.

TABLE 22

T (^{o}K)	$1/T$ ($^{o}K^{-1}$)	$m=d\sigma/d\ln\dot{\varepsilon}$ (dynes/cm^2)	kT (dyne cm)	$V = \frac{kT}{m}$ (cm^3)	l (cm)
1046	0.955	5.2×10^{6}	1.44×10^{-13}	2.8×10^{-20}	1.1×10^{-5}
996	1.0	6.1×10^{6}	1.37×10^{-13}	2.2×10^{-20}	8.8×10^{-6}
978	1.02	6.7×10^{6}	1.35×10^{-13}	1.7×10^{-20}	6.8×10^{-6}
893	1.12	11.2×10^{6}	1.23×10^{-13}	1.1×10^{-20}	4.4×10^{-6}
839	1.19	13.9×10^{6}	1.16×10^{-13}	0.83×10^{-20}	3.3×10^{-6}
793	1.26	22.6×10^{6}	1.09×10^{-13}	0.5×10^{-20}	2.0×10^{-6}

Knowing the activation volume (V) and distance (l) between the dragging points at various temperatures, we can derive an equation representing the thermal equilibrium of the dragging points. A plot of ln V versus $1/T$ gives a good straight line (Fig.32). Hence we conclude that the thermal equilibrium of the dragging points is represented by :

$$V = c \exp \frac{-E}{kT} \quad \ldots\ldots \quad (16.4)$$

$$\text{or} \quad l = c' \exp \frac{-E}{kT} \quad \ldots\ldots \quad (16.5)$$

with c, c' constants.

We can derive the activation energy E controlling the thermal equilibrium from the slope of the graph. The slope is :

$$\frac{d \ln V}{d\, 1/T} = -\frac{E}{k} \qquad \ldots\ldots \qquad (16.6)$$

From which $E = 0.44$ e.v.

i.e. $V = c \exp \frac{-0.44 \text{ e.v.}}{kT}$

$$l = c' \exp \frac{-0.44 \text{ e.v.}}{kT}$$

(2) The slope $d\sigma/d \ln \dot{\varepsilon}$ at a given temperature is independent of the dislocation density of the specimen. Hence the activation volume is independent of the dislocation density of the specimen. Therefore dislocations in the deformed and annealed specimens, at a given temperature, have the same distance (l) between dragging points. This indicates that the fundamental nature of a dislocation is not irreversibly altered by high temperature annealing.

Therefore the strain rate results enable us to make two important deductions as to the nature of the dislocations :

(1) The distance between dragging points along a dislocation changes reversibly with changes in temperature.

(2) High temperature annealing does not irreversibly alter the fundamental nature of a dislocation.

16.3 Effect of temperature.

From equation (16.1), at a constant strain rate, the slope $d\sigma/dT$ is given by :

$$\frac{d\sigma}{dT} = \frac{k}{V} \ln \frac{\dot{\varepsilon}}{\dot{\varepsilon}_o} \quad \ldots\ldots \qquad (16.7)$$

From the experimental results we find that the slope $d\sigma/dT$ is not linear (Figs.27,28). This is consistent with the ideas discussed in the previous section. If the activation volume remained constant, then the slope $d\sigma/dT$ would be linear. Hence the observed result, that the slope is not linear, confirms the previous conclusion that the activation volume is temperature dependent.

By measuring the tangents at various points on the σ versus T curve, we can derive values of $\frac{k}{V} \ln \frac{\dot{\varepsilon}}{\dot{\varepsilon}_o}$.

These values are required in the calculation of the rate determining activation energy U_o.

16.4 Effect of dislocation density.

A model of flow stress for germanium must explain the reduction in flow stress on retesting, after high temperature annealing. It seems probable that the reduction in flow stress is associated with the reduction in the number of the dislocations. A reduction in dislocation density gives a reduction in

the internal stress field (σ_G) due to the elastic interaction of parallel dislocations. The internal stress field (σ_G) is given by :

$$\sigma_G = \alpha b G \sqrt{\rho} \quad \ldots\ldots\ldots \quad (16.8)$$

α - depends on nature and distribution of dislocations.
b - Burgers vector.
G - shear modulus.
ρ - dislocation density.

Hence we must determine if the internal stress field provides an appreciable contribution to the flow stress, and its magnitude in deformed and annealed specimens. Previous experiments indicate that the elastic stress fields around dislocations in germanium and silicon are extensive, and likely to give rise to an appreciable elastic interaction with parallel dislocations. Infra red[78] photographs through silicon have shown that the stress field extends for about 20 microns from the centre of the dislocation. Observations[79,80,81] on dislocation doublets in low angle grain boundaries in germanium have shown that the minimum separation of the two dislocations is about 10 microns.

A reduction in dislocation density (ρ) also gives a positive stress increment ($\Delta\sigma_v$) due to the

dislocations having to move at a higher velocity ($\bar{v}$) to maintain the applied strain rate ($\dot{\varepsilon}$).

Hence the change in the observed flow stress ($\Delta\sigma$) on retesting after high temperature annealing is given by :

$$\Delta\sigma = \Delta\sigma_G + \Delta\sigma_v \quad \ldots\ldots\ldots \quad (16.9)$$

The magnitude of the increment in stress ($\Delta\sigma_v$) required to accommodate the change in the velocity of the dislocations can be determined in two ways :

(1) From the strain rate results.

The strain rate (ε) is given by :

$$\dot{\varepsilon} = b \rho \bar{v} \quad \ldots\ldots\ldots \quad (6.12)$$

$\bar{v}$ - average dislocation velocity.

We have derived experimentally that :

$$\sigma = B \ln \dot{\varepsilon} \qquad B \text{ - constant.}$$

Then, as $\dot{\varepsilon} \sim \bar{v}$

$$\sigma = B \ln \bar{v}$$

$$\text{or} \quad \Delta\sigma_v = B\Delta \ln \bar{v} \quad \ldots\ldots\ldots \quad (16.10)$$

Hence knowing the change in dislocation density we can determine $\Delta\sigma_v$ from equation (6.12) and (16.10).

(2) From the temperature results.

We have

$$\sigma = \sigma_G + \frac{U_o}{V} + \frac{kT}{V} \ln \frac{\dot{\varepsilon}}{\dot{\varepsilon}_o} \quad \ldots\ldots\ldots \quad (16.1)$$

$$\text{i.e.} \quad \Delta\sigma = \Delta\sigma_G + \Delta\left(\frac{U_o}{V} + \frac{kT}{V} \ln \frac{\dot{\varepsilon}}{\dot{\varepsilon}_o}\right)$$

$$\text{hence} \quad \Delta\sigma_v = \Delta\left(\frac{U_o}{V} + \frac{kT}{V} \ln \frac{\dot{\varepsilon}}{\dot{\varepsilon}_o}\right)$$

We also know that :

(1) The activation volume (V) is the same in the deformed and annealed condition.

(2) At a constant strain rate, $\frac{d\sigma}{dT} = \frac{k}{V} \ln \frac{\dot{\varepsilon}}{\dot{\varepsilon}_o}$

Hence we can express $\Delta\sigma_v$ as :

$$\Delta\sigma_v = T \frac{d\sigma}{dT} \qquad \ldots\ldots\ldots \qquad (16.11)$$

We can then derive $\Delta\sigma_v$ at any temperature by measuring the tangents to the graphs of stress versus temperature obtained for the deformed and annealed specimens. This method is not very sensitive as it is difficult to make accurate measurements of the tangents.

The magnitude of the internal stress field (σ_G) can also be determined in two ways :

(1) <u>From the relaxed stress</u>

The relaxed stress observed experimentally may provide a measure of the internal stress field (σ_G) of the specimen. The characteristics of the relaxed stress are :

(1) The stress relaxes to approximately the same value for a given specimen regardless of the initial strain rate.

(2) An annealed specimen with lower dislocation density always relaxes to a lower stress than a deformed specimen.

(3) The relaxed stress can be correlated with the observed elastic limit of the specimen.

It seems likely that the relaxed stress would be the flow stress at an infinitely small strain rate; i.e. being the stress to overcome the internal stress field (σ_G).

(2) From $\Delta\sigma$ and $\Delta\sigma_v$

Knowing values of $\Delta\sigma$ and $\Delta\sigma_v$ we can derive $\Delta\sigma_G$ from equation (16.9). The internal stress field (σ_G) is given by :

$$\sigma_G = A\sqrt{\rho} \quad \text{.....(16.12)}$$

A - constant.

$$\text{i.e.} \quad \Delta\sigma_G = A\,\Delta\sqrt{\rho}$$

Hence knowing $\Delta\sigma_G$, we can calculate A. Then we can determine the value of the internal stress field at any given dislocation density by using equation (16.12).

Substituting experimental values in the various equations, we find :

For Type B specimens in the deformed and annealed conditions at 620°C, $\dot{\varepsilon} = 4 \times 10^{-6} sec^{-1}$, we have

From (1) $\Delta\sigma_v = 240$ gms/mm^2

(2) $\Delta\sigma_v \sim 300$ gms/mm^2

and for the deformed specimen ($\rho = 1 \times 10^7 cm^{-2}$)

$$\underline{\sigma_G \text{ deformed}} = \underline{540 \text{ gms/mm}^2}$$

for the annealed specimen ($\rho = 1 \times 10^6 cm^{-2}$)

$$\underline{\sigma_G \text{ annealed}} = \underline{170 \text{ gms/mm}^2}$$

The observed values of the relaxed stress (σ_r) at this temperature (620°C) were :

$$\sigma_r \text{ deformed} = \underline{540 \text{ gms/mm}^2}$$

$$\sigma_r \text{ annealed} = \underline{260 \text{ gms/mm}^2}$$

The agreement of the calculated values of σ_G and the relaxed stress (σ_r) is reasonable, as σ is difficult to determine experimentally. Any temperature fluctuations make difficult long time tests required to test that σ_r has become constant.

We conclude that :

(1) The internal stress field (σ_G) constitutes an important fraction of the observed flow stress.

(2) The internal stress field of an annealed specimen is much smaller than that of a deformed specimen. The reduction in internal stress field, due to the reduction in dislocation density produced by high

temperature annealing, is larger than the positive stress increment due to the dislocations having to move at a higher velocity to maintain the applied strain rate. The net effect is a reduction in the observed flow stress on retesting.

16.5 The variation of the internal stress field (σ_G) with temperature.

The internal stress field (σ_G) is given by

$$\sigma_G = \alpha b G \sqrt{\rho} \quad \ldots \quad (16.8)$$

α - depends on nature and distribution of dislocations.
b - Burgers vector.
G - shear modulus.
ρ - dislocation density.

In metals, the internal stress field has only a small variation with temperature, due to small changes in the elastic constants. However in germanium the variation of the internal stress field with temperature is large. Both the observed relaxed stress and the calculated values of σ_G, decreased markedly with increasing temperature.

We have, at 773°C :

	(1) From σ_G	(2) From calculation
For a deformed specimen ($\rho = 1 \times 10^7 cm^{-2}$) $-\sigma_{G\ deformed}$	= 220gms/mm^2	220gm/mm^2
For an annealed specimen ($\rho = 1 \times 10^6 cm^{-2}$) $-\sigma_{G\ annealed}$	= 170gms/mm^2	80gm/mm^2

Comparing these values of σ_G with those obtained at 620°C, we find that σ_G has decreased by about 60% in ~ 150°C.

The large variation of the internal stress field can be due to :

(1) Possible experimental errors.

For the calculated σ_G to remain nearly constant with temperature, the decrease of $d\sigma/d \ln \dot{\varepsilon}$ with increasing temperature would have to be offset by a divergence of the stress-temperature graphs of the deformed and annealed specimens towards higher temperatures. In fact, a convergence of the stress-temperature graphs is observed. The convergence of the graphs may be explained by the annealing out of some of the dislocations in the deformed specimens at the higher temperatures, or by an increase in the number of dislocations in the annealed specimens. However cycling the tests between various temperatures gave reproducible values of flow stress and gives confidence that such effects are negligible.

Moreover the steady decrease of the relaxed stress with temperature gives a direct check as to the validity of the calculated values of σ_G.

(2) Changes in shear modulus (G)

No measurements of the appropriate shear modulus have been made in the range of temperature used.

However, studies of the variation of Young's Modulus (E) with temperature indicate that the change in elastic constant is small (~ 10% over 900°C), although certain anomalies giving a large change in E have been observed[82]. It seems unlikely that any large change in the shear modulus does occur.

(3) Changes in the nature and distribution of the dislocations.

The term α in equation (16.8) depends on the nature and distribution of the dislocations.

(a) The nature of the dislocations.

In metals, the term α associated with a screw dislocation is several times larger than α associated with an edge dislocation. We have shown that the nature of dislocations in germanium varies with temperature. The number of dragging points along a dislocation changes reversibly with temperature, the thermal equilibrium of the dragging points being given by :

$$l = c' e^{\frac{-0.44}{kT}} \text{ e.v.}$$

where l is the distance between dragging points.

Each dragging point may have an associated elastic distortion. Then the integral of the individual dragging point elastic distortions along the whole dislocation, would contribute to the stress field around the dislocation. Hence any change in

the number of dragging points might affect the stress field around a dislocation and alter the elastic interaction between parallel dislocations.

A test of this hypothesis is to determine the relation between and the number of dragging points (n) along a dislocation. We can derive values of $\Delta\sigma_G$ and A ($= \alpha b G$) at various temperatures. Then as G, b are practically constant :

$$\alpha \propto A$$

The number of dragging points (n) is inversely proportional to the activation volume (V). Hence a plot of A versus 1/V will give the relation between α and n. The values of A and 1/V are shown in Table 23.

TABLE 23

T (^oC)	$\Delta\sigma$ gms/mm^2	$\Delta\sigma_v$ gms/mm^2	$\Delta\sigma_G$ gms/mm^2	A gms/mm	V (cm^3)	1/V (cm^{-3})
773	30	120	150	0.75×10^{-2}	2.8×10^{-20}	0.36×10^{20}
723	50	140	190	0.95×10^{-2}	2.2×10^{-20}	0.46×10^{20}
705	60	180	240	1.2×10^{-2}	1.7×10^{-20}	0.59×10^{20}
620	130	240	370	1.9×10^{-2}	1.1×10^{-20}	0.91×10^{20}
566	150	320	470	2.3×10^{-2}	0.83×10^{-20}	1.21×10^{20}
520	200	520	720	3.6×10^{-2}	0.56×10^{-20}	2.0×10^{20}

From the graph (Fig.33)we find that a plot of A versus 1/V gives a reasonable straight line. Therefore

we can conclude that α depends on the number of dragging points along a dislocation.

The actual nature of the elastic distortion around a dragging point is not yet understood.

It is a possibility that the width of the dislocation may depend in some way on the number of dragging points along a dislocation. Then changes in the number of dragging points will affect the width of the dislocation and hence the nature of the elastic distortion.

We conclude that the reduction of σ_G with increasing temperature results from a decrease in the term α, which is associated with the reduction in the number of dragging points along a dislocation line.

(b) The distribution of dislocations.

Cycling tests between various temperatures gave reproducible values of post yield flow stress. Hence it is concluded that changes in distribution did not occur.

16.6. The activation energy (U_o)

Knowing values of σ_G, the activation volume (V) and $d\sigma/dT$, we can calculate values of the activation energy (U_o) from equation (16.1). U_o probably represents the activation energy to move a dislocation dragging point. We find that U_o is about 2 e.v. for both deformed and annealed specimens.

16.7 Other factors which may affect the post yield flow stress.

(a) Forest dislocations.

Two types of forest dislocations were present in the experiments :

(1) Grown in dislocations ($\sim 10^3 cm^{-2}$) which intersect the active slip planes.

(2) Glide dislocations produced by the secondary slip which was observed near the shoulders (at ~ 80^o to the tensile axis), in about 40% of the specimens.

Forest dislocations may conceivably act in a similar manner to the dragging points. To differentiate between forest dislocations and the dragging points associated with the glide dislocations, we can express the flow stress as :

$$\sigma = \sigma_G + \underbrace{\frac{U_o}{V} + \frac{kT}{V} \ln \frac{\dot{\varepsilon}}{\dot{\varepsilon}_o}}_{\text{Dislocation dragging points}} + \underbrace{\frac{U_o'}{V'} + \frac{kT}{V'} \ln \frac{\dot{\varepsilon}'}{\dot{\varepsilon}_o'}}_{\text{Forest dislocations}}$$

We assume that the activation energy (U_o) to move a dragging point is of the same order as the activation energy (U_o') to cut a forest dislocation. Then for the cutting of the forest dislocations to contribute a significant fraction (say 0.1) to the post yield flow stress, the activation volume V' must not be greater

than 10 times V. Hence :

$l_f \geq 10\, l$

l_f - distance between forest dislocations.

l - distance between dragging points.

From the experimental results, we find :

l varies from 2.5×10^{-6} cm at $520^{\circ}C$

to 1×10^{-5} cm at $773^{\circ}C$

i.e. $l_f \geq 1 \times 10^{-4} - 2.5 \times 10^{-5}$

Now $\rho_f \sim 1 / l_f$

ρ_f - density of forest dislocations.

i.e. $\rho_f \neq 10^8 - 10^{10}\ cm^{-2}$.

Hence for the forest dislocations to contribute a significant fraction to the post yield flow stress, the forest dislocation density must be greater than $10^8 cm^{-2}$. This was higher than the total dislocation density observed experimentally.

We conclude that the effect of the forest dislocation on flow stress is small compared with the effect of the dislocation dragging points.

(b) "Debris" hardening.

Gilman has suggested that "debris" hardening is produced by the interaction of dislocations with trails left by preceding dislocations. However in the present experiments easy glide continued at

a constant stress, indicating that any such effect is negligible.

16.8 General conclusions.

From the discussion we can make the following conclusions :

(1) The post yield flow stress of germanium single crystals can be described by a modified form of Seeger's equation.

The modified equation is :

$$\sigma = \sigma_G + \frac{U_o}{V} + \frac{kT}{V} \ln \frac{\dot{\varepsilon}}{\dot{\varepsilon}_o}$$

with

(a) $\sigma_G = \alpha\, b\, G \sqrt{\rho}$

where $\alpha = f(T)$

(b) $V = c \exp \frac{-0.44 \text{ e.v.}}{kT}$

c – constant.

(2) The contributions to the post yield flow stress are :

(a) The internal stress field (σ_G) due to the elastic interaction of parallel dislocations.

(b) The stress required to move the dragging points situated along a dislocation. This term depends on the velocity at which the dislocations are made to move.

(3) The number of dragging points along a

dislocation changes reversibly with temperature. The thermal equilibrium of the distance (l) between the dragging points is given by :

$$l = c' \exp \frac{-0.44 \text{ e.v.}}{kT}$$

c'- constant

The reduction in number of dragging points along a dislocation with increasing temperature has the following effects :

(a) The term , dependent on the nature of the dislocations is reduced. Hence the internal stress field is reduced.

(b) The stress to move a dislocation is reduced.

The total effect is a reduction of the observed post yield flow stress with temperature.

(4) High temperature annealing of a deformed specimen reduces the dislocation density, and hence the magnitude of the internal stress field (σ_G). This reduction more than offsets the positive stress increment, due to the dislocations having to move at a higher velocity to maintain the applied strain rate. The net effect is a reduction in the observed flow stress.

High temperature annealing does not change the fundamental nature of a dislocation. The activation energy to move a dragging point, and the number of dragging points along a dislocation remain constant.

(5) Forest dislocations and "debris" hardening effects make a negligible contribution to the post yield flow stress.

16.9 Other flow stress models.

Van Bueren has proposed an equation of flow stress (see Review of Literature) which has certain similarities to that derived from Seeger's model. Van Bueren's equation, in a comparable form, may be written as:

$$\sigma = \frac{Q_1}{V} + \frac{kT}{V} \ln \frac{\dot{\varepsilon}}{\dot{\varepsilon}_o}$$

A similar temperature dependent volume (V) is proposed. However Van Bueren does not include an internal stress field (σ_G) term due to the elastic interaction of parallel dislocations.

The omission of an internal stress field term (σ_G) leads to difficulties in trying to interpret our observed results on the reduction in flow stress on retesting after high temperature annealing. An interpretation of the results in terms of a reduction in the internal stress field, i.e. a dislocation number effect, is not possible. Instead an interpretation of the results in terms of Van Bueren's model suggests that the reduction in flow stress is due to a reduction in Q_1, the activation energy to move a dragging point.

At a given temperature we have :

(1) The flow stress of an annealed specimen is less than that of a deformed specimen.

(2) The activation volume (V) is the same for an annealed and deformed specimen.

(3) The slope $d\sigma/dT = \frac{k}{V} \ln \frac{\dot{\varepsilon}}{\dot{\varepsilon}_o}$ of a deformed specimen is greater (more negative) than the slope of an annealed specimen.

Therefore an interpretation of the results in terms of Van Bueren's equation, suggests that the reduction in flow stress after high temperature annealing is due to a reduction in Q_1, the activation energy to move a dragging point, and not to the change in dislocation number. However this conclusion is not consistent with the conclusions from the strain rate results, which have the same significance using Van Bueren's equation. It was shown that, at a given temperature, the number of dragging points was the same in a deformed and annealed specimen. Therefore a change in Q_1 can only be explained by a change in the nature of the dragging points. However if this occurred, there is no reason why E, the energy describing the thermal equilibrium of the dragging points, should be the same in the deformed and annealed specimens as was observed.

We conclude that our theory, of the reduction in flow stress being a dislocation number effect, provides a more reasonable explanation.

17. The yield point phenomenon.

17.1 The effects of number and velocity of dislocations.

Johnston and Gilman showed that the yield point in lithium fluoride can be understood in terms of the number and velocity of dislocations. The properties required by other materials, for a similar yield point mechanism to be applicable, are :

(1) A high crystalline perfection, i.e. a significant increase in dislocation number and decrease in dislocation velocity will occur on deformation.

(2) The stress to move a dislocation must be sufficiently sensitive to changes in dislocation velocity for a significant drop in stress to occur.

The properties of germanium single crystals are:

(1) A high crystalline perfection.

(2) Considerable dislocation multiplication occurs on deformation.

(3) The upper yield stress and the post yield flow stress are sensitive functions of the strain rate. As the strain rate is proportional to the average dislocation velocity, there is a similar sensitive relation between stress and average dislocation velocity.

Hence the properties of germanium suggest that the yield point may be understood in terms of the number and velocity of dislocations. A qualitative explanation of the phenomenon in terms of these parameters is as follows :

(1) The yield point on first loading.

The constant applied strain rate ($\dot{\varepsilon}$) is a function of the density (ρ) and average velocity (v) of the dislocations :

$$\dot{\varepsilon} = \rho b \bar{v} \qquad \ldots\ldots\ldots \qquad (6.12)$$

At the elastic limit "certain"dislocations sources start to emit dislocation loops. To maintain the applied strain rate the first glide dislocations move at a velocity, given by

$$\bar{v} = \dot{\varepsilon} / b\rho \qquad \ldots\ldots\ldots \qquad (17.1)$$

As dislocation multiplication occurs, the velocity of the dislocations required to maintain the applied strain rate decreases .

$$\bar{v} = \dot{\varepsilon} / b(\rho + \Delta\rho) \qquad \ldots\ldots(17.2)$$

The stress to move a dislocation is a function of the dislocation velocity. Hence the decrease in velocity is accompanied by a decrease in stress giving a yield point.

We can explain certain of the experimental observations in terms of these ideas.

The size of the yield point depends on the amount of the decrease in dislocation velocity, i.e. on the difference between the dislocation density in the undeformed state and at the lower yield point. Hence a Type B specimen exhibits a larger yield point than a Type A specimen.

Annealing the undeformed specimen at 900°C, does not affect the yield point on testing, as the dislocation density is not altered.

(2) Reloading and annealing effects.

(a) On reloading the specimen after the lower yield point, dislocation multiplication does not occur and a yield point is not observed.

(b) On retesting annealed specimens of dislocation density $> 1 \times 10^5 cm^{-2}$ dislocation multiplication does not occur and a yield point is not observed.

(c) However on retesting annealed specimens of dislocation density $< 1 \times 10^5 cm^{-2}$, dislocation multiplication does occur and a yield point is observed. The size of the yield point depends on the increase in dislocation density. Hence the size of the yield point increases as the dislocation density of the annealed specimen is further reduced.

We conclude that at dislocation densities greater than $1 \times 10^5 cm^{-2}$ sufficient dislocations are present

for deformation to proceed at a constant stress. At densities less than $1 \times 10^5 cm^{-2}$, the small dislocation density demands a "high" dislocation velocity to maintain the applied strain rate. Hence dislocation multiplication occurs and a yield point is observed.

The size of the regained yield point is much smaller than the initial yield point. This is explained by the smaller increase in dislocation density and change in velocity on deformation. It was shown that an undeformed specimen, of similar density to an annealed specimen, gave a similar yield point.

The discussion of the post yield flow stress leads to a fuller understanding of the nature of the yield point. The stress at any time during the yield point is determined by two opposing effects. These are:

(1) The increase in dislocation number results in a decrease in the dislocation velocity required to maintain the applied strain rate. As the stress to move a dislocation is a function of the dislocation velocity, a drop in stress occurs.

(2) The increase in dislocation number increases the magnitude of the internal stress field (σ_G).

The increase in the internal stress field (σ_G) is not likely to be significant until the dislocation density is of the order $10^6 cm^{-2}$, i.e. when slip has

occurred over the whole specimen (0.5 - 1.0 % glide strain).

Hence the initial "fast" decrease of stress from the upper yield point is due to the change in dislocation velocity ($\Delta\sigma_v$). After a certain strain the increase in the internal stress field ($\Delta\sigma_G$) becomes significant and the stress decreases at a slower rate to the lower yield point.

We can calculate values of $\Delta\sigma_v$ and $\Delta\sigma_G$ for various specimens and predict the approximate magnitude of the yield points. The following are some examples of this evaluation :

(1) Type A specimen at 560°C.

(a) Determination of $\Delta\sigma_v$

$$\rho_{\text{undeformed}} = 1 \times 10^3 \text{cm}^{-2}$$

$$\rho_{\text{L.Y.P.}} = 7 \times 10^6 \text{cm}^{-2}$$

At constant $\dot{\varepsilon}$

$$\Delta \bar{v} = \Delta \rho$$

i.e. $\Delta \bar{v} = 7 \times 10^3$

As $\bar{v} \propto \dot{\varepsilon}$

from the graph of σ versus $\ln \dot{\varepsilon}$ we obtain :

$$\Delta\sigma_v \sim - 1360 \text{ gms/mm}^2$$

This value is only approximate as it involves extrapolation of the curve to higher strain rates.

(b) Determination of $\Delta\sigma_G$

At 0% strain $\sigma_G = 0$

At L.Y.P. $\sigma_G = 700$ gms/mm^2 (from relaxed stress)

$$\therefore \quad \Delta\sigma_G = + 700 \text{ gms/mm}^2.$$

The change in the observed stress during the yield point is given by :

$$\Delta\sigma = \Delta\sigma_G + \Delta\sigma_v$$

$$\therefore \quad \Delta\sigma \sim - \underline{660 \text{ gms/mm}^2}$$

This compares with the experimentally observed decrease of :

$$250 - 1000 \text{ gms/mm}^2.$$

(2) Type B specimens at 620°C.

(a) Determination of $\Delta\sigma_v$

ρ undeformed $= 5 \times 10^2$ cm^{-2}

ρ L.Y.P. $= 1 \times 10^7$ cm^{-2}

At constant $\dot{\varepsilon}$

$$\Delta \bar{v} = \Delta \rho$$

i.e. $\Delta \bar{v} = 2 \times 10^4$

As $\bar{v} \propto \dot{\varepsilon}$

from σ versus $\ln \dot{\varepsilon}$ we obtain :

$$\Delta\sigma_v \sim - 1080 \text{ gms/mm}^2.$$

(b) Determination of $\Delta\sigma_G$

At 0% strain $\sigma_G = 0$

L.Y.P. $\sigma_G = 540$ gms/mm^2 (from relaxed stress and calculation)

i.e. $\Delta\sigma_G = 540$ gms/mm^2

The change in the observed stress ($\Delta\sigma$) during the yield point is given by :

$$\Delta\sigma = \Delta\sigma_G + \Delta\sigma_v$$

$$\therefore \Delta\sigma \sim 540 \text{ gms/mm}^2.$$

This compares with the experimentally observed decrease of :

$$150 - 320 \text{ gms/mm}^2.$$

(3) Type A specimen (in annealed condition) at 560°C.

(a) Determination of $\Delta\sigma_v$

$\rho_{\text{annealed}} = 9 \times 10^4 \text{cm}^{-2}$

$\rho_{\text{L.Y.P.}} = 6 \times 10^5 \text{cm}^{-2}$

At constant $\dot{\varepsilon}$

$\Delta \bar{v} = \Delta \rho$

i.e. $\Delta \bar{v} = 7$

As $\bar{v} \propto \dot{\varepsilon}$

from σ versus $\ln \dot{\varepsilon}$ we obtain

$$\Delta\sigma_v \sim -270 \text{ gms/mm}^2.$$

(b) Determination of $\Delta\sigma_G$

σ_G annealed = 84 gms/mm^2 (from calculation

σ_G L.Y.P. = 184 gms/mm^2 and observation

$\therefore$ $\Delta\sigma_G$ ~ 100 gms/mm^2 of relaxed stress)

The decrease in the observed stress ($\Delta\sigma$) during the yield point is given by

$$\Delta\sigma = \Delta\sigma_G + \Delta\sigma_v$$

$$\therefore \Delta\sigma \sim 170 \text{ gms/mm}^2.$$

This compares with the experimentally observed decrease of : 40 - 160 gms/mm^2.

The agreement of the calculated and observed decreases in stress is reasonable, as the calculations are only approximate, their importance is in demonstrating that the large yield point observed experimentally can be quantitatively satisfied by a theory dependent on the number and velocity of dislocations.

We conclude that the number and velocity theory provides a reasonable quantitative explanation of the yield point in germanium.

17.2 The effects of impurity.

The best argument in favour of the number and velocity of dislocations theory of the yield point phenomenon in germanium is the positive one that it provides a satisfactory explanation of the experimental

results. However certain of the qualitative arguments against an explanation in terms of the impurity locking theory are included for completeness.

Certain features of the deformation behaviour are consistent with the effects of the impurity locking of dislocations. These are :

(1) The yield point observed during the first loading.

(2) The absence of a yield point on immediate reloading.

(3) The return of a yield point after a suitable annealing treatment.

However there are certain differences between the observed results and the yield point effects in metal crystals. These are :

(1) In metals where the dislocations are locked by impurity atoms, yielding is an abrupt process. When the dislocations are released from the impurity atoms, the stress decreases rapidly to the lower yield point. One or more Luders bands then spread through the specimen at the lower yield point stress.

The yield point in germanium is a "slow" process. The stress decreases from the upper yield point at less than the maximum relaxation rate of the machine, with Luders bands spreading through the specimen after the

upper yield point. About 1 - 2% glide strain (depending on experimental conditions) occurs between the upper and lower yield point. Easy glide continues after the lower yield point at a constant dislocation density.

(2) In metal crystals, the yield point is regained after strain ageing has allowed the impurity atoms to re-lock the dislocations.

In germanium crystals, even ones diliberately contaminated with impurity, the yield point is only regained after the dislocation density of the specimen has been reduced to less than $1 \times 10^5 cm^{-2}$. Hence the return of the yield point appears to depend on the dislocation density of the specimen and not on a strain ageing process.

There are various impurity elements which may act as dislocation locks in germanium. However none of the possible elements completely satisfy the observed experimental conditions.

(1) Gallium and indium.

(a) The addition of gallium or indium in small amounts to intrinsic germanium does not significantly affect the yield point. This suggests that, if gallium or indium were the locking impurity, sufficient is already present in the intrinsic germanium to lock all the dislocations.

(b) Annealing the undeformed specimens at 900°C did not affect the nature of the yield point. This suggests that the condensation temperature of the locking impurity is in excess of 900°C (the melting point is 937°C). Hence the binding energy between the dislocation and the impurity atom is likely to be large (> 2 e.v.) The interaction between a dislocation and a gallium or indium atom would be expected to be elastic; i.e. the binding energy would be small ($\frac{1}{2}$ 0.5 e.v.) and the condensation temperature "low".

Therefore it seems unlikely that gallium or indium atoms act as dislocation locks.

(2) Copper and nickel.

(a) The interaction between a dislocation and a copper or nickel atom would be expected to be elastic, with a small binding energy and low condensation temperature.

(b) Copper and nickel both diffuse rapidly in deformed germanium. Shorter annealing times (of order 1 hr. at 700°C) than those observed should effect a return of the yield point.

Hence it seems unlikely that copper or nickel atoms act as dislocation locks.

(3) Oxygen.

(a) The interaction between a dislocation and

an oxygen atom may be chemical, with a large binding energy and high condensation temperature. However whether the atoms would remain condensed at 900°C is doubtful. This would indicate that a yield point could be obtained on testing at this temperature. In fact a yield point has not been observed experimentally above 800°C.

(b) Annealing a deformed or annealed specimen in air at temperatures below 900°C does not effect a return of the yield point. This treatment is likely to increase the oxygen concentration in the specimen and hence, if oxygen atoms act as dislocation locks, should facilitate a return of the yield point.

(c) The diffusion coefficient of oxygen in germanium has not been accurately determined. However diffusion coefficient measurements of oxygen[83] in silicon, suggest that shorter annealing times than those observed would effect a return of the yield point. It was found that for silicon, an anneal at 800°C (i.e. T/Tm = 0.56) for 2 hours would allow sufficient oxygen diffusion to re-lock dislocations. The equivalent annealing temperature in germanium (i.e. T/Tm = 0.56) is about 530°C. Obviously the diffusion coefficient of oxygen in silicon, and oxygen in germanium, will not be exactly the same. However, due to the similarity in structure, it seems unlikely

that the diffusion coefficients would be completely unrelated. It seems likely that, say 2 - 100 hrs at 500 - 600°C, would allow sufficient oxygen diffusion to re-lock dislocations. In fact a minimum annealing treatment of 90 hours at 900°C (T/Tm = 0.96) was required to regain the yield point.

We conclude that, although oxygen is the most possible dislocation lock, it seems unlikely that it does fulfil this function.

Therefore, considering :

(1) The absence of a suitable impurity to act as a dislocation lock,

(2) The "slow" nature of the yield point,

(3) The sensitivity of the regained yield point to dislocation number,

we conclude that an explanation of the yield point phenomena in terms of the impurity locking theory is not satisfactory.

17.3 Dislocation sources.

It was not possible by direct observation of slip lines to determine whether grown in, fresh (i.e. newly created) or surface dislocations were the operative dislocation sources. However, certain experimental observations allow an indirect assessment of the nature of the sources to be made. The observations were :

(1) The upper yield stress increased as the grown in dislocation density decreased.

(2) The upper yield stress was independent of the surface condition of the specimen.

From these observations, we conclude :

(1) Surface sources are not important.

(2) Fresh dislocations are unlikely to provide many sources. (If fresh dislocations acted as sources and the grown in dislocations only provided a network of pinning points, then the stress to operate a source ($\sigma = G\ b/\ l$) would decrease as the distance between the pinning points increased. Hence the upper yield stress would be expected to decrease as the grown in dislocation density decreased. In fact the reverse condition was observed experimentally).

(3) Grown in dislocations provide most of the operative dislocation sources.

It seems likely that on loading the specimen suitably oriented grown in dislocations can act as sources and emit dislocations. The number of suitably oriented dislocations will depend directly on the grown in dislocation density. Hence the greater the grown in dislocation density the smaller is likely to be the upper yield stress.

18. Other results.

Concurrently with the present research, Patel and his co-workers have been publishing abstracts of their continuing research. Some of their results are as follows:

(1) The upper yield stress of germanium single crystals, deformed in tension between 500 - 700°C, is raised by a factor of 2 on lowering the initial density from 10^6 to 0 cm^{-2}.

(2) The ductile brittle transition temperature is raised on decreasing the specimen dislocation density.

(3) There is a substantial pre yield strain.

(4) A yield point is not regained by reloading or annealing after the lower yield point.

(5) Dissolved gases or contamination have little effect on the yield point.

Points (1), (3) and (5) are in agreement with our own observations. The inability to regain a yield point by annealing was probably due to an insufficient annealing treatment.

Patel measured average dislocation velocities under various stress pulses, by the Stein and Low method. He compared these velocities with those calculated from measurements of the dislocation density and strain rate and concluded that all the dislocations in a sample being deformed are not mobile. However

details of the work are not available and a critical discussion is not possible.

Recently Patel has suggested that the yield point phenomenon in silicon is not an impurity locking effect. Again no details are available and a critical discussion is not possible.

During the writing of this thesis, Alexander[84] has published the results mentioned in the discussion of Van Bueren's model (see Review of Literature). Alexander studied the effect of strain rate and temperature on the flow stress in stages I, II and III of the stress-strain curve. He did not study in detail the yield point and also did not determine the effect of dislocation density on the flow stress. From his results he obtained a similar basic empirical equation of flow stress to that derived by ourselves, i.e. :

$$\sigma \sim \ln \dot{\varepsilon} \quad \exp (1/T)$$

Alexander's plots of stress against temperature show a similar exponential form. However the variation of flow stress with strain rate was only determined at three strain rates and is not very conclusive. The results were discussed in terms of the flow stress models of Haasen and Van Bueren.

Two points of difference between Alexander's results and our own are :

(1) Alexander found that the stress increased slightly with strain during the easy glide region. We found that the stress remained constant during this region. However the difference may be due to a difference in orientation. Alexander's specimens were not oriented so nearly to a direction at the centre of the unit triangle as our own.

(2) Alexander observed that the slope $d\sigma/d\varepsilon$ during stage II is independent of temperature. This is contrary to our observation that the slope does vary with temperature. It does not also seem compatible with our observations that the post yield flow stress is temperature dependent.

ACKNOWLEDGEMENTS

It is a pleasure to record my appreciation of the stimulating supervision of Dr. R. L. Bell during the three years of this project. I am also indebted to Professor J. G. Ball for the provision of the laboratory facilities, and to Dr. W. Bardsley, of the Royal Radar Establishment, for the supply of germanium single crystals. Finally, I gratefully acknowledge the maintenance support received from the Department of Scientific and Industrial Research.

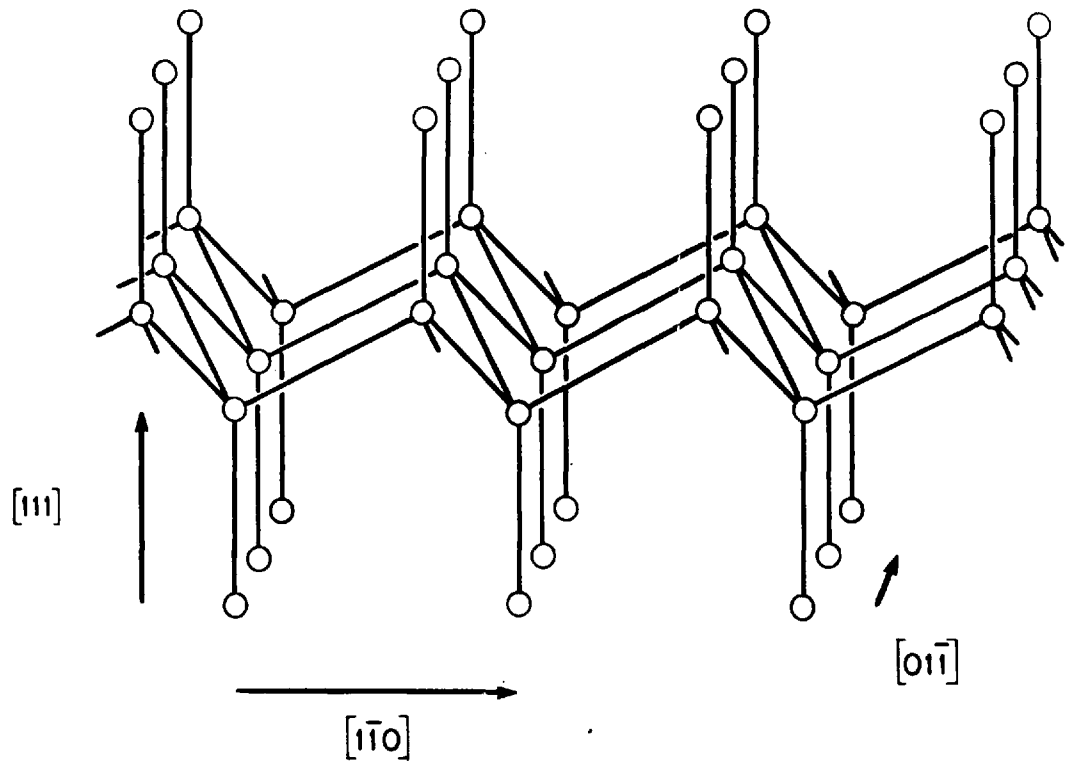

FIGURE 1a Normal diamond structure (after Schockley).

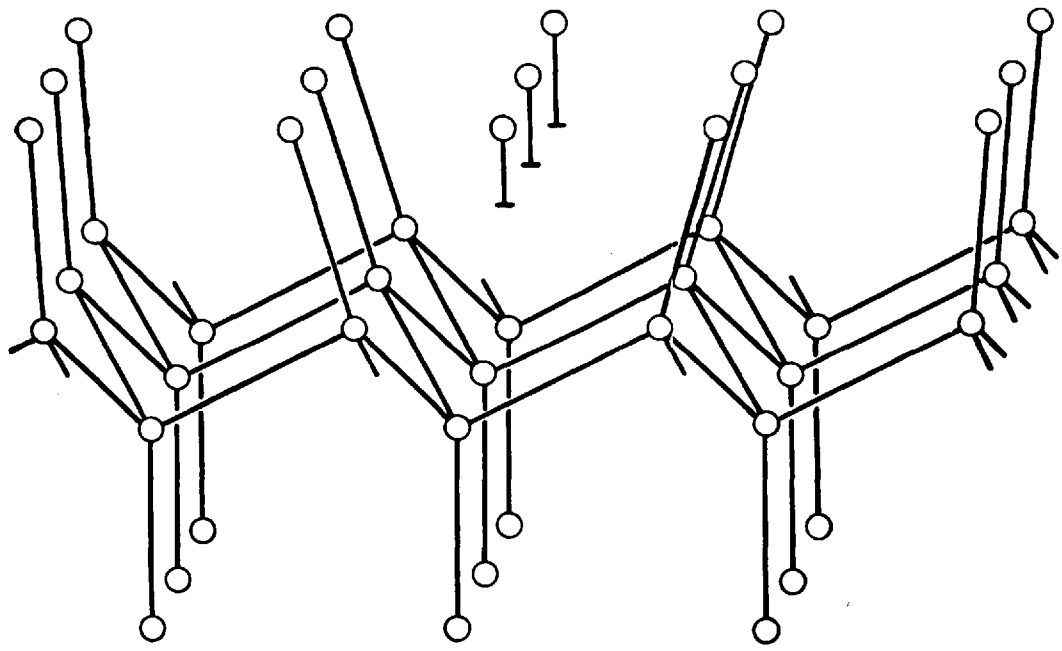

FIGURE 1b 60° dislocation (after Schockley).

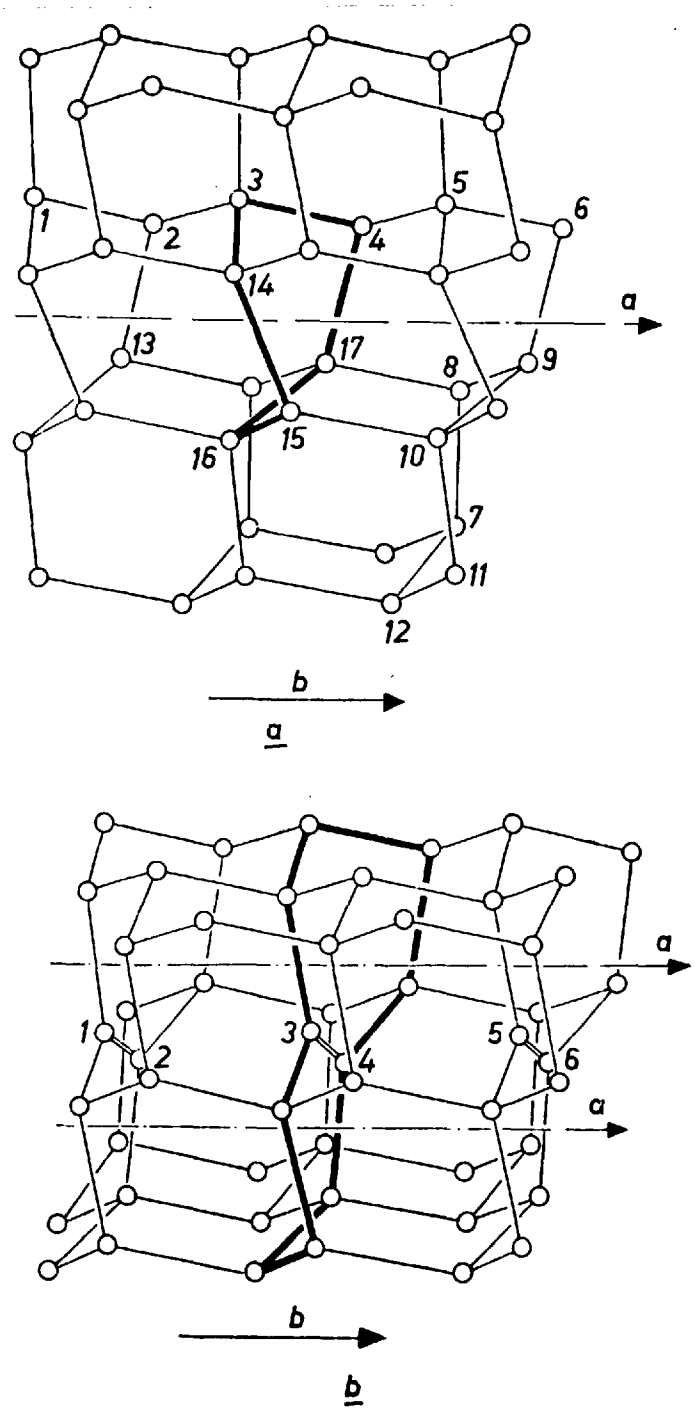

FIGURE 2. Screw dislocation (after Hornstra)
(a) Simplest form.
(b) Alternative form with double bonds
a - axis b - Burgers vector.

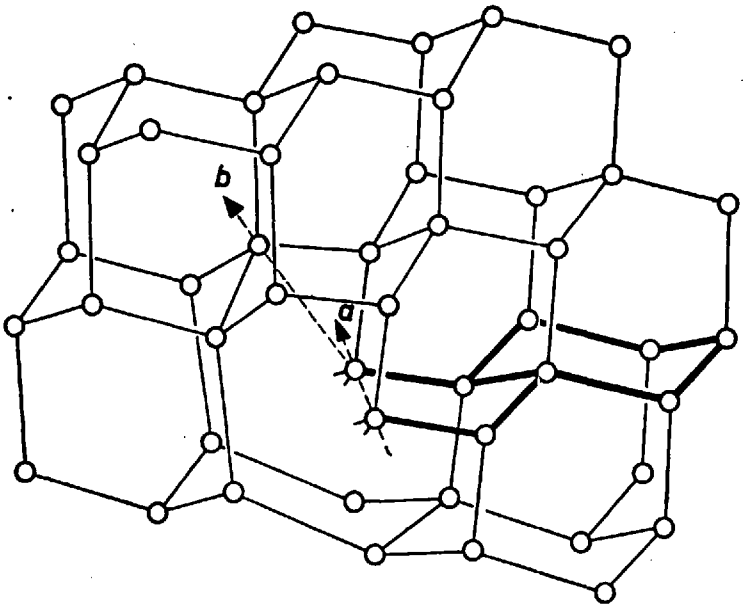

a

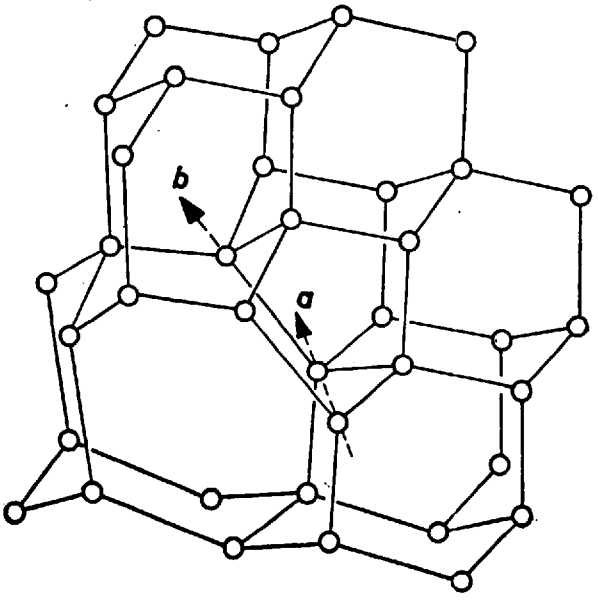

b

FIGURE 3 Edge dislocation (after Hornstra)
(a) Simplest form.
(b) Alternative form without dangling bonds.
a - axis. b - Burgers vector.

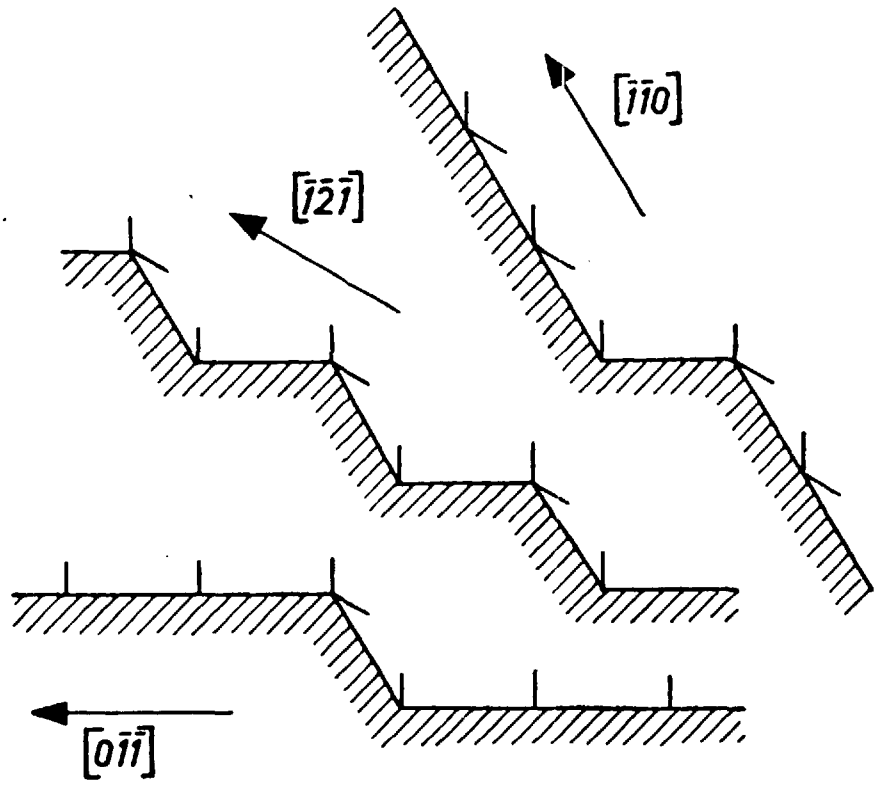

FIGURE 4. Schematic drawing of edge of the extra half plane of three dislocations with the same Burgers vector ⟨ 110 ⟩ (After Hornstra).

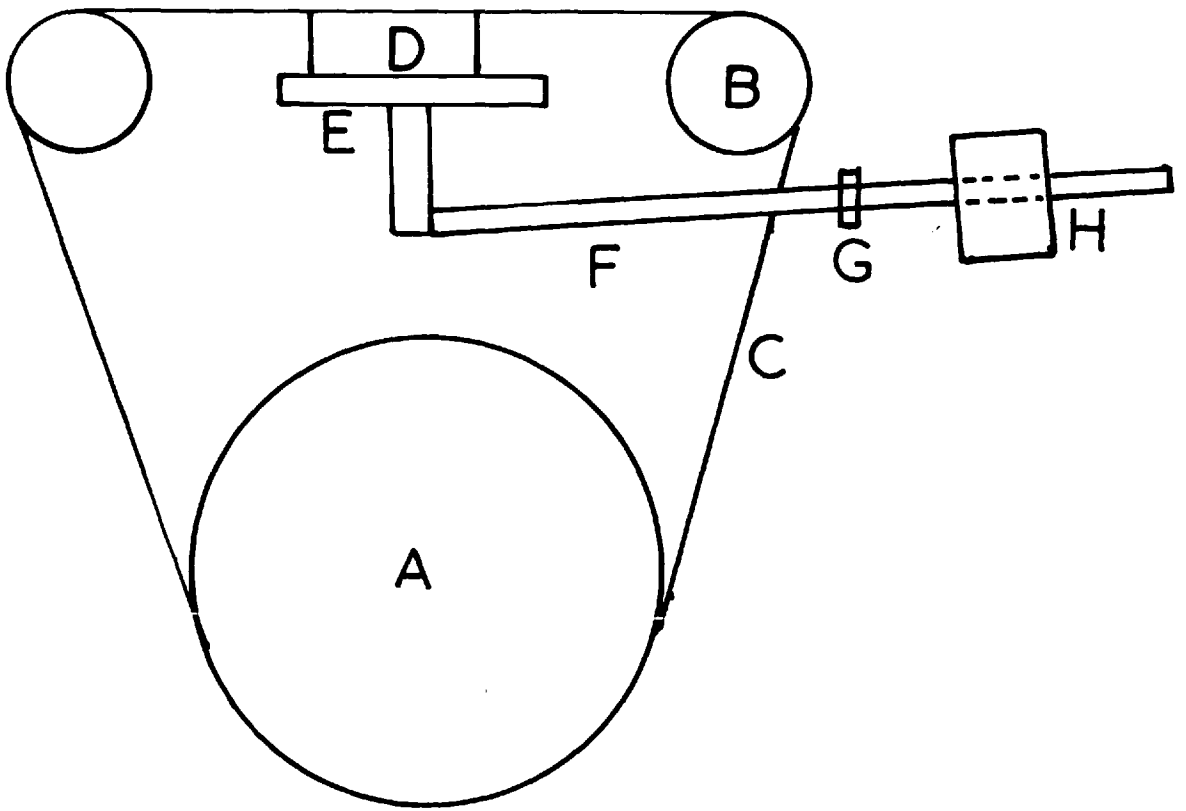

FIGURE 5. Diagram of the wire saw.

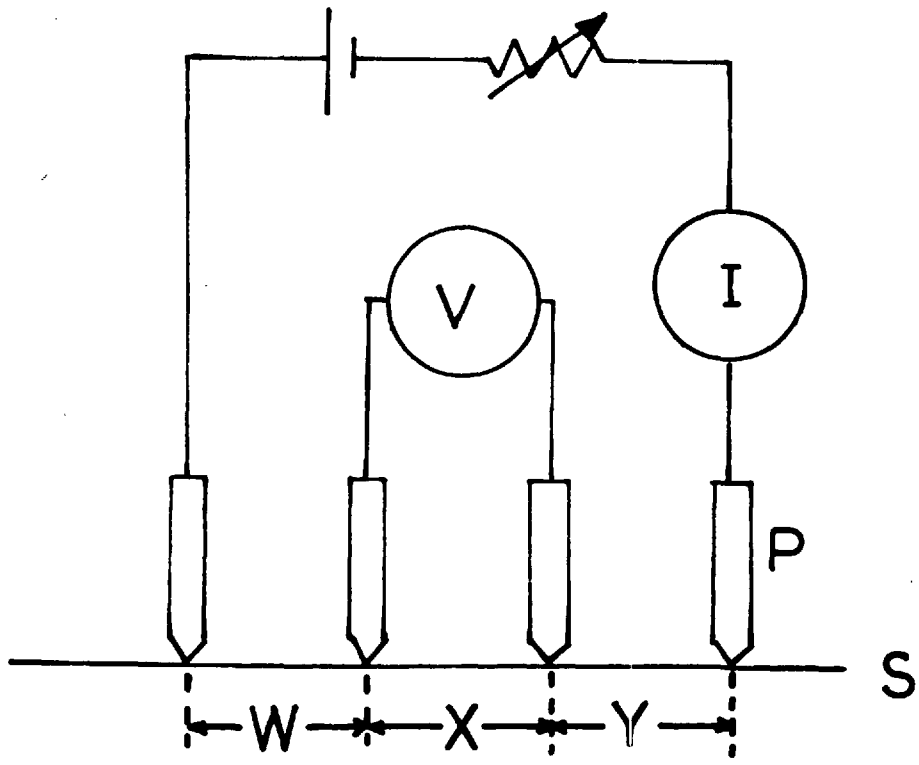

FIGURE 6 The principle of the four probe method.

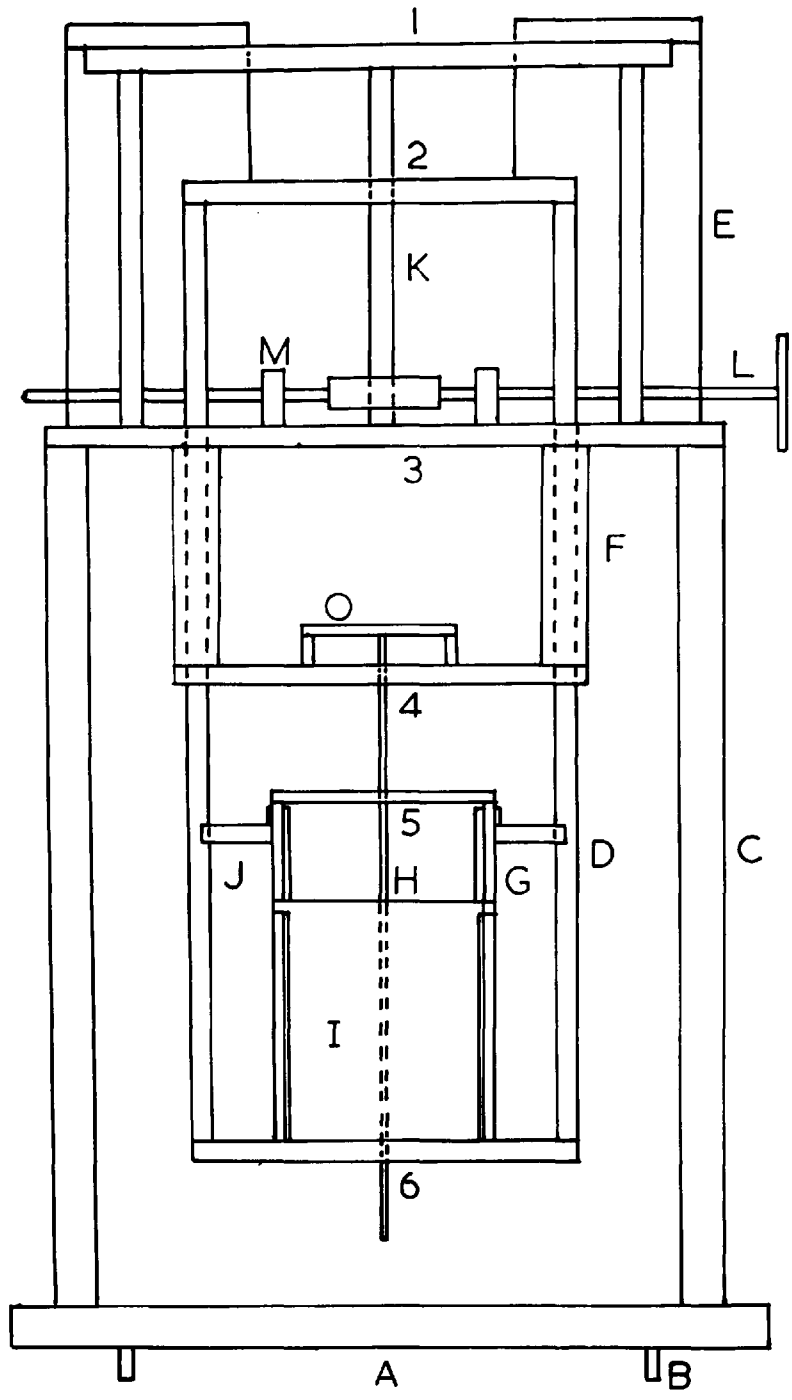

FIGURE 7 Schematic arrangement of tensile machine.

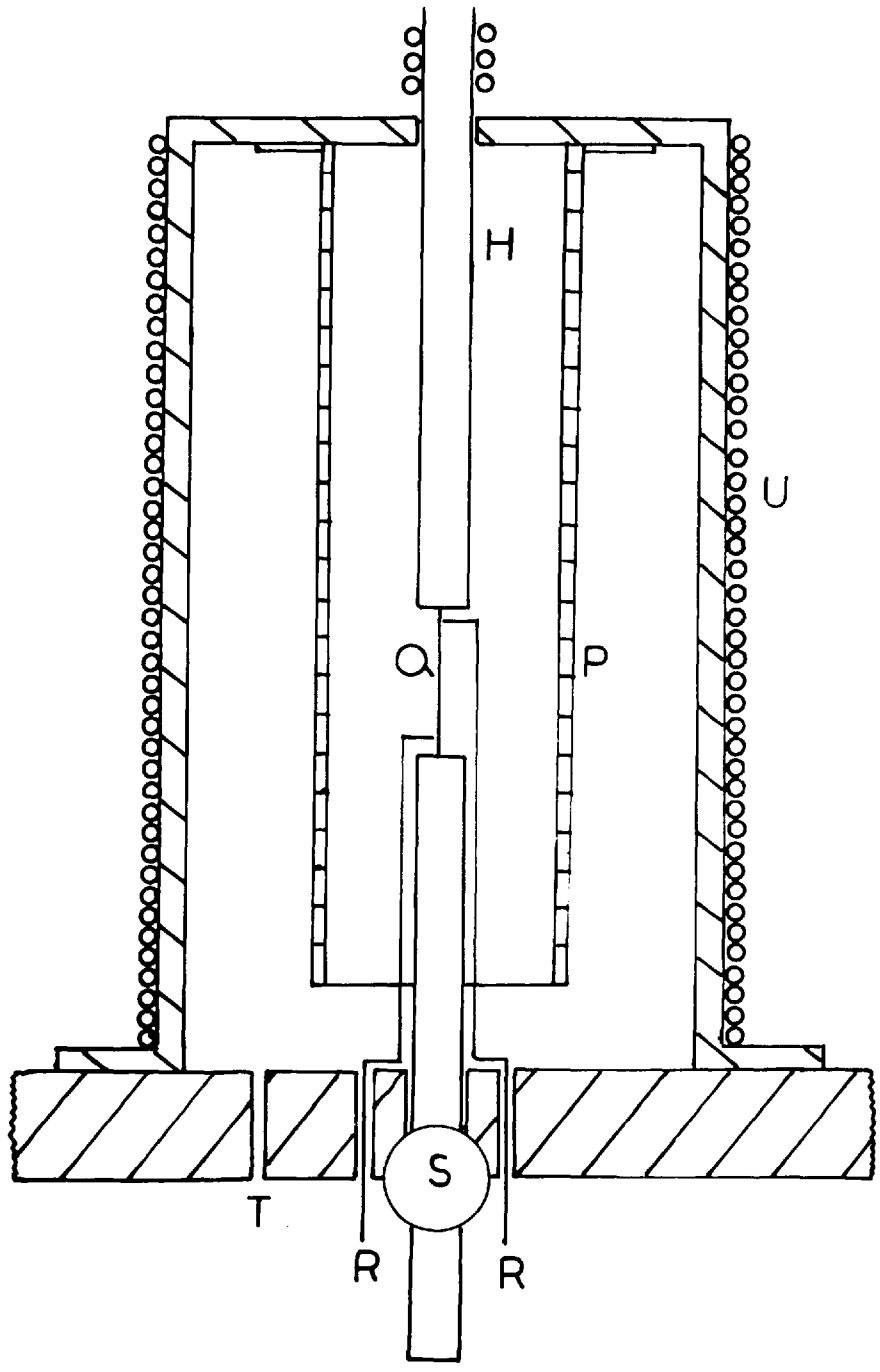

FIGURE 8 Schematic arrangement of furnace.

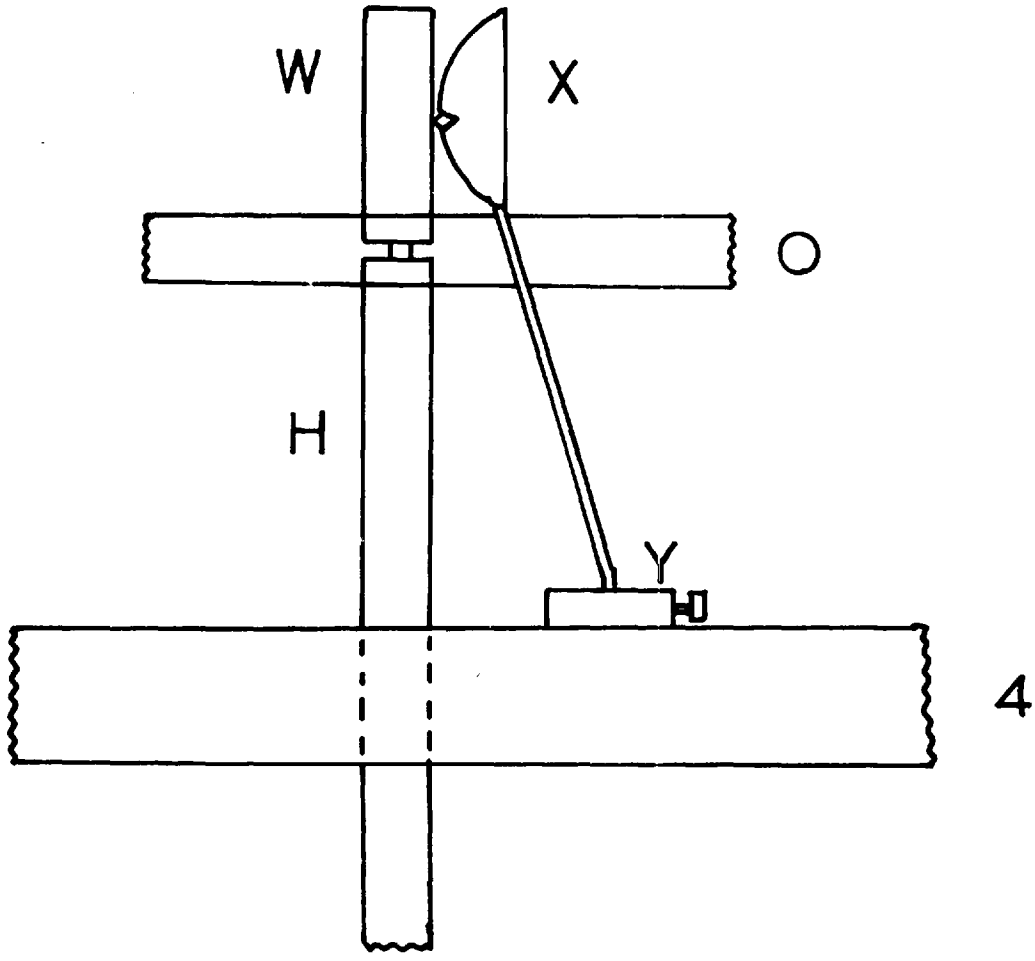

FIGURE 9 Details of deflection measurement.

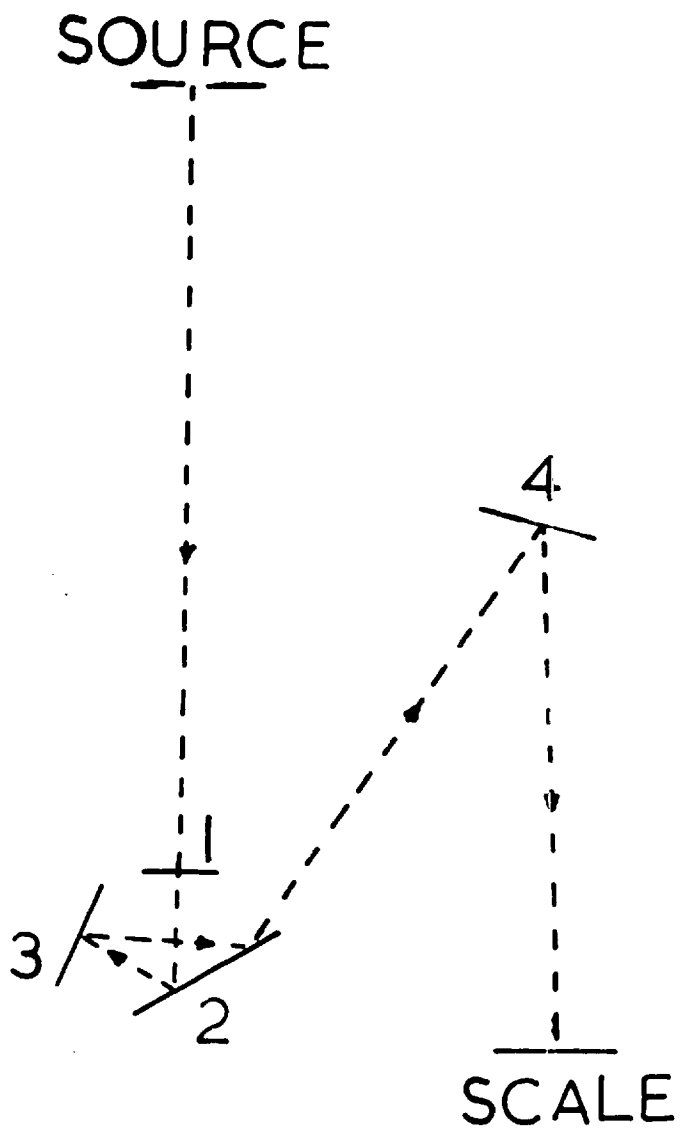

FIGURE 10 Arrangement of optical system.

(1) Convex lens. (2) Plane mirror on rhomb.
(3) Plane mirror. (4) Plane mirror.

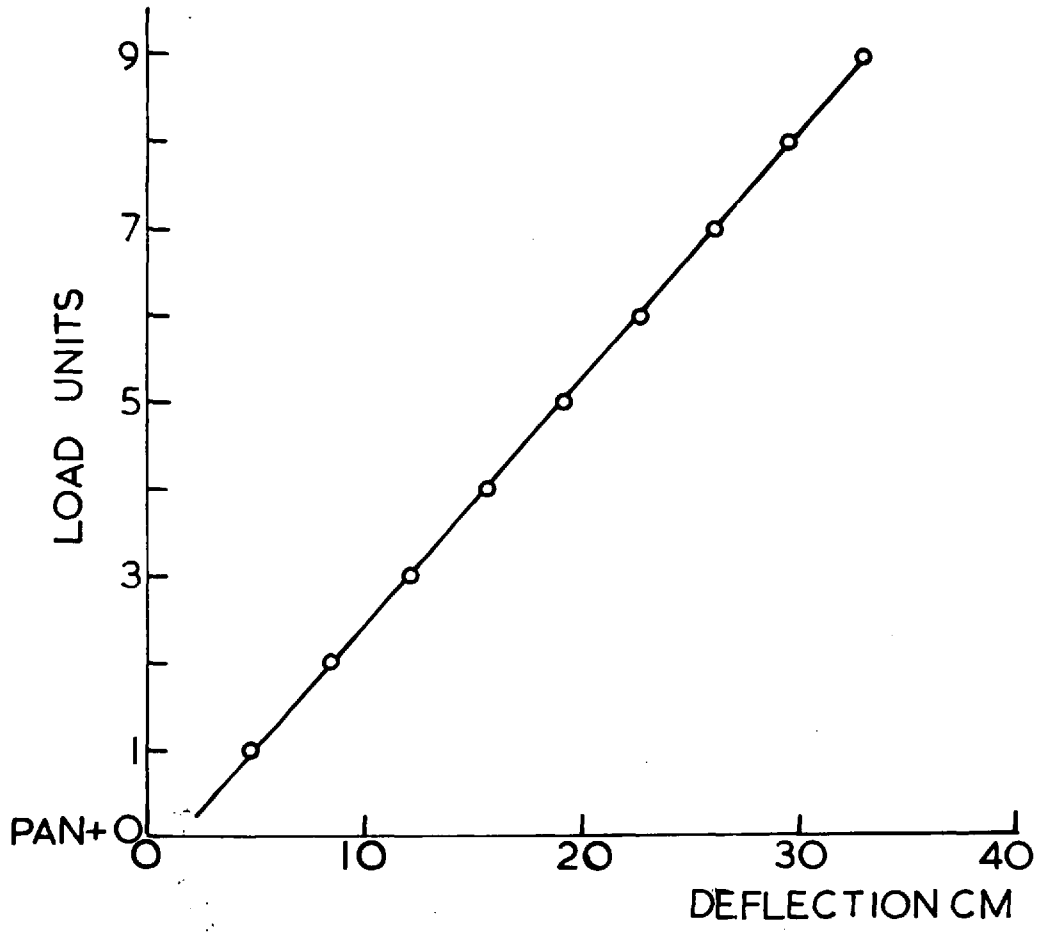

FIGURE 11 Calibration of beam deflection.

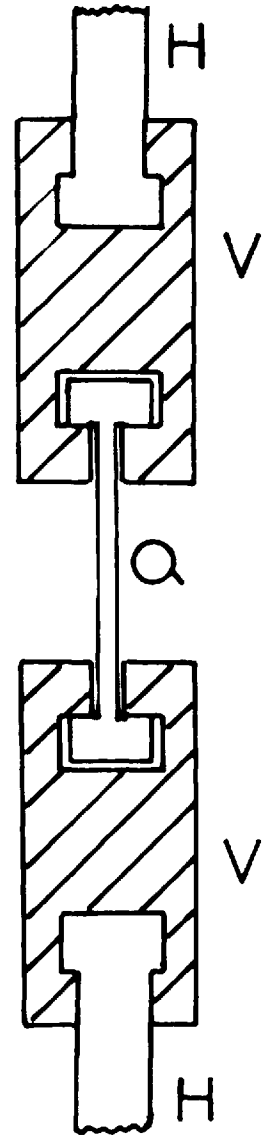

FIGURE 12. Specimen - chuck arrangement.

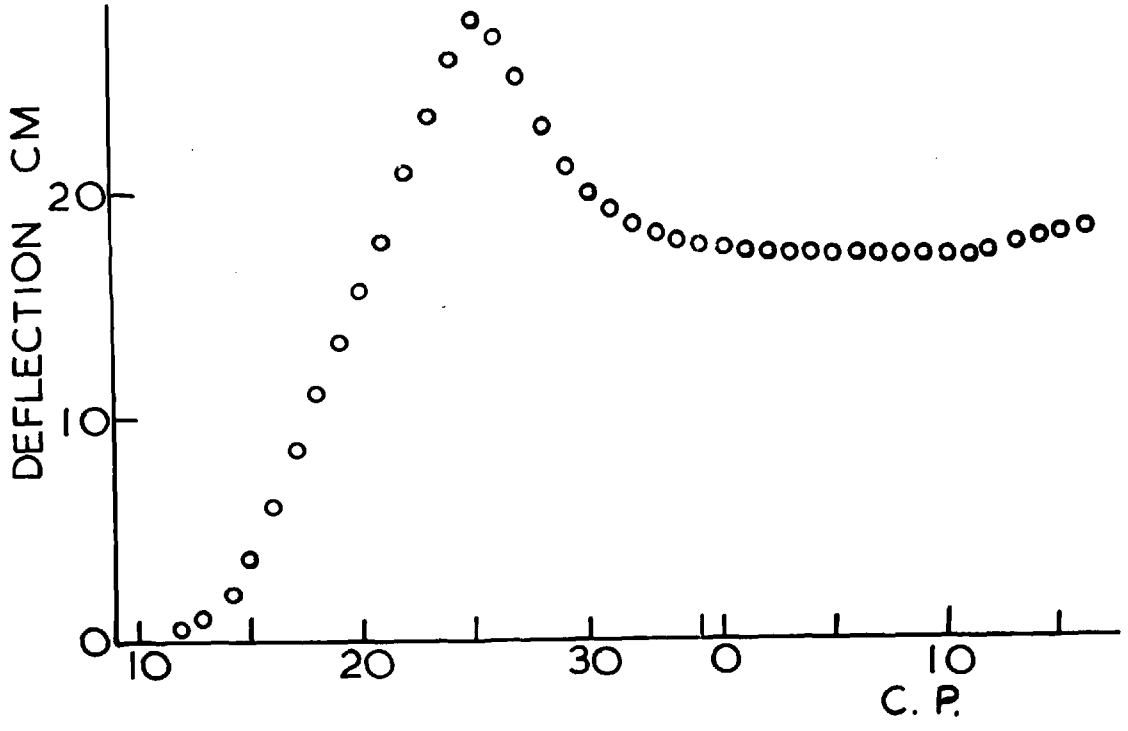

FIGURE 13a. Experimental graph of deflection (load) versus carriage position (extension). Type A specimen, strain rate 1 x 10^{-4} $sec.^{-1}$ temperature 560°C.

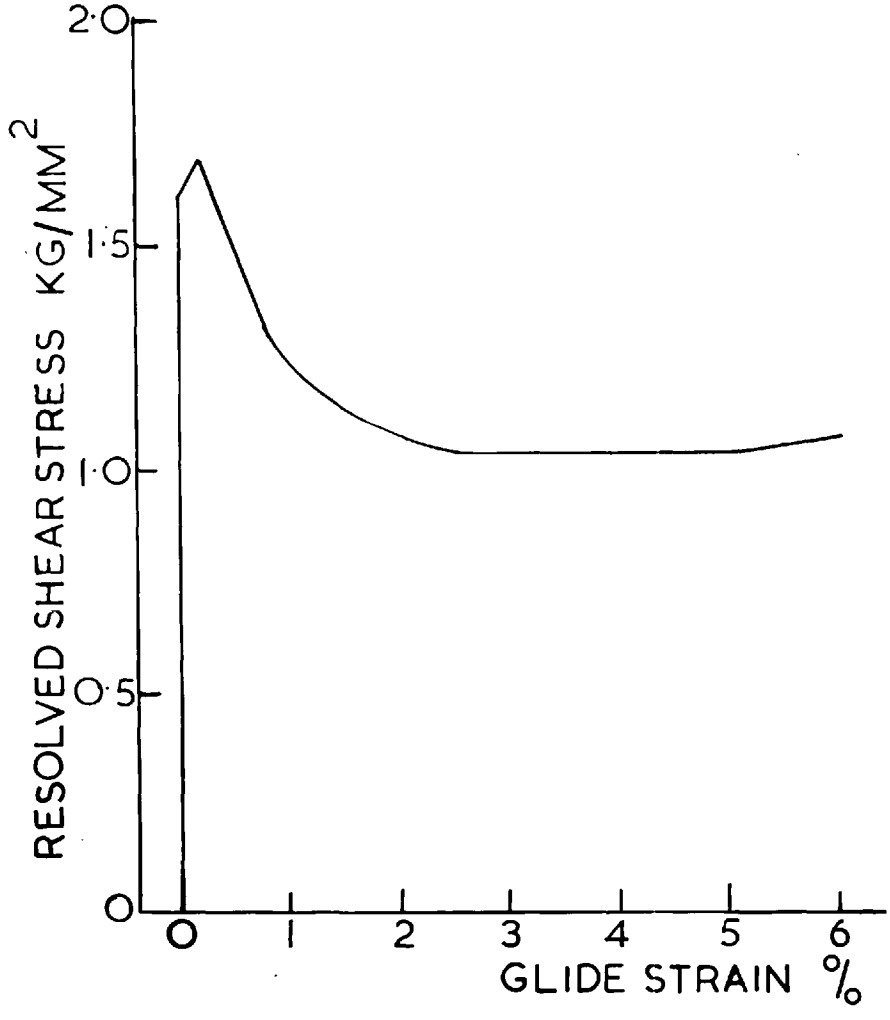

FIGURE 13b Derived graph of resolved shear stress versus glide strain.
Type A specimen, strain rate 1 x 10^{-4} sec.$^{-1}$ temperature 560^{0}C.

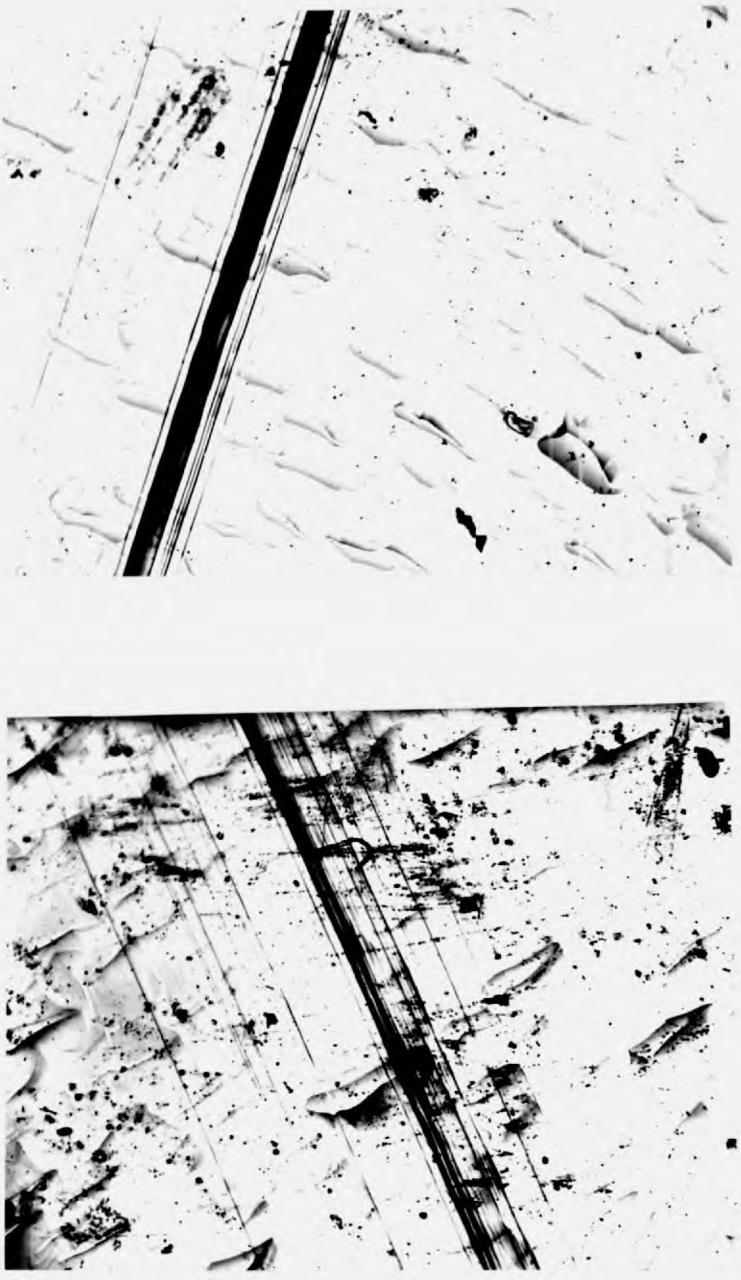

FIGURE 14. Luders band. x 740.

FIGURE 15. Dislocation configuration at the lower yield point. ($\rho = 7 \times 10^{6} cm^{-2}$) x.640.

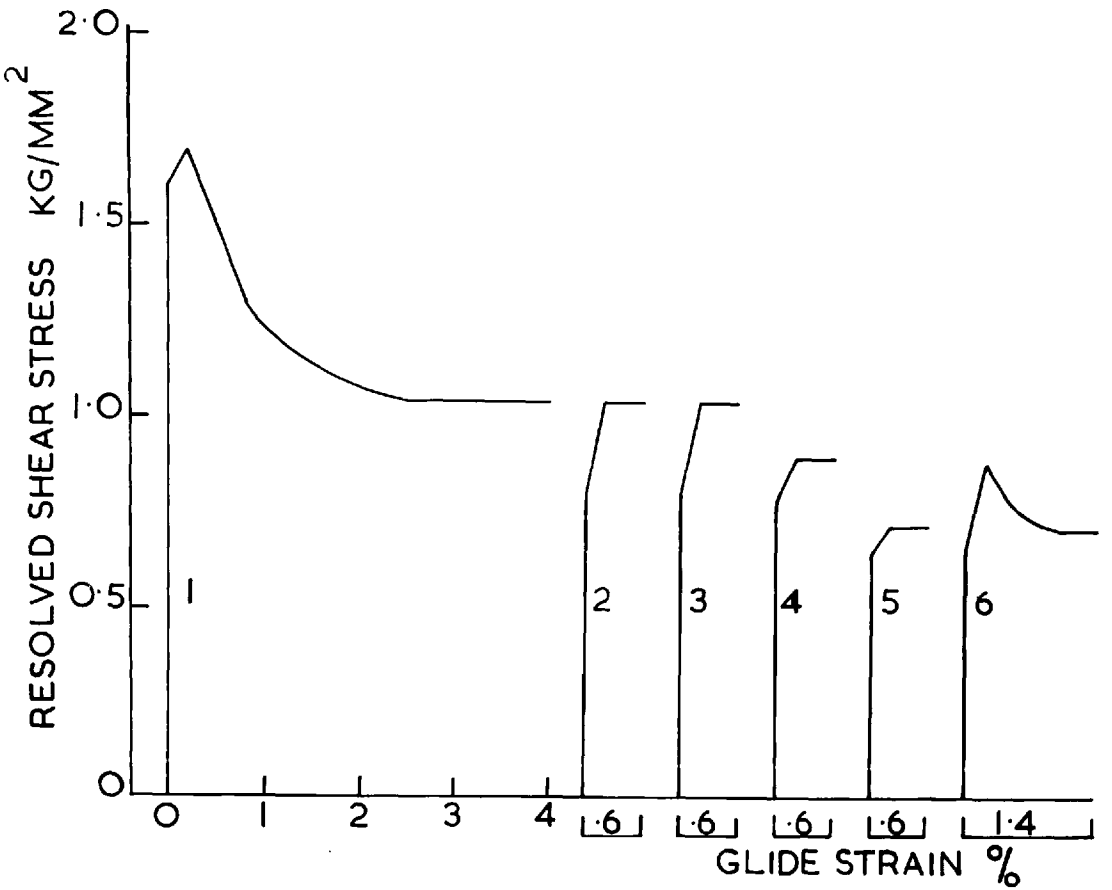

FIGURE 16. Type A specimens, strain rate $1 \times 10^{-4} sec^{-1}$, Temperature 560°C.

(1) First loading.
(2) Effect of unloading, reloading.
(3) Testing after anneal at 600°C for 70 hrs.
(4) Testing after anneal at 700°C. for 70 hrs.
(5) Testing after anneal at 800°C for 70 hrs.
(6) Testing after anneal at 900°C. for 236 hrs.

FIGURE 17. Dislocation configuration after anneal at 800°C for 70 hrs. ($\rho = 5 \times 10^5$ cm^{-2}) x 440.

FIGURE 18. Dislocation configuration after anneal at 900°C for 236 hrs. ($\rho = 9 \times 10^4 cm^{-2}$) x 440.

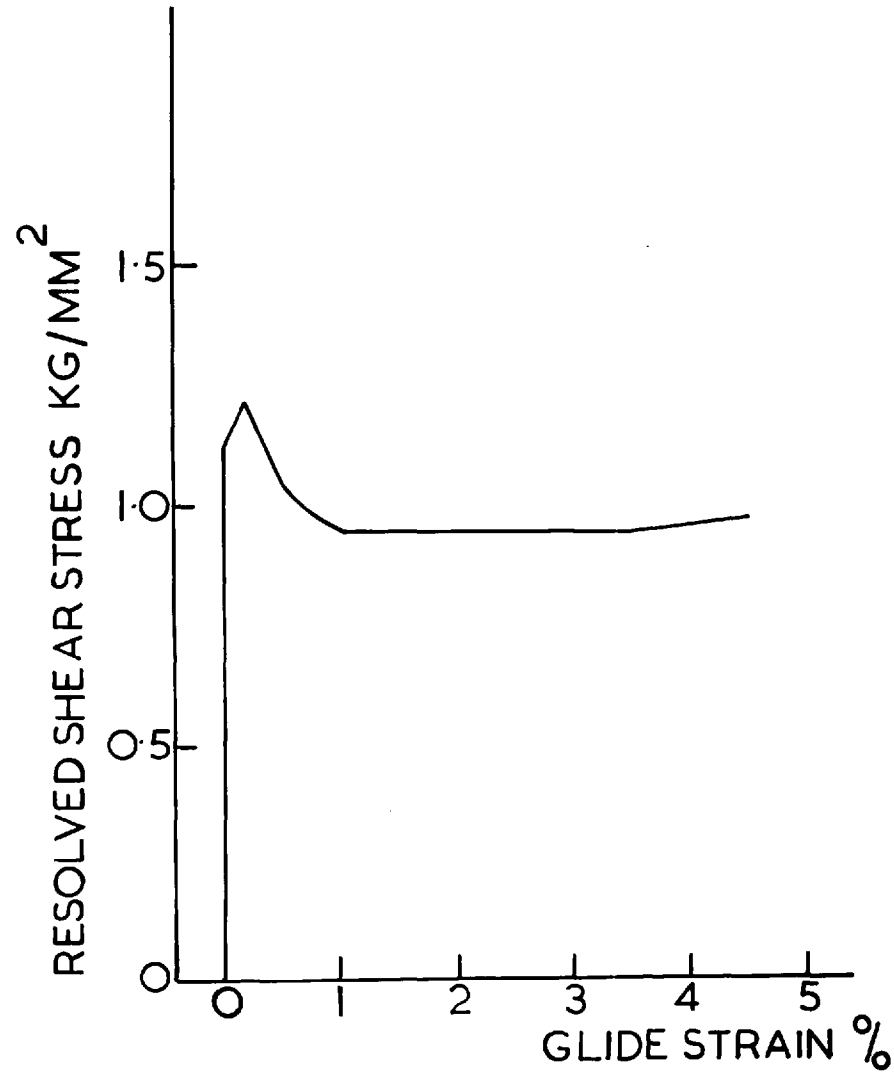

FIGURE 19. Type B specimen, strain rate 1 x 10^{-4} sec^{-1} temperature 620°C.

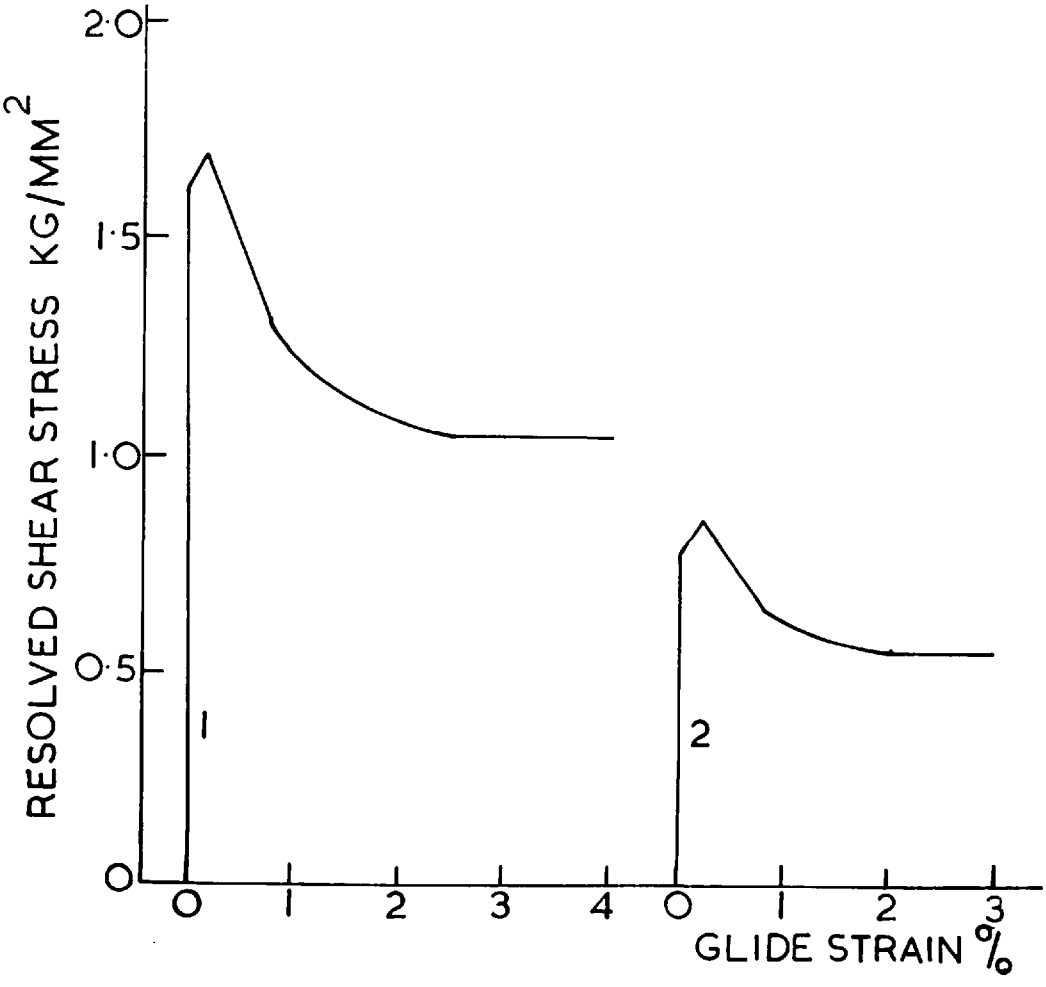

FIGURE 20 (1) Type A specimen, strain rate 1 x 10^{-4} sec^{-1} Temperature 560°C.
(2) Type A specimen, strain rate 2 x 10^{-5} sec^{-1} Temperature 560°C.

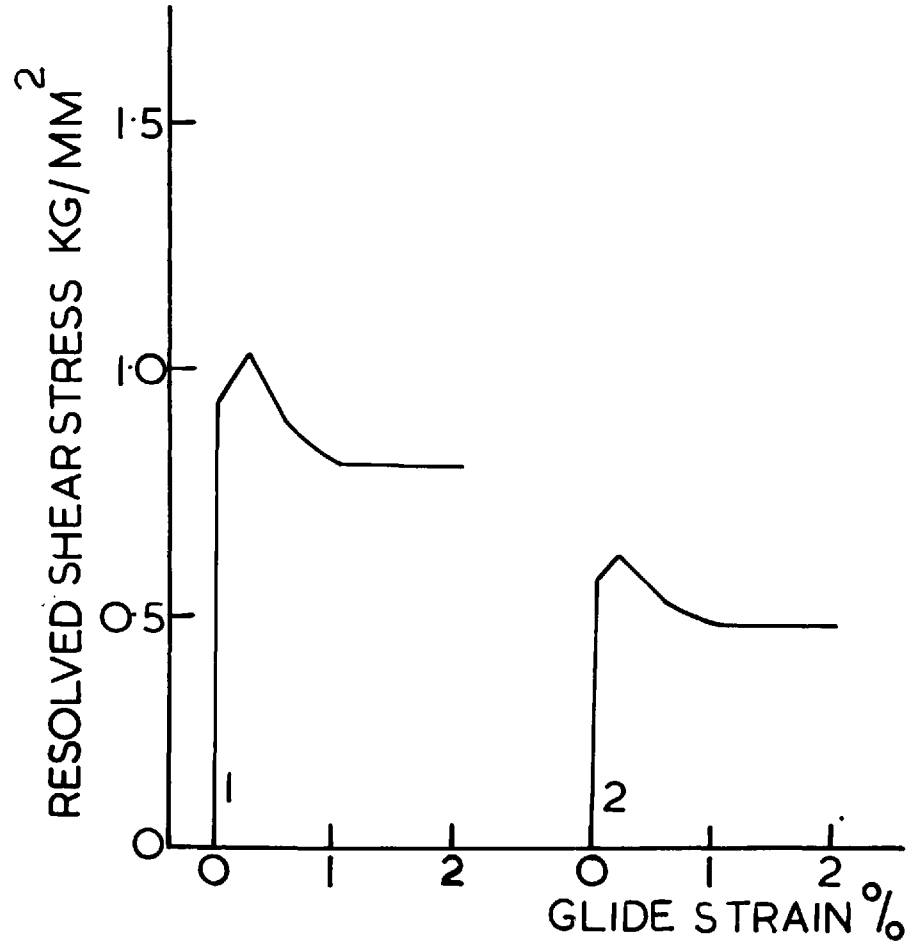

FIGURE 21 (1) Type B specimen, strain rate 1 x 10^{-4} sec^{-1} Temperature 650°C.
(2) Type B specimen, strain rate 2 x 10^{-5} sec^{-1} Temperature 650°C.

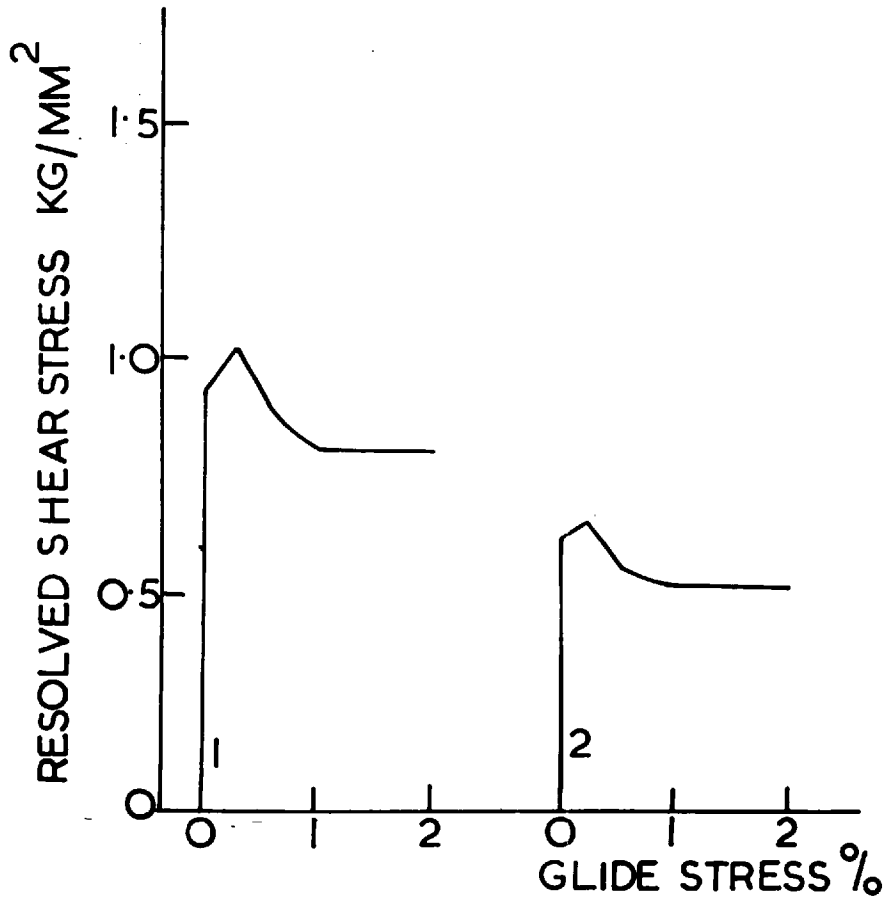

FIGURE 22. (1) Type B specimen. Strain rate 1 x 10^{-4} sec^{-1} Temperature 650°C.
(2) Type A specimen. Strain rate 1 x 10^{-4} sec^{-1} Temperature 650°C.

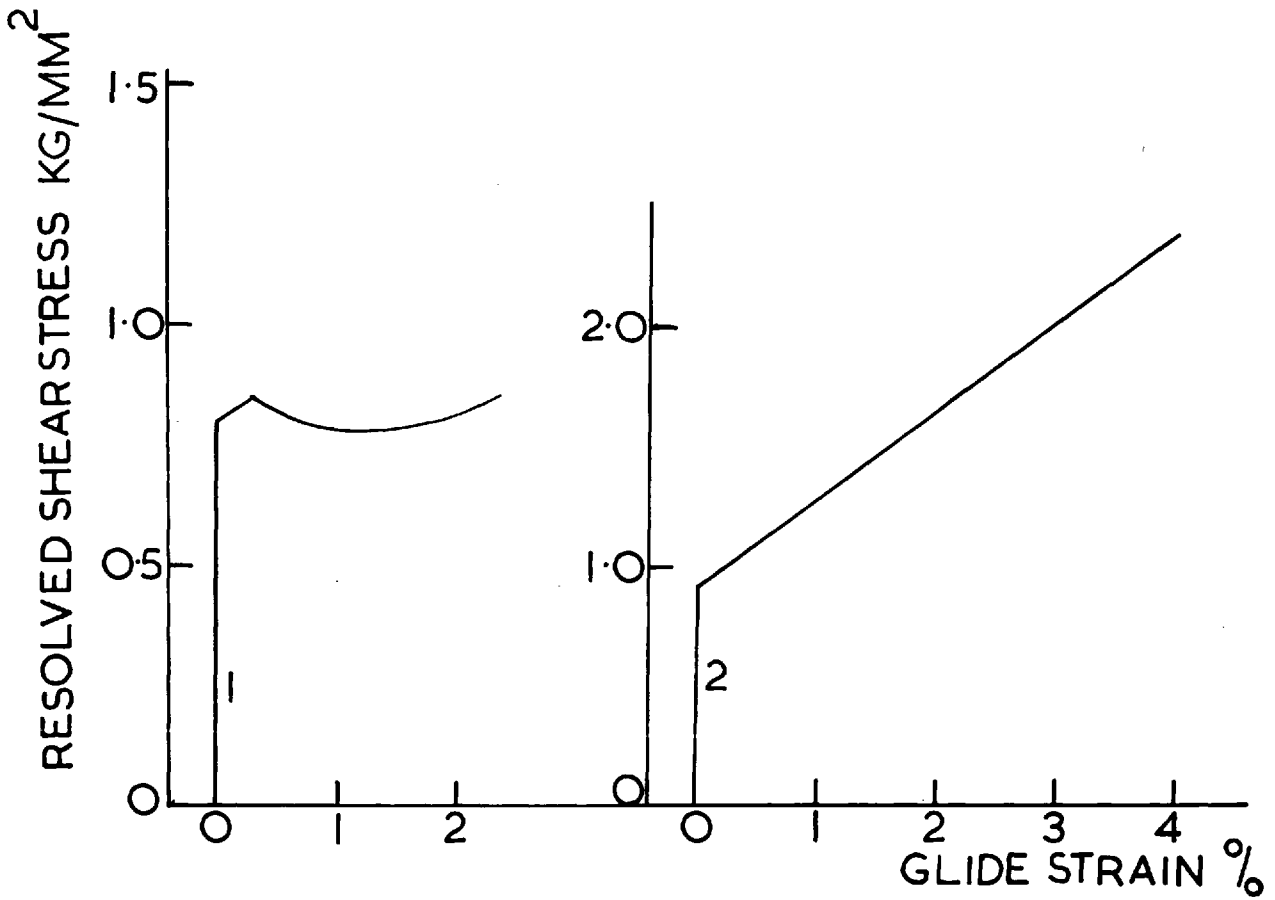

FIGURE 23. The effect of orientation.
Type A specimens, strain rate 1 x 10^{-4}sec^{-1}, temperature 560°C
(1) Orientation near 111 110 boundary (2) <111> orientation.

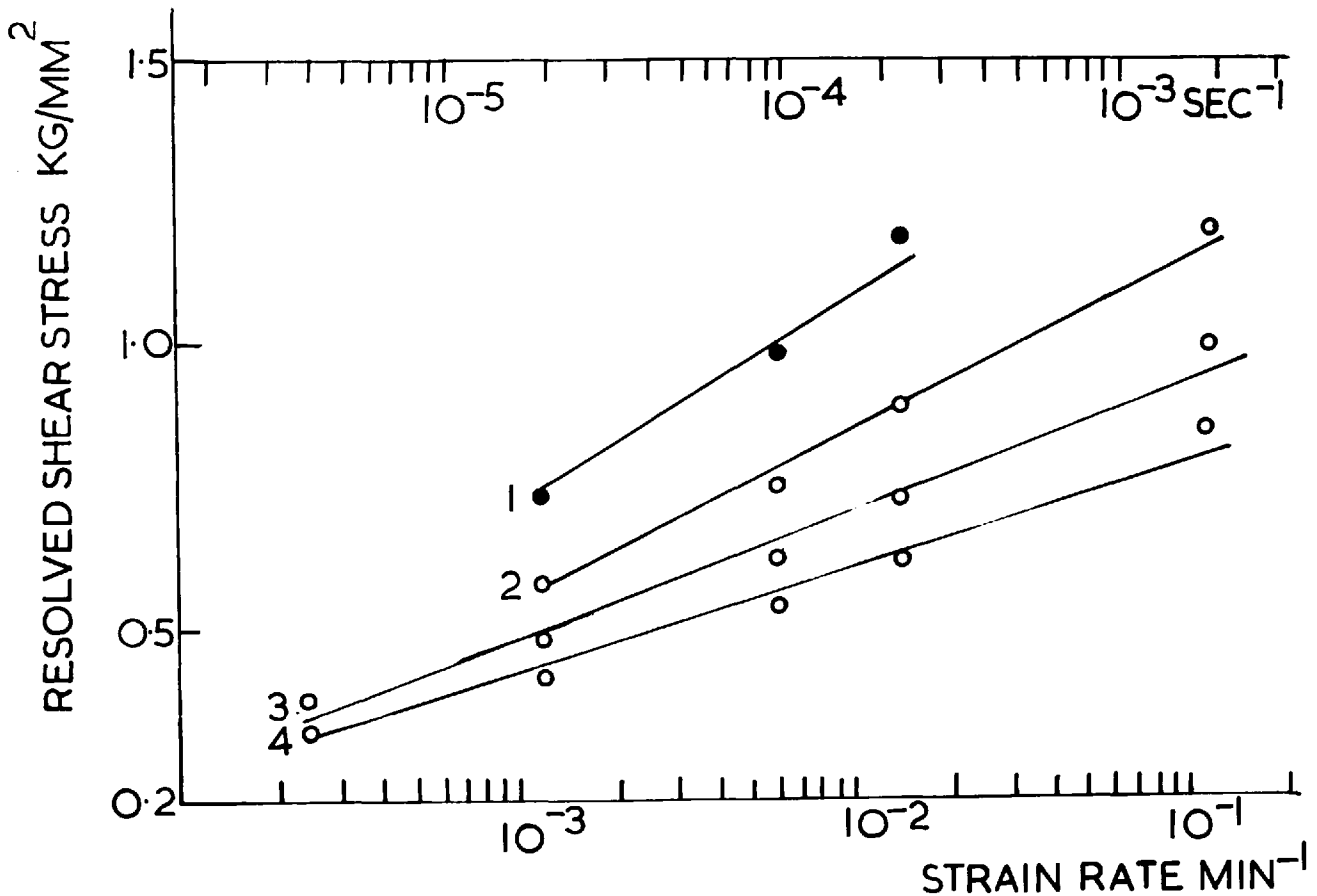

FIGURE 24. Type A specimens.
(1) Deformed specimen at 560°C. (2) Annealed specimen at 560°C.
(3) Annealed specimen at 620°C. (4) Annealed specimen at 670°C.

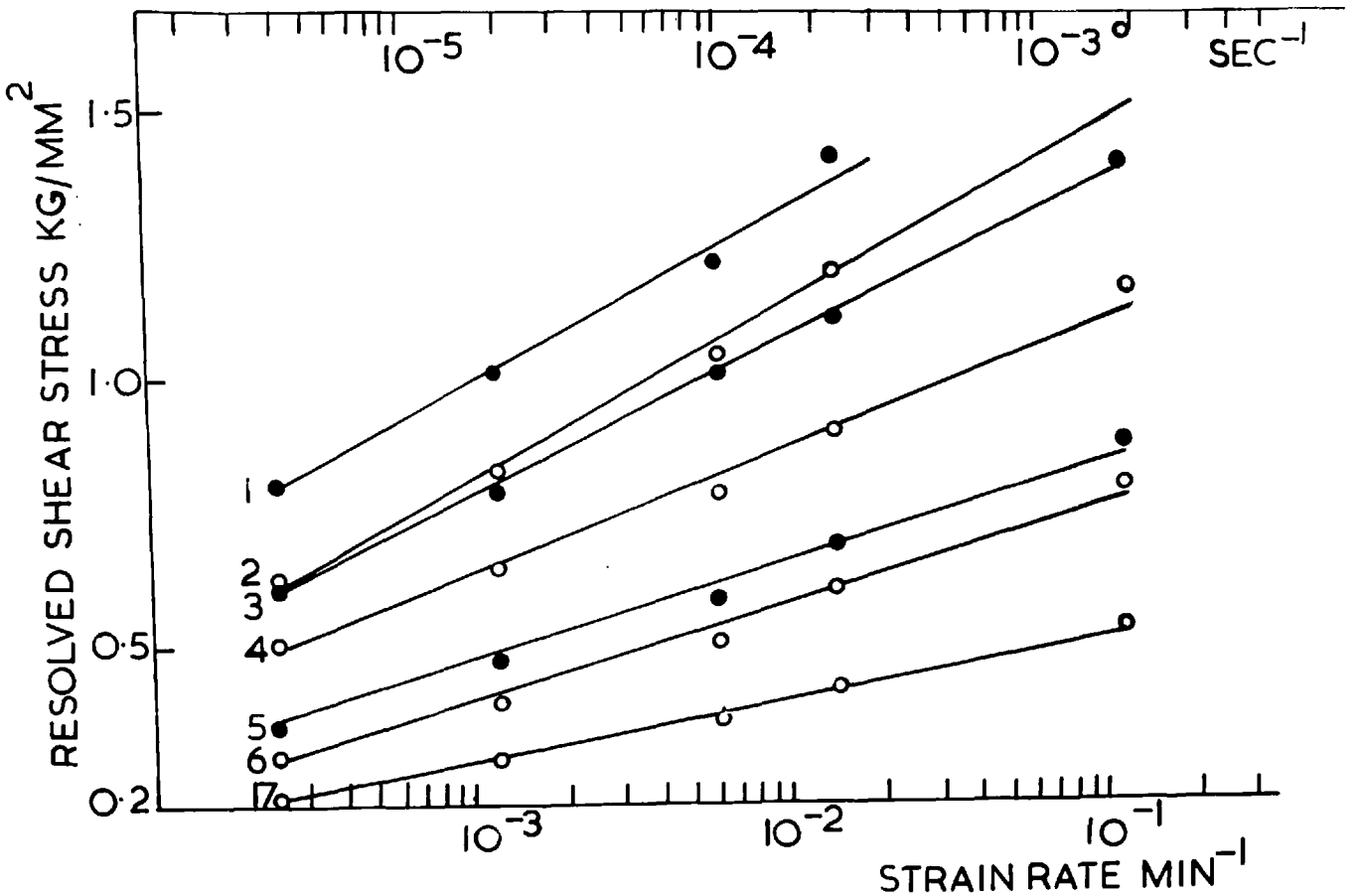

FIGURE 25 Type B specimens.

(1) Deformed specimen at 560°C.
(2) Annealed specimen at 560°C.
(3) Deformed specimen at 620°C.
(4) Annealed specimen at 620°C.
(5) Deformed specimen at 705°C.
(6) Annealed specimen at 705°C.
(7) Annealed specimen at 775°C.

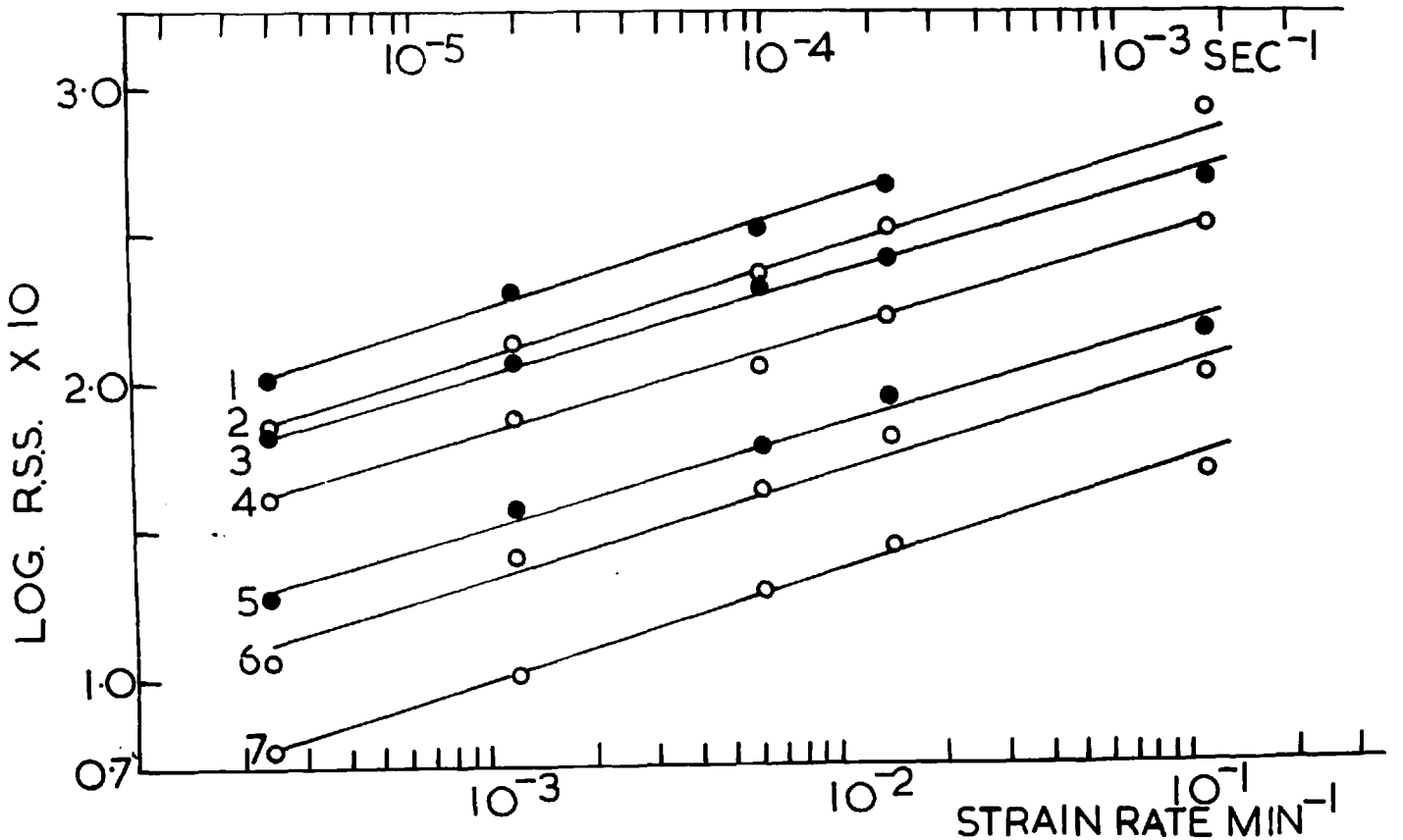

FIGURE 26 Type B specimens.

(1) Deformed specimens at 560°C.
(2) Annealed specimens at 560°C.
(3) Deformed specimens at 620°C.
(4) Annealed specimens at 620°C.
(5) Deformed specimens at 705°C.
(6) Annealed specimens at 705°C.
(7) Annealed specimens at 775°C.

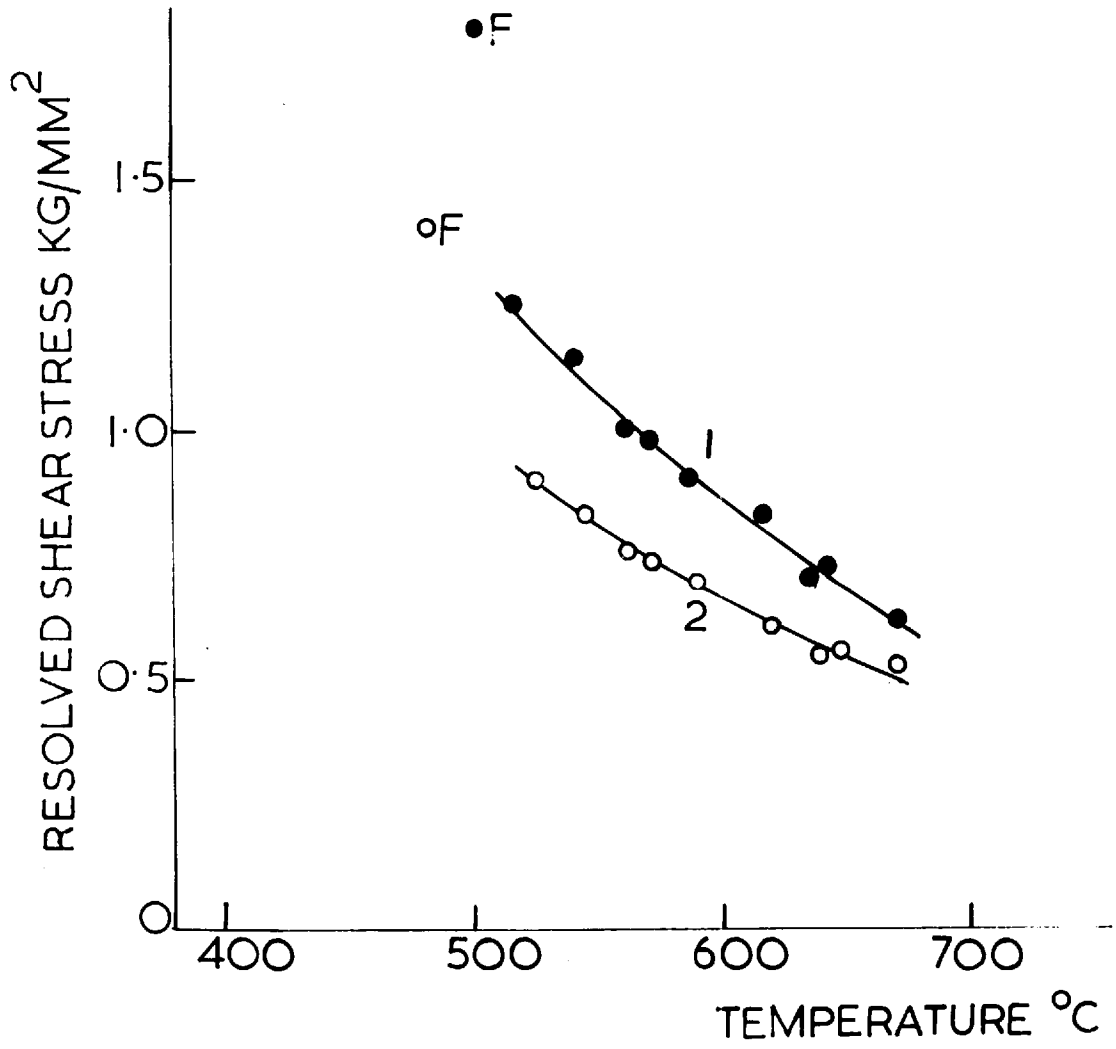

FIGURE 27 Type A specimens.
(1) Deformed specimens at 1 x 10^{-4} sec^{-1}.
(2) Annealed specimens at 1 x 10^{-4} sec^{-1}.

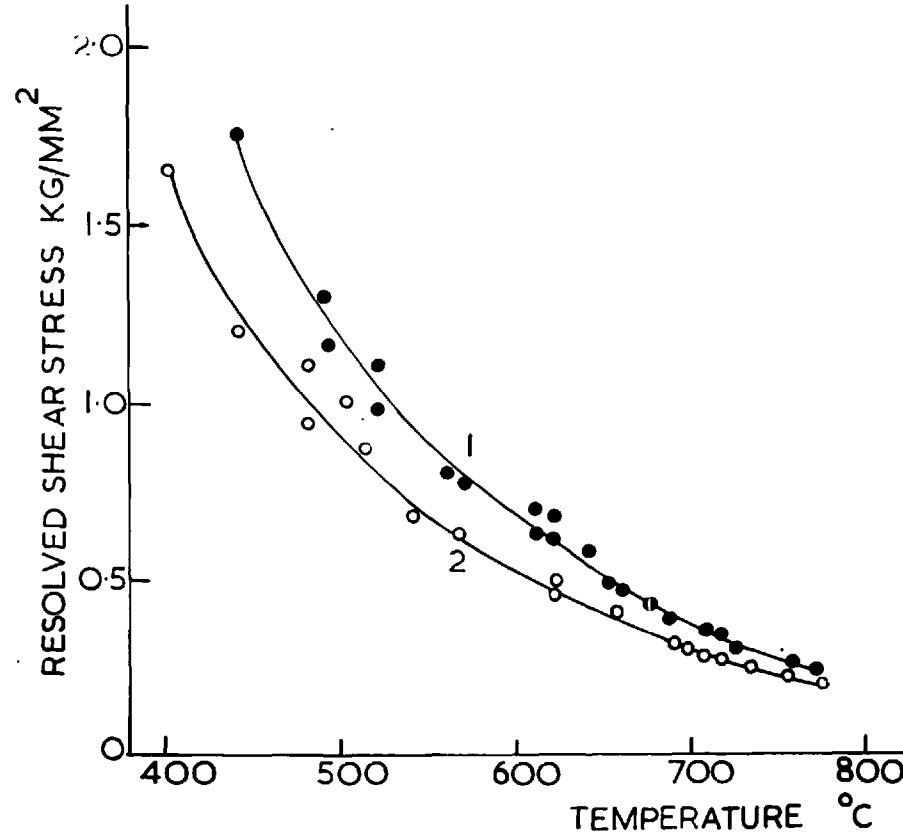

FIGURE 28 Type B specimens.
(1) Deformed specimens at $4 \times 10^{-6} sec^{-1}$.
(2) Annealed specimens at $4 \times 10^{-6} sec^{-1}$.

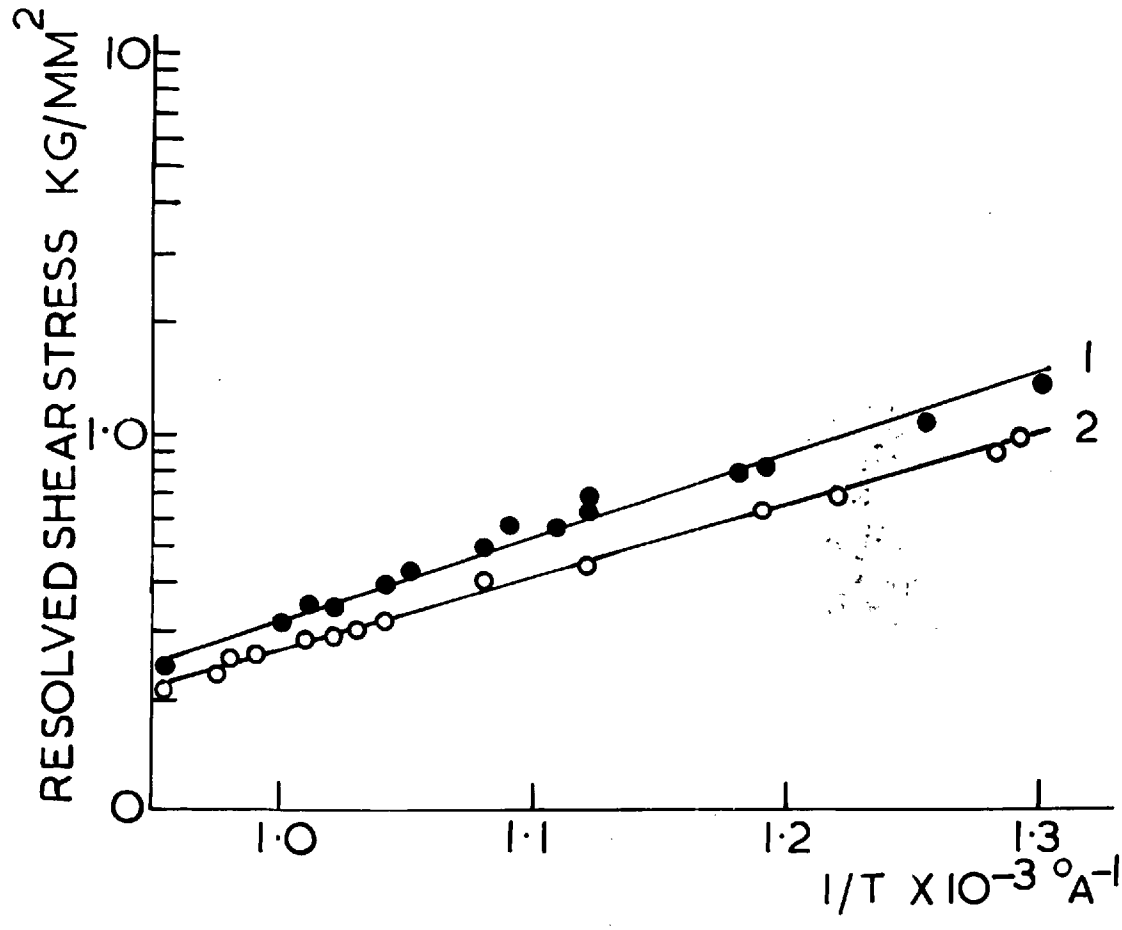

FIGURE 29 Type B specimens.
(1) Deformed specimens at $4 \times 10^{-6} sec^{-1}$.
(2) Annealed specimens at $4 \times 10^{-6} sec^{-1}$.

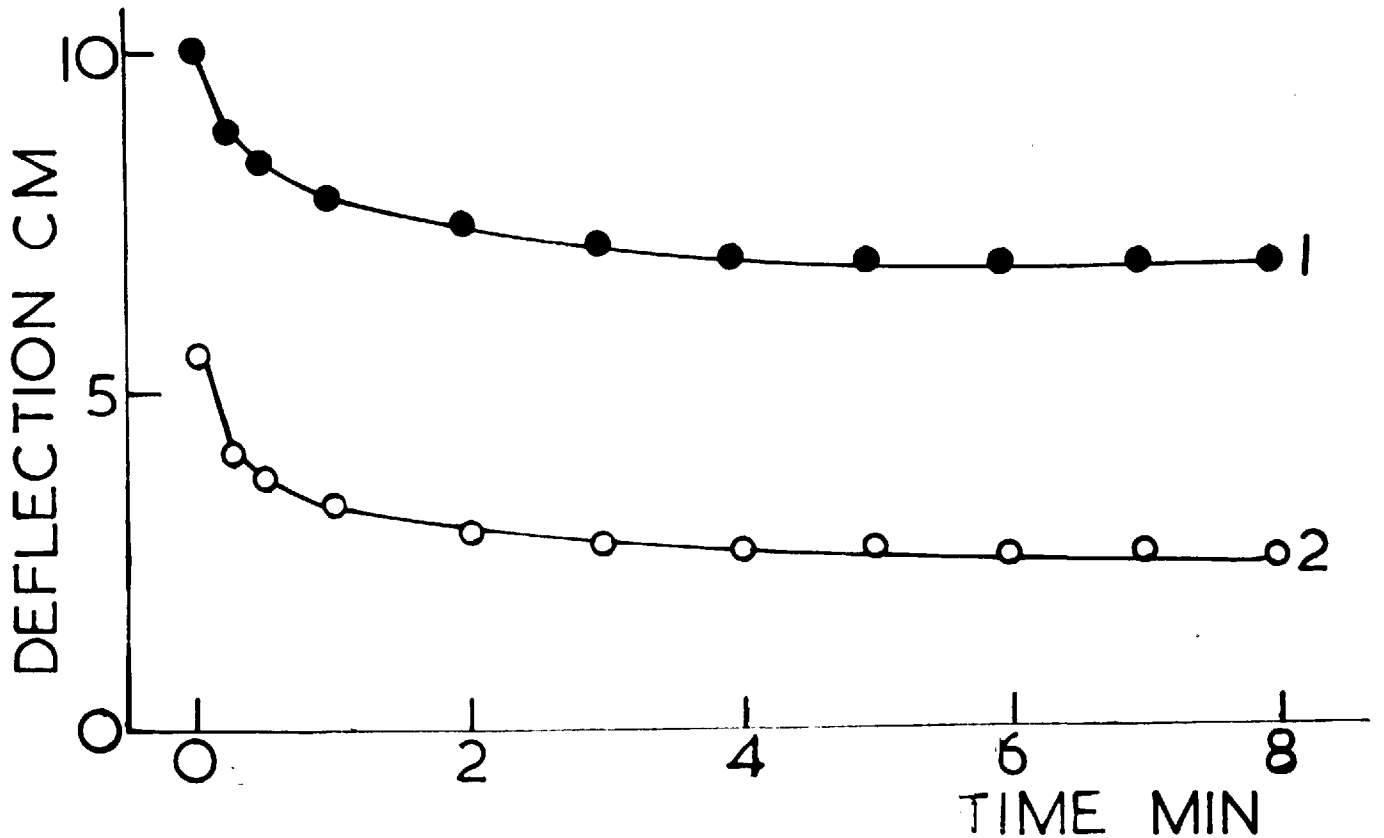

FIGURE 30 The relaxation of deflection (load) with time.
(1) Deformed specimen. (2) Annealed specimen.

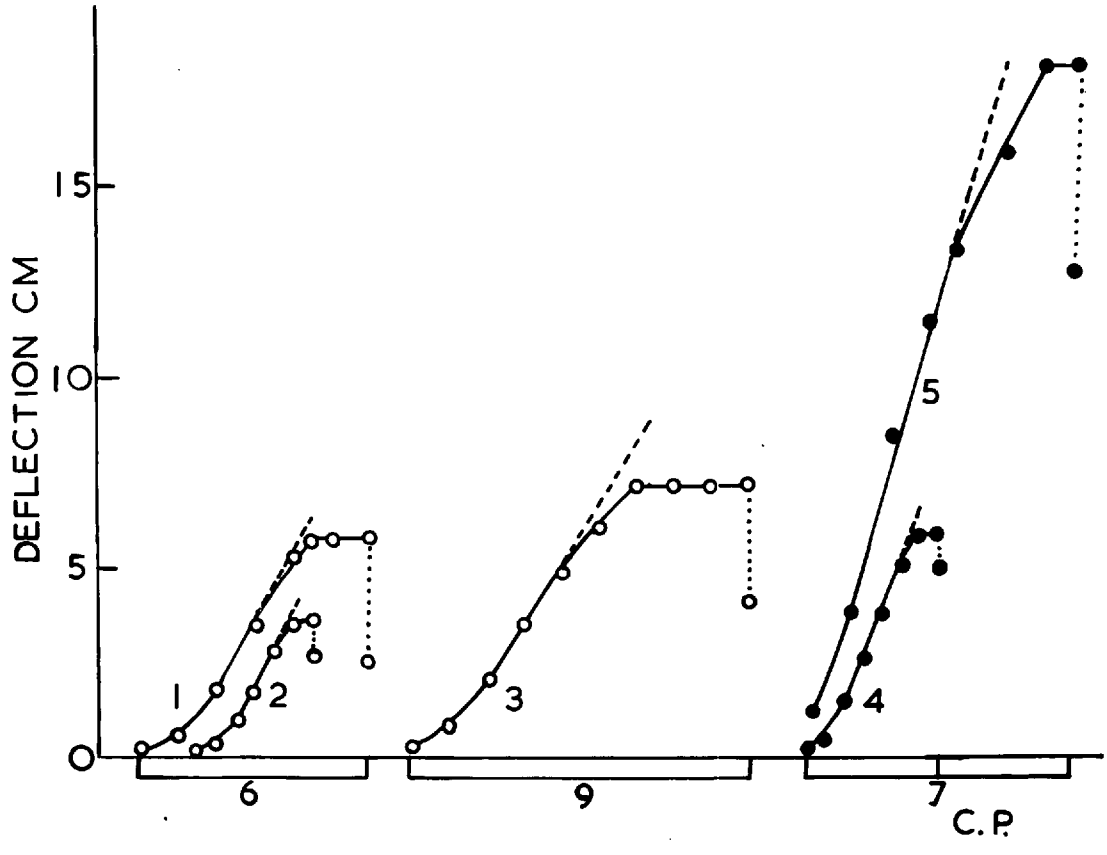

FIGURE 31 Relaxed stress effects.

(1) Type B annealed specimen, temperature 620°C. strain rate 1 x 10^{-4} sec^{-1}.

(2) Type B annealed specimen, temperature 620°C. strain rate 2 x 10^{-5} sec^{-1}.

(3) Type B annealed specimen, temperature 620°C. strain rate 1 x 10^{-4} sec^{-1}

(4) Type B deformed specimen, temperature 620°C. strain rate 1 x 10^{-4} sec-1.

(5) Type A deformed specimen, temperature 560°C. strain rate 1 x 10^{-4} sec^{-1}.

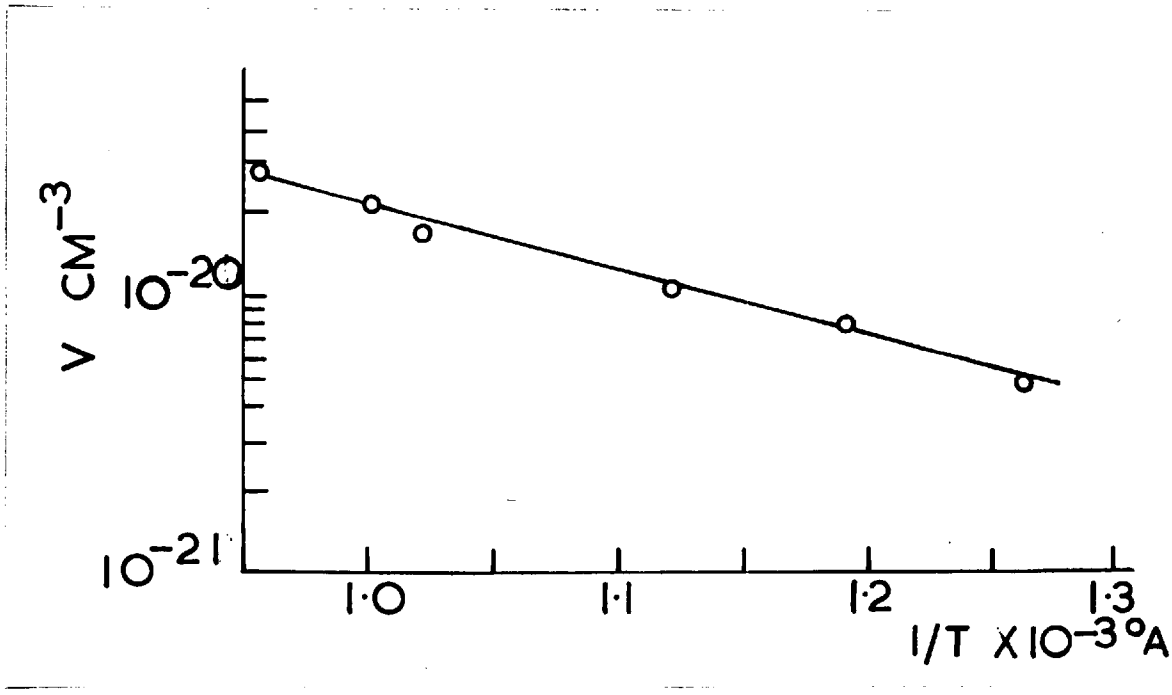

FIGURE 32.

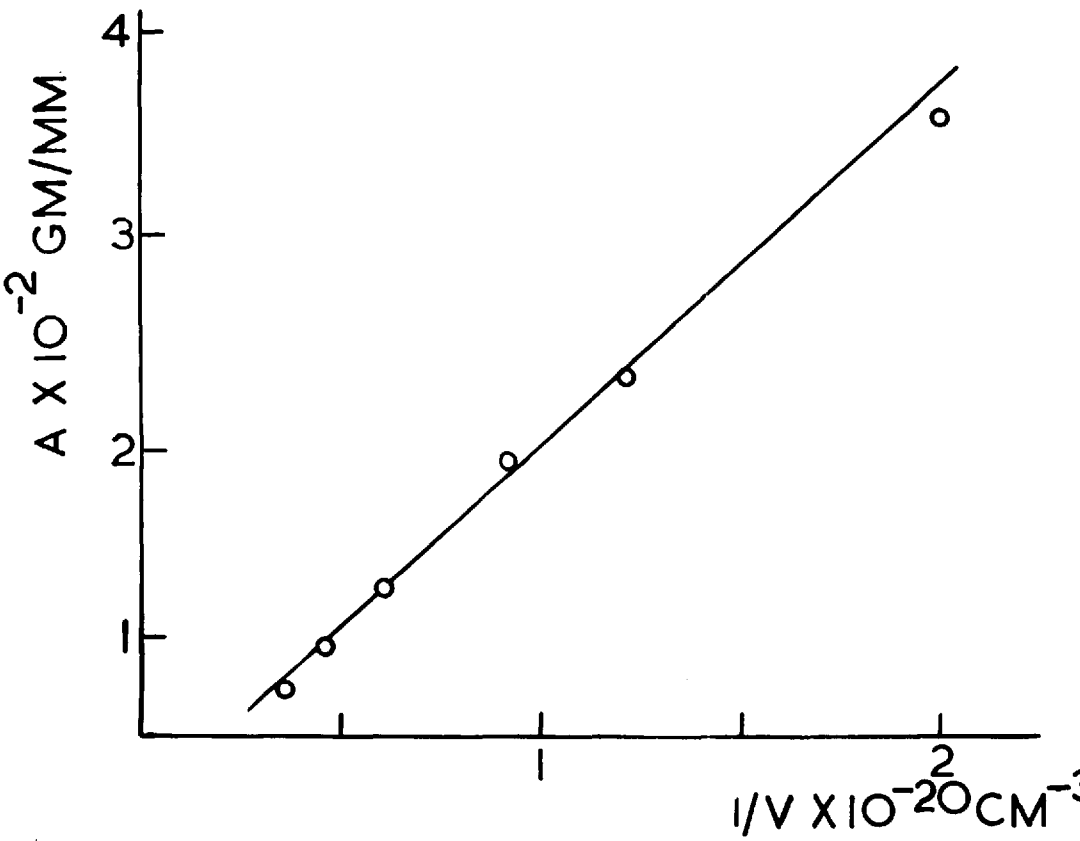

FIGURE 33.

REFERENCES

1 W.T.Read. Phil. Mag. 45, 775 (1954)

2 W.T.Read. Phil. Mag. 46, 111 (1955)

3 W.Schockley. Phys. Rev. 91 228 (1953)

4 J. Hornstra. J.Phys. Chem. Solids 5, 129 (1958)

5 P. Haasen and A.Seeger. Halbleiterplobleme IV, Vieweg, (1958).

6 F.L.Vogel, W.G.Pfann, H.E.Corey and E.E.Thomas. Phys. Rev. 89, 489 (1953).

7 F.L.Vogel. Acta Met. 3, 245 (1955)

8 F.L.Vogel. Acta Met. 8, 946 (1956)

9 W.C.Dash. Dislocations & Mechanical properties of crystals - Fisher et al., Wiley, (1957).

10 R.Phillips - The Institute of Metals Symposium on metallurgical aspects of semi-conductors (Feb.1958)

11 C.J.Gallacher. Phys. Rev. 88, 721 (1952)

12 F.Seitz. Phys. Rev. 88, 721 (1952)

13 J.R.Patel. Phys. Rev. 101, 143 (1956)

14 R.G.Treuting. J. of Metals. 7, 1027 (1955)

15 H.G. van Bueren. Physica 24, 821 (1958)

16 P.Penning and G.de Wind. Physica 25, 765 (1959)

17 H.G. van Bueren. Physica 25, 775 (1959)

18 J.R.Patel and B.H.Alexander. Acta.Met. 4, 385 (1956)

19 R.P.Carreker. J. of Metals 8, 111, (1956)

20 H.G. van Bueren. Physica 26, 997 (1960)

21 P.Haasen. Acta Met. 5, 598 (1957)

22 A.R.Chaudhuri, and J.R.Patel. Bull.Am.Phys. Soc. 5, 264 (1959)

23 R.L.Cummerow and A.R.Cherry. Phys.Rev. Letters 3 367 (1959)

24 T.Suzuki - International Union of Crystallography Congress (1960)

25 E.Billig. Proc. Roy. Soc. A 235, 37 (1956)

26 P.Penning. Philips Res. Reports 13, 79 (1958)

27 G.L.Pearson, W.T.Read and W.L.Feldmann. Acta Met. 5, 197 (1957)

28 W.D.Sylwestrowicz - Private communication.

29 A.G.Tweet. Phys. Rev. 106 221 (1957)

30 H.C.Theurerer, J.H.Scaff. Tr.A.I.M.E. 191, 59 (1951)

31 C.Golberg. Phys. Rev. 89, 920 (1952)

32 L.Esaki. Phys. Rev. 89, 722 (1952).

33 C.S.Fuller and J.D.Struthers. Phys.Rev. 87, 526 (1952)

34 W.P.Slichter and R.O.Kolbs. Phys.Rev. 87, 527 (1952)

35. G.Finn. Phys. Rev. 91, 754 (1953)

36 S.Mayburg. Phys. Rev. 95, 38 (1954)

37 R.Logan. Phys. Rev. 101, 1455 (1956)

38 R.L.Hopkins and E.N.Clarke. Phys. Rev. 100, 1786 (1955)

39 S.Mayburg. Phys. Rev. 103, 1130 (1956)

40 H.Letaw. J.Phys. Chem. Solids 1, 100 (1956)

41 A.Seeger. Solid State Physics in Electronics & Telecommunications Vol.I. (Acad.Press) 1959.

42 A.T.Churchman and A.H.Cottrell. Nature 167, 943 (1950).

43 P.Tury and S.Krausz. Nature 139, 30 (1937)

44 G.W.Ardley and A.H.Cottrell. Proc.Roy.Soc. A 219, 328 (1953).

45 D.F.Gibbons and A.H.Cottrell. Nature 162, 488 (1947

46 H.L.Wain and A.H.Cottrell. Proc.Roy.Soc. B 63, 339 (1950).

47 R.E.Smallman, G.K.Williamson and G.W.Ardley. Acta Met. 1, 126 (1953)

48 V.A.Phillips, A.J.Swain and R.E.Eborall. J.I.M. 81, 625 (1953)

49 A.H.Cottrell. Dislocations & Plastic Flow in Crystals, Oxford (1953)

50 A.H.Cottrell and R.A.Bilby. Proc. Phys. Soc. A.62, 49 (1949)

51 A.D.Heidenreich and W.Schockley. Rep. Conf. Strength of Solids, Bristol (1947)

52 J.C.Fisher. Trans. A.S.M. 47, 451 (1955)

53 A.H.Cottrell. Conf. Mech. Engineers (1957)

54 H.Suzuki - Dislocations & Mechanical Properties of Crystals, Fisher et al., Wiley (1957)

55 G.Schoeck and A.Seeger. Acta Met. 7, 469 (1958)

56 H.Lange and K.Lücke. Z.fur Metall. 44, 183 (1952)

57 T.H.Blewitt. Phys. Rev. 91, 1115 (1953)

58 C.R.Cupp and B.Chalmers. Acta Met. 2, 803 (1954)

59 P.Haasen and A.Kelly. Acta Met. 5, 192 (1957)

60 M.J.Makin. Phil. Mag. 3, 287 (1958)

61 A.T.Thomas. Nature 181, 1728 (1958)

62 H.W.Paxton. J.A.P. 24, 104 (1953)

63 G.F.Bolling. Phil. Mag. 4, 537 (1959)

64 A.H.Cottrell and R.J.Stokes. Acta Met. 2, 341 (1954)

65 A.H.Cottrell and R.J.Stokes. Proc.Roy.Soc. A 233, 17 (1955)

66 G.I.Taylor. Proc.Roy.Soc. A 145, 362 (1934)

67 A.Seeger. Dislocations and Mechanical Properties of Crystals - Fisher et al., Wiley (1957)

68 J.Friedel. Dislocations and Mechanical Properties of Crystals - Fisher et al., Wiley (1957)

69 J.E.Bailey and P.B.Hirsch. International Union of Crystallography Congress (1960)

70 P.B.Hirsch. International Union of Crystallography Congress (1960)

71 J.J.Gilman and W.G.Johnston - Dislocations and Mechanical Properties of Crystals, Fisher et al., Wiley (1957)

72 W.G.Johnston & J.J.Gilman. J.A.P. 30, 129 (1959)

73 J.J.Gilman. J.A.P. 30, 1584 (1959)

74 W.G.Johnston & J.J.Gilman. J.A.P. 31, 632 (1960)

75 J.J.Gilman & W.G.Johnston. J.A.P. 31, 687 (1960)

76 L.B.Valdes. Proc. I R E. 420 (1954)

77 E.Schmid & W.Boas - Plasticity of Crystals, F.A.Hughes & Co. (1950)

78 W.L.Bond & J.Andrus. Phys.Rev. 101, 1211 (1956)

79 J.J.Oberly. J. of Metals 6, 1026 (1954)

80 J.Okada. J.Phys.Soc. Japan 10, 1018 (1955)

81 Y.Uemura. J.Phys.Soc. Japan 10, 1020 (1955)

82 C.S.Baker, L.M.Slifkin & J.W.Marx. J.A.P.24,1331 (1953)

83 R.A.Logan & A.J.Peters. J.A.P. 30, 1627 (1959)

84 H.Alexander. Z.fur Metall. 52, 344 (1961)